Simulating the Characteristics and Influences of the Botswana High over Southern Africa using the Model for Prediction Across Scales (MPAS)

MOLULAQHOOA LINDA MAOYI
(MYXMOL001)

Thesis Presented for the degree of

DOCTOR OF PHILOSOPHY

Department of Environmental & Geographical Science

Faculty of Science

UNIVERSITY OF CAPE TOWN

Supervisor:

Assoc. Prof Babatunde J. Abiodun

December 2021

DECLARATION I

I know the meaning of plagiarism and declare that all the work in this thesis, save for that is properly acknowledged, is my own.

Signature: Signed by candidate

Molulaqhooa Linda Maoyi

DECLARATION II

Parts of this thesis have been published or are under review for publication in the following papers:

- Maoyi ML, Abiodun BJ (2021) How well does MPAS-Atmosphere simulate the characteristics of the Botswana High? Published - *Climate Dynamics*.

- Maoyi ML, Abiodun BJ (2022b) The influence of the Botswana High on drought modes over Southern Africa in observation and MPAS. Under review - *International Journal of Climatology*.

- Maoyi ML, Abiodun BJ (2022a) Investigating the Response of the Botswana High to El Niño Southern Oscillation using a Variable-Resolution Global Climate Model. Published - *Theoretical and Applied Climatology*.

ABSTRACT

The Botswana High is a prominent mid-tropospheric system that modulates rainfall over subtropical Southern Africa, but the capability of a Global Climate Model (GCM) to reproduce the characteristics and influences of this system on drought remains unknown. Furthermore, the summer variability of the Botswana High has been linked to the El Niño Southern Oscillation (ENSO). However, it remains unknown whether the high's variability is a direct response to ENSO. To that end, this thesis examines the capability of a GCM with quasi-uniform resolution (Model Prediction Across Scales, hereafter MPAS) in simulating the characteristics and influences of the Botswana High on drought modes over the subcontinent as well as the influence of ENSO on the high. To simulate the characteristics of the Botswana High and its influence on drought modes, the MPAS model is applied to simulate the global climate at 240km quasi-uniform resolution over the globe for the study period 1980-2010. The model results are validated against gridded observation dataset (Climate Research Unit, CRU), satellite dataset (Global Precipitation Climatology Project, GPCP), and reanalysis datasets (Climate Forecast System Reanalysis, CFSR; the National Oceanic and Atmospheric Administration, NOAA; and ERA-Interim reanalysis 5, ERA5). To investigate the response of the Botswana High to ENSO, this thesis carried out two MPAS model experiments. The first model experiment used observed SSTs everywhere during the study period, while the second experiment used observed SSTs everywhere except over the Pacific Ocean, where monthly climatological SSTs are imposed.

The results of this thesis show that MPAS replicates all the essential features in the climatology of climate variables (e.g. temperature, rainfall, 500 hPa geopotential height and vertical motion) over Southern Africa, reproduces the spatial and temporal variation of the Botswana High, and captures the influence of the Botswana High on droughts and deep convections over the subcontinent. In all the datasets (CRU, ERA5, 20C and MPAS), the most dominant five Drought Modes (hereafter DM1-DM5) over Southern Africa jointly explain more than 60% of the interannual variability in the 3-month summer droughts for SPEI and for SPI. ERA5 and MPAS agree that the Botswana High influences the interannual variability of DM1; however, the influence is strong in ERA5 ($r = -0.85$) and moderate in MPAS ($r = -0.42$). In addition to that, wet years (+ve SPEI and SPI) are characterized by a weak Botswana High and drought years (-ve SPEI and SPI) by a strong Botswana High.

In addition to that, the wet and dry years correspond to the -ve and +ve phases of El Niño Southern Oscillation (ENSO), respectively. Given this, the results of this thesis suggest that the Botswana High might be a conduit pipe through which ENSO signals influence DM1 over the region. Investigation into the impact of ENSO on the Botswana High reveals that the absence of ENSO forcing reduces the amplitude of the Botswana High variability, but the signal of the variability remains. While ENSO enhances the strength of the Botswana High, it does not aid the formation of the High. The result of the thesis has application in the improvement and application of MPAS for drought early warning systems over Southern Africa.

ACKNOWLEDGEMENTS

First and foremost, I would like to express my deepest gratitude to my Supervisor, Prof Babatunde Joseph Abiodun, for taking me under his wing and training me into a specialist climate modeller and researcher. In addition to that, I would like to thank the great Professor for his constant support, guidance, and motivation throughout this mammoth of a degree. I was ready to quit many times when things were not working out, but you kept calling me "Kinetic Doctor Maoyi", which made all the difference. Thank you very much, Babs!

I would also like to express my sincere gratitude to Mr Phillip Mukwenha for his selfless assistance and incredible work ethic when I had trouble installing the various software packages I needed to conduct my research. Thank you very very much Mr Phillip, and may God bless you more and more!

A big thank you to my PhD colleagues, Dr Roland Takong and Dr Sabina Abba Omar, for always being available when I needed to pick their brains. Thank you, guys, for taking time from your busy schedules for the advice and insightful discussions, which were vital for this research.

I would also like to thank the Centre for High-Performance Computing (CHPC) for allocating me resources so I can run my model experiments. Gratitude also goes out to the support team, who have always accommodated my requests even under challenging circumstances.

My gratitude goes out to the University of Cape Town, of which the university's PhD staff bursary partly supported this research.

To my colleagues at the SAS Institute, thank you for showing interest in my work and always encouraging me to finish this thesis, especially when I was in complete darkness. I would especially like to thank my line manager Mr Adesh Nathalal for giving me his full support and encouragement during my doctoral journey. Thank you so much, boss, and I really appreciate all that you have done for me.

I would also like to express my deepest gratitude to my Cape Town friends and family for their support, encouragement, and love. Most notably, I would like to thank Tendai Mbanje, Alupheli Gxavu, Fungai Jani, the late Aunty Lizzy, Joel Guy Chabata, Lynette Van Schalkwyk, Ngonidzashe Edwards SJ, Fr Matsepane Morare SJ, Fr Jean Claude Havyarimana SJ and members of the Society of Jesus (Jesuits) in Cape Town. Thank you, guys, for taking the time to listen to me going on and on about the Botswana High and climate modelling. I am sure most of you are well-versed in Atmospheric Science by now.

To my friends and brothers from Mohlakeng, thank you, gents, for being a pillar of strength during my study time. You never complained when I wasn't around during weekends or for *chillas* because you understood the important work that I was undertaking. A big thank you to the late Fr Sixtus Moahludi, Tshepo Monyatsi, Kabelo Mnisi, Sabata Moeketsi, Kagiso Moiloa and Lucky Lentswe. *Dankie,* gents, for being there when I needed you the most.

To my wonderful and loving family, without whose unfailing love and support I could have never achieved such a great accomplishment, ke re ho lona, kea leboha! To Mampho and Teboho Maoyi, you are doing great and on the right track. Keep focused, and the world will be your oyster. To my father, Israel Maoyi and mother, Tsholofelo Maoyi, thank you for supporting and encouraging me all these years during my academic endeavours and for never having any doubt in my ability to succeed. It's been a long and hard road, but I have finally reached my destination with you by my side. I love you, Mom and Dad!

Most importantly, I would like to thank God for bringing together everyone I mentioned above into my life and this journey. Thank you again, God, for keeping me and blessing me with life, courage, and strength in undertaking this degree. It was really tough and challenging, and I have the scars to prove it. But through your grace Lord, I overcame the challenges, persevered, and finally conquered. To you, Glory and Praise forever, Lord!

~ God Bless You All ~

DEDICATION

I would like to dedicate this thesis to my father, Israel Maoyi, who has been a role model and inspiration and supported me from the first day I went to elementary school to the first day I went to University. To my mother, Tsholofelo Maoyi, who has been a constant pillar of strength and support.

A Molimo a le hlohonolofatse, mme a le boloke- May God bless and keep you

I would also like to remember those who passed on and were an integral part of this journey.

My Parish Priest Fr Lionel Sham (2009)
My Grandfather Moses Mogorosi (2009)
My Aunt Maria Maoyi (2015)
My Uncle Andile Maoyi (2016)
My Grandmother Francina Nobadula (2019)
My Aunt Lydia Mogorosi (2020)
My Priest and Brother Fr Sixtus Moahludi (2020)
My Aunt Lizzy Isaacs (2020)

LIST OF ACRONYMS

20C	20th Century reanalysis II
AAO	Antarctic Oscillation
AOI	Antarctic Oscillation Index
AGBM	Australian Government Bureau of Meteorology
AGCM	Atmospheric General Circulation Model
AIDS	Acquired Immunodeficiency Syndrome
AMJ	April to June
ARW	Advanced Research WRF
CAM	Community Atmosphere Model
CESM	Community Earth System Model
CFSR	Climate Forecast System Reanalysis
CHPC	Centre for High-Performance Computing
CMIP5	Coupled Model Intercomparison Project Phase 5
CRU	Climate Research Unit
CTRL	Control
DJF	December to February
DM	Drought Mode
DRC	Democratic Republic of Congo
EAM	East Asian Monsoon
ECMWF	European Centre for Medium-Range Weather Forecasts
ENSO	El Niño Southern Oscillation
EOF	Empirical Orthogonal Function
ERA5	ERA-Interim reanalysis 5
GCM	Global Climate Model
GDP	Gross Domestic Product

GMTED2010	Global Multi-resolution Terrain Elevation Data 2010
GPCP	Global Precipitation Climatology Project,
HIV	Human Immunodeficiency Virus
IOD	Indian Ocean Dipole
IOM	Indian Monsoon
IOSD	Indian Ocean Subtropical Dipole
ITCZ	Intertropical Convergence Zone
JFM	January to March
JJA	June to August
MAM	March to May
MC	Mozambique Channel
MPAS	Model for Prediction Across Scales
MSD	Mid-Summer Drought
NASH	North Atlantic Subtropical High
NCEP	National Centers for Environmental Prediction
NOAA	National Oceanic and Atmospheric Administration
NPSH	North Pacific High Subtropical High
OLR	Outgoing Longwave Radiation
OND	October to December
PCA	Principal Component Analysis
PET	Potential Evapotranspiration
RCM	Regional Climate Model
RMSE	Root Mean Square Error
SADC	Southern African Development Community
SAH	South Atlantic High
SAM	Southern Annular Mode
SAMI	Southern Annular Mode Index
SASD	South Atlantic Subtropical Dipole

SASH	South Atlantic Subtropical High
SACZ	South Atlantic Convergence Zone
SICZ	South Indian Convergence Zone
SIH	South Indian High
SIOD	Subtropical Indian Ocean Dipole
SOM	Self-Organising Map
SPEI	Standard Precipitation Evapotranspiration Index
SPH	South Pacific High
SPI	Standard Precipitation Index
SST	Sea Surface Temperature
SVD	Singular Value Decomposition
TNA	Tropical North Atlantic
TTT	Tropical Temperate Troughs
USGS	U.S. Geological Survey
VRGCM	Variable-Resolution Global Climate Model
WNPSH	Western North Pacific Subtropical High
WPSH	Western Pacific Subtropical High
WRF	Weather Research and Forecasting

TABLE OF CONTENTS

LIST OF FIGURES

LIST OF TABLES

CHAPTER ONE: INTRODUCTION

1.1 What is the Botswana High?

The Botswana High is a semi-permanent mid-level anticyclone located over central Namibia and western Botswana. It is also referred to as the Botswana Upper High. The Botswana High is an important component of regional atmospheric circulation over Southern Africa during the austral spring, summer, and autumn (Reason, 2016; Reason, 2018). This mid-level anticyclone is more prominent in the 500 hPa geopotential height from January to March (JFM), which is the rainiest part of the rainfall season in Southern Africa. It is a prominent feature to weather and seasonal forecasters in the various countries in the Southern African region (Fig 1.1).

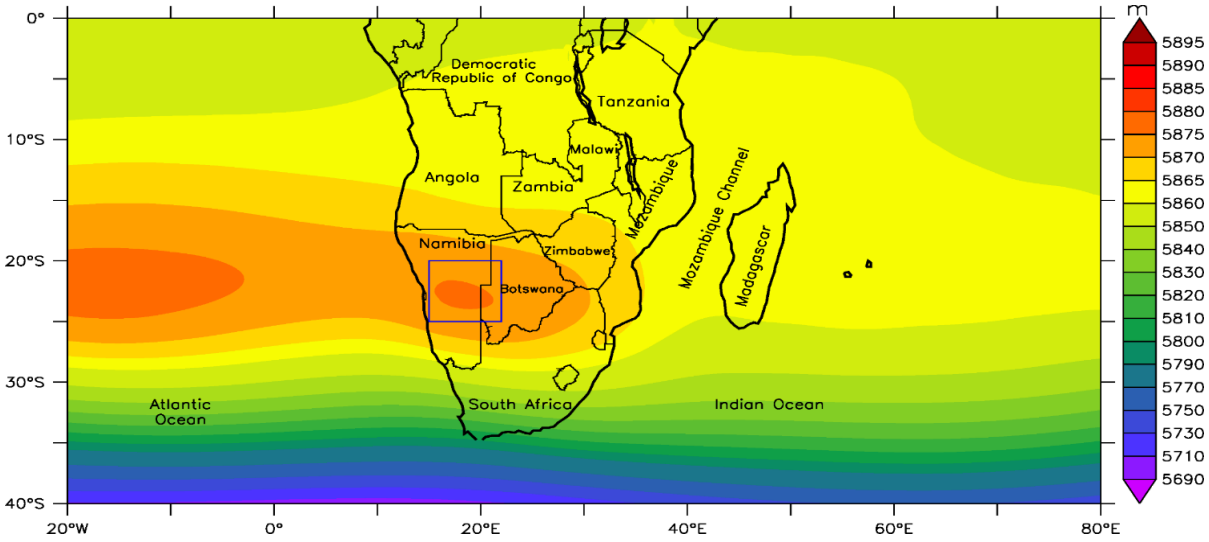

Fig 1. 1: The January-March climatology of 500 hPa geopotential height (m) over Southern Africa (1980-2010) as depicted by the European Centre for Medium-Range Weather Forecasts reanalysis 5. The blue box shows the Botswana High Area (15-22º E; 20-25º S)

Generally speaking, anticyclones or high-pressure systems like the Botswana High are regions where the atmospheric pressure is greater than its surrounding environment (University Corporation for Atmospheric Science, 2021). As a result, winds within anticyclones flow outward from the higher-pressure areas near their centres towards the lower-pressure areas farther from their centres. Gravity adds to the forces that cause this general movement because the higher pressure compresses the column of air near the centre of the high into greater density – and greater weight than the air outside the centre. However, because of the earth's rotation, the airflow from the centre to the exterior is not direct but twisted due to the Coriolis effect (Persson, 1998). Given that, the circulation around the highs is clockwise in the Northern

Hemisphere and counterclockwise in the Southern Hemisphere. At sea level, anticyclones typically originate as cold, shallow circulations that move equatorward and evolve into warm, subtropical high-pressure systems penetrating well into the troposphere. Aloft, anticyclones may appear at the middle and higher latitudes on isobaric surfaces. In addition, anticyclones aloft are typically stationary or westward drifting and thus may block the eastward progress of other weather systems (Colucci, 2003).

The Botswana High can be classified as a subtropical high. Subtropical highs are semi-permanent synoptic-scale features that influence weather and climate over the world's subtropical regions. These systems are characterised by anticyclonic wind curl, subsidence, and low-level atmospheric divergence (He et al., 2017). The centres of the high are characterised by weak pressure gradients, light winds, and clear skies due to subsidence, while their borders have more intense winds. They are located between 20^{o} and 40^{o} of latitude in both the Northern and Southern Hemispheres (Britannica, 2017) and occupy 40% of the Earth's total surface area (Rodwell and Hoskins, 2001). Although subtropical highs are not as actively researched as their low counterparts (e.g. tropical cyclones), these anticyclones are important because the clear and dry condition associated with them usually allows for increased temperatures and below-average rainfall (Driver and Reason, 2017), which may lead to heatwaves and drought conditions. Furthermore, increased subsidence from subtropical highs may allow air pollutants to concentrate near the Earth's Surface.

1.2 Evolution of the Botswana High

The Botswana High evolves in austral spring and summer from August until April (Fig 1.2). In August, a band of high pressure exists between 5^{o} and 15^{o}S over the tropical Atlantic Ocean, extending over much of Angola and the western parts of Zambia (Fig 1.2a). By September, the high pressure forms a closed anticyclone (which is reminiscent of the Botswana High) over southern Angola while the band extending from the high into the Atlantic Ocean dissipates (Fig 1.2b). In October (Fig 1.2c), the centre of the Botswana High increases in size and strengthens and shifts southward towards the northern parts of Namibia and Botswana. The high continues to move southward during November (Fig 1.2d) into northern Namibia and Botswana (Fig 1.2d); however, the high's strength decreases, and its centre becomes broader by December (Fig 1.2e). In January (Fig 1.2f), the high develops a small centre over central Namibia and increases in strength in February through to March (Figs 1.2g and 1.2h). By April (Fig 1.2i),

the Botswana Highs centre dissipates and shifts farther north. The location of the high and its shift south and south-eastward have been linked to the movement of the region of highest precipitation over the Congo basin and the Intertropical Convergence Zone (ITCZ), which lie northeast of the high (Driver and Reason, 2017).

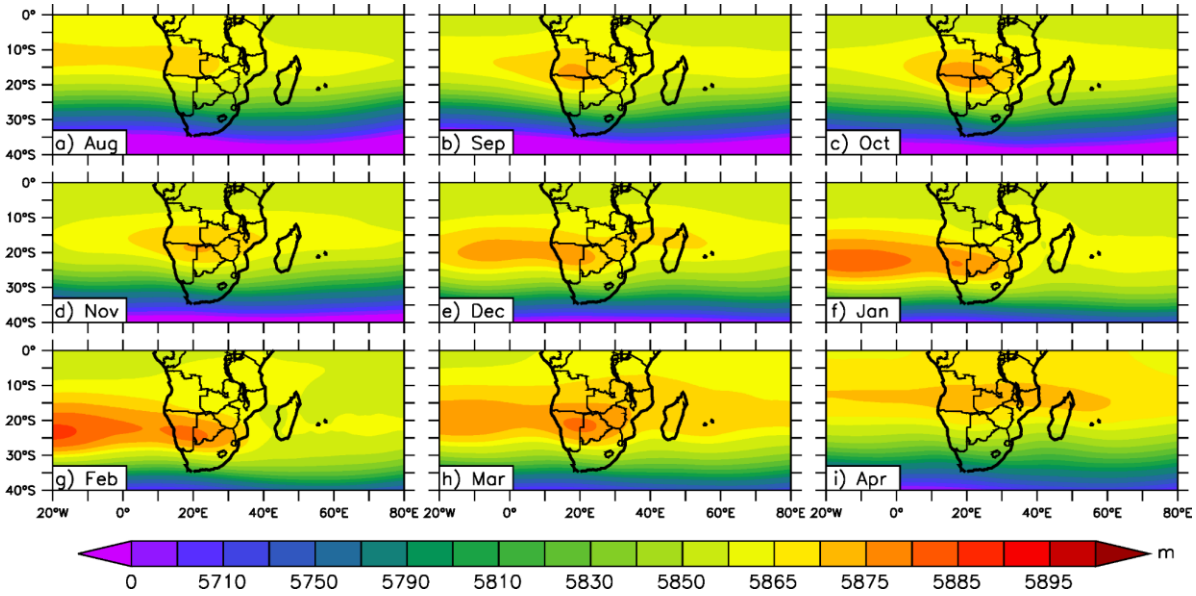

Fig 1. 2: The climatology of 500 hPa geopotential height (m) for August-April over Southern Africa (1980-2010) as depicted by the European Centre for Medium-Range Weather Forecasts reanalysis 5

1.3 Southern Africa and socio-economic developments

Southern Africa is the southernmost region of the African continent and consists of 16 developing countries that unite to form the Southern African Development Community (SADC). The SADC member states include Angola, Botswana, Comoros, Democratic Republic of Congo (DRC), Eswatini, Lesotho, Madagascar, Malawi, Mauritius, Mozambique, Namibia, Seychelles, South Africa, Tanzania, Zambia, and Zimbabwe (Fig 1.3). The Southern African region, which covers about 556781 km^2, accommodates more than 345 million people with an average life expectancy of 61 years (SADC, 2018). Poverty and underdevelopment remain daunting challenges for social and human development in the SADC region, with approximately half of the population living below the international poverty line of US $1 per day (SADC, 2012a). Poverty is further compounded by complex challenges, which include social and civic conflicts, gender inequalities, exploitation, high unemployment, high morbidity, and HIV and AIDS. However, climate variability, which manifests in the form of floods, heatwaves, and droughts, has a huge impact on the region's livelihoods and economic activity (SADC, 2012b). A better understanding of how atmospheric processes (like Botswana Highs) influence climate variability over Southern Africa would contribute toward the

development of socio-economic activities and the protection of lives, property, and the environment.

Fig 1. 3: The Southern African Development Community member states (Source: SADC, 2012c)

The agricultural sector is of social and economic importance in the SADC region. Its performance has a strong influence on food security, economic growth, and social stability in the area. Agriculture contributes between 4% and 27% of the Gross Domestic Product (GDP) in the different SADC member states and 13% of overall export earnings (SADC, 2012d). Approximately 70% of the region's population depends on agriculture, primarily practised under rain-fed conditions (Cooper et al., 2008; Zinyengere et al., 2013) for food, income, and employment (see Fig 1.4). In light of this, the region's socio-economic development depends heavily upon the agricultural sector's performance and growth, which is often vulnerable to and constrained by weather and climate extremes such as heatwaves, floods and droughts (Ziervogel et al., 2008). Several other factors also affect the agricultural sector, such as pests, diseases, and inappropriate government policy decisions that adversely affect agricultural input costs such as seeds, fertilisers, and agrochemicals (Food and Agriculture Organisation of the United States, 2016). Furthermore, the agriculture industry is labour-intensive, and the high prevalence of diseases such as HIV/AIDS in the labour force further compounds the food security crisis (SADC, 2012d), making the region's population more vulnerable to weather and climate extremes. To better understand these extreme events and reduce their impacts over the region, the present study focuses on a subtropical high, called the Botswana High (Driver,

2014; Driver and Reason, 2017; Reason, 2018), which has been shown to impact dry and wet spells over Southern Africa.

Fig 1. 4: Southern African rural women farming crops (Source: SADC, 2012e)

Mining is also a crucial industrial sector in several SADC nations (Fig 1.5), and roughly half of the world's vanadium, platinum, and diamonds originate in the region, along with 36% of gold and 20% of cobalt (SADC, 2012f). These minerals contribute significantly to several member states' GDPs (~10%) and employment (~5%), and many of them depend on mineral exports for their foreign exchange earnings (~60%) (SADC, 2001). In addition, minerals processing and extraction are industries that influence energy and electricity production and are vulnerable to weather and climate change (Naik, 2015). For instance, coal supplies most of the region's power generation (SADC, 2012g) and 90% of South Africa’s electricity (Scholvin, 2014). In 2014, heavy rains soaked South Africa's major coal-fired power plants leading to a national energy crisis (Dames, 2014). As a result, the national power supplier (Eskom) implemented a full-day power rationing for the first time since 2008, which impacted the national economy. The unprecedented national blackout in December 2019 (Smilie, 2019) was also attributed to 'wet coal,' as was the January 2021 South African nationwide stage-2 load shedding (O'Regan, 2021). Again, wet coal had a direct economic impact, demonstrating that weather and climate impact many socio-economic sectors in Southern Africa.

Fig 1. 5: Mine Workers working deep underground at Harmony Gold Mine's Cooke shaft near Johannesburg, September 22, 2005 (Source: Spector, 2012)

1.4 The climate of Southern Africa

The climate of Southern Africa is characterised by various climatic zones, which range from a Mediterranean climate in the southwestern tips, dry steppe over the central and eastern regions of South Africa and Botswana to tropical rainforests along the equator (see Fig 1.6). Unlike the rest of the region, only Namibia's interior has a desert climate. Much of the region has a distinct wet season, with most of its rainfall falling during the austral summer (December-February; DJF), while the dry season occurs in the austral winter (June-August; JJA). In contrast, the southwestern region of South Africa (i.e., Western Cape province), which has a Mediterranean climate, is characterised by dry summers and receives most of its rainfall during the winter because of cut-off lows and the passage of mid-latitude cyclones (Reason et al., 2006; Davis-Reddy and Vincent, 2017).

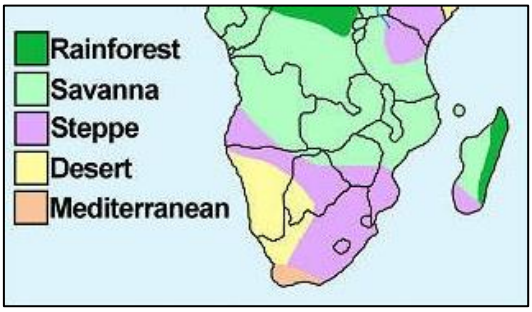

Fig 1. 6: The climatic zones of Southern Africa (Source: Bolton Geography Portfolio, nd, with some modification)

1.5 Factors influencing the weather and climate of Southern Africa

1.5.1 Ocean Currents

The Southern African climate is influenced by different factors, including topography, tropical, subtropical, mid-latitude systems and oceans currents that drive the region's climatology and seasonal cycle (Engelbrecht et al., 2014; Jury, 2013; Abba Omar, 2020). Southern African ocean currents are known to influence areas that are adjacent to them (Fig 1.7). For instance, the cold Benguela Current (Nicholson & Entekhabi, 1987) on the west coast of Southern Africa draws cold waters from the South Atlantic and carries them northward along the region's west coast. These cold waters cause cold air above the ocean contributing to low moisture and very little rainfall in coastal areas adjacent to the current. Furthermore, these cold waters may contribute to the parched climate of the Kalahari and Namib deserts. On the other hand, the warm Agulhas current (Lutjeharms, 2006), which flows southward on the southeast coast of Mozambique and South Africa, causes warm air above the Indian Ocean, leading to increased humidity, convection, and rainfall over the region. Thus, oceans moderate temperatures near Southern African coasts, making summers less hot and winters less cold than in the interior.

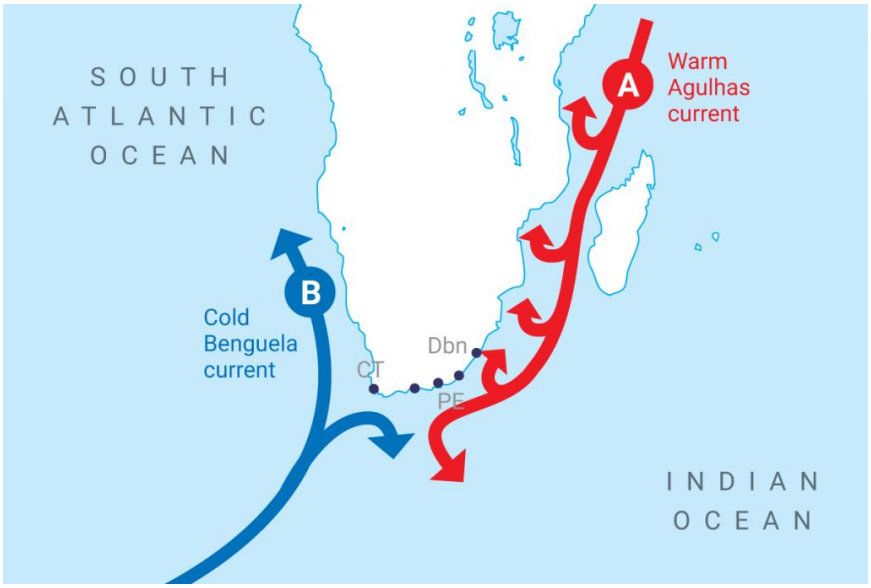

Fig 1. 7: Ocean Currents of the Southern African coast (Source: Ingpen, 2015)

1.5.2 Topography

The Great Escarpment is a notable feature of Southern African topography (see Fig 1.8), consisting of steep slopes from the high central-Southern African plateau southward in the

direction of the oceans that surround the region on the east (Indian Ocean), west (Atlantic Ocean), and south (Antarctic Ocean) (Naik, 2015). The escarpment's average height ranges from around 1500 m above sea level in the southwest to around 3500 m towards the KwaZulu-Natal Drakensberg area (Bhaktawar and Van Niekerk, 2012). Furthermore, the plateau is distinguished by broad plains that rise to around 1200 metres above sea level. Coastal mountains and escarpments abutting high ground can be found in northern Mozambique, South Africa, Namibia, Angola, and between the borders of Mozambique and Zimbabwe. Coastal plains, on the other hand, border the Indian Ocean in Mozambique and the Atlantic Ocean in Namibia and Angola. The region's topography is crucial as it creates spatial gradients in temperature and rainfall and sets up areas that exhibit different microclimates (Naik, 2015; Abba Omar, 2020).

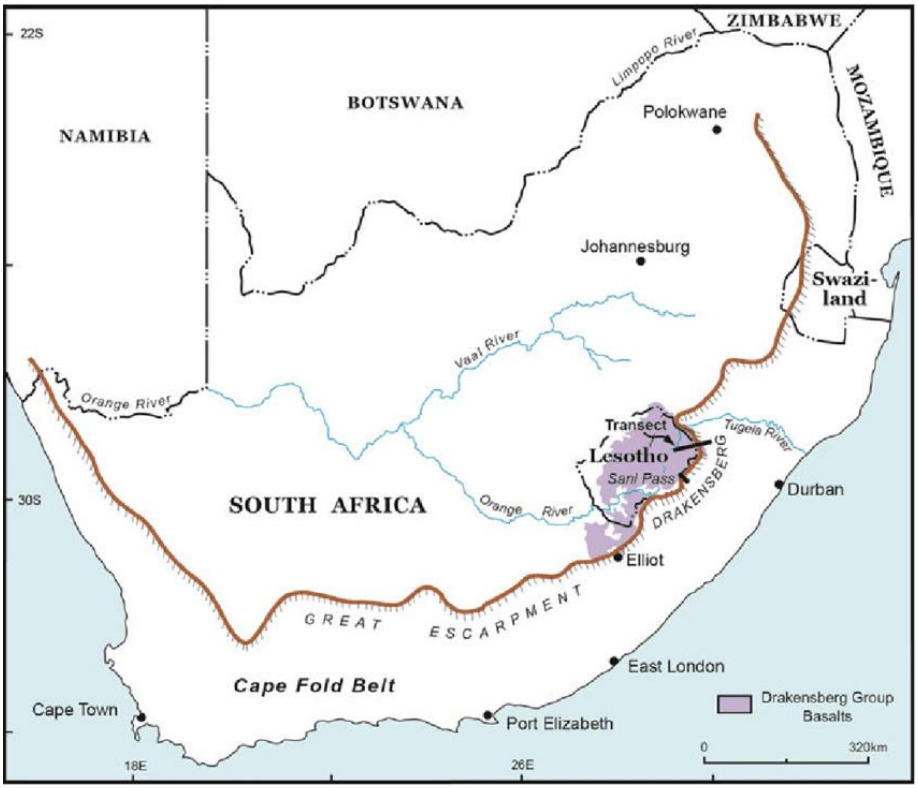

Fig 1. 8: Location of the Great Escarpment across South Africa (Source: Knight and Grab, 2015)

1.5.3 Intertropical convergence zone

The ITCZ, a region of cloud band and heavy rainfall caused by the convergence of north-easterly and south-easterly trade winds, is one of the atmospheric factors that play a significant influence in Southern African rainfall variability (Driver, 2014). The location of the ITCZ varies throughout the year and follows the thermal equator (Fig 1.9; Meque, 2015). During the

austral summer, the ITCZ shifts southwards along with the easterly waves and lows, bringing summer rainfall over most parts of Southern Africa (Pontes et al.,2020). With the southward shift of the ITCZ, the semi-permanent subtropical anticyclones (also known as subtropical highs) also shift farther south, allowing for rainy conditions to dominate over much of the subcontinent. During winter, subtropical anticyclones move north along with the northward shift of the ITCZ, leading to dry conditions over the region and wet conditions in the southern tip.

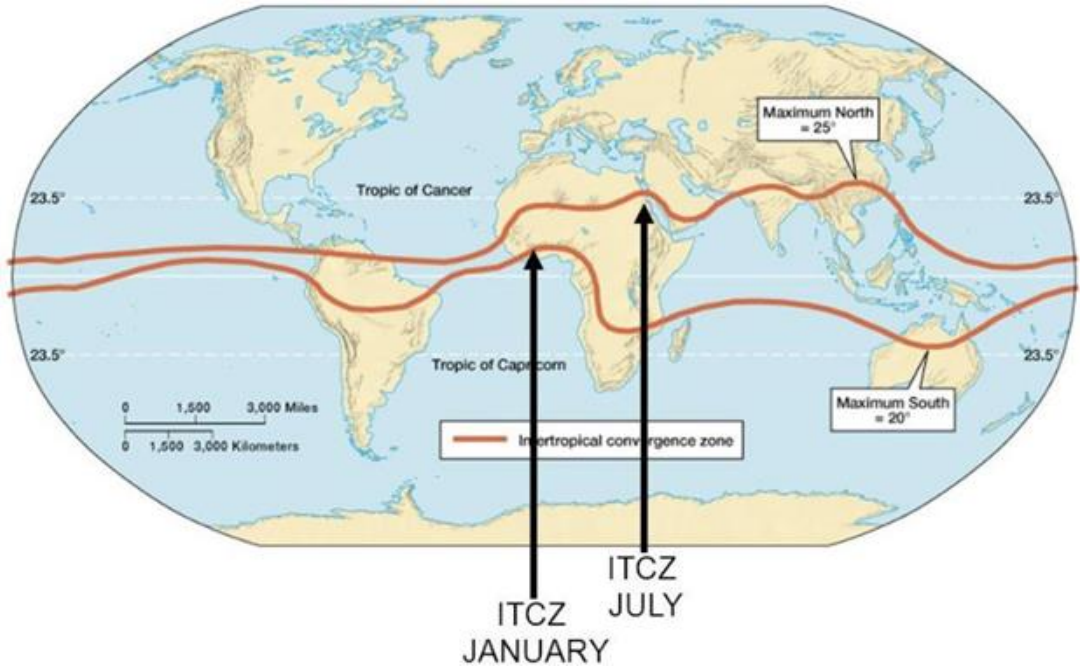

Fig 1. 9: Position of the January and July ITCZ (Source: Siddharta, 2020)

1.5.4 Tropical Temperate Troughs and Cut-off Lows

Southern African rainfall is mainly seasonal (Mason and Jury, 1997; Richard et al., 2001; Driver, 2014). The peak of the rainfall season occurs in austral summers (i.e. December, January, and February), except for the southwestern regions, which are in austral winter (i.e. June, July and August) (Lawal, 2015). The region's significant contributors to summer rainfall are tropical temperate troughs (TTTs) and their associated cloud bands (Mason and Jury, 1997) (see Fig 1.10). TTTs typically form when a tropical low is coupled to a mid-latitude trough in the upper atmosphere and tend to propagate eastward from Southern Africa to the Mozambique Channel and southern Madagascar. In the SADC region, the Angola Low is a tropical source region for these TTTs and their associated cloud bands (Chikoore and Jury, 2010), and the presence of a strong Angola Low generally results in higher levels of rainfall (Crétat et al.,

2018). Although TTTs contribute to widespread rainfall over much of the SADC region, the heaviest downpours are usually associated with cut-off lows (Singleton and Reason, 2007). As a result, these systems are known to cause floods in mid-latitude and subtropical regions in both the Northern and Southern Hemispheres (Abba Omar, 2020). Cut-off lows are closed, cold-cored lows in the upper troposphere that start as a high-amplitude trough in the upper Rossby wave, which advects cold polar air equatorward (Porcù et al., 2006). The trough then becomes unstable as it increases in amplitude and sometimes decreases in wavelength. The instability of the trough causes it to tear off from the primary wave, resulting in a closed low-pressure system with a cold polar air pool.

1.5.5 Summertime Highs

The SADC region is dominated by the Botswana High and two ocean-based semi-permanent anticyclones that form part of the ~35°S subtropical high belt during summer (see Fig 1.10). The two ocean-based anticyclones are the South Atlantic High (SAH) or St. Helena anticyclone (Sun et al., 2017) and the South Indian High (SIH) or Mascarene anticyclone (Xulu et al., 2020). The position of these subtropical highs has an impact on the summer rainfall in the region. For example, the Botswana High has been linked to rainfall anomalies over a few Southern African countries (Matarira, 1990; Magadza, 1994; Unganai and Mason, 2002; Ratna et al., 2012; Driver and Reason, 2017). Strong Botswana High years, for example, are frequently associated with unusually dry summers, whereas weak Botswana High years result in wet summers. Furthermore, the passage of upper westerlies of mid-latitude origin influences rainfall variability across the region, and hence the influence of these waves is occasionally impacted by the presence of a strong Botswana High. Moreover, the SAH and SIH are located in their respective oceans throughout the summer, creating favourable conditions for moisture transport inland and associated rainfall. However, during the winter period, the St. Helena and Mascarene High move closer to their respective coasts and form a massive high-pressure cell that extends from the Atlantic Ocean to the Indian Ocean. This situation results in subsidence over much of Southern Africa and inhibits rainfall since the atmosphere is relatively stable (Nicholson, 2011).

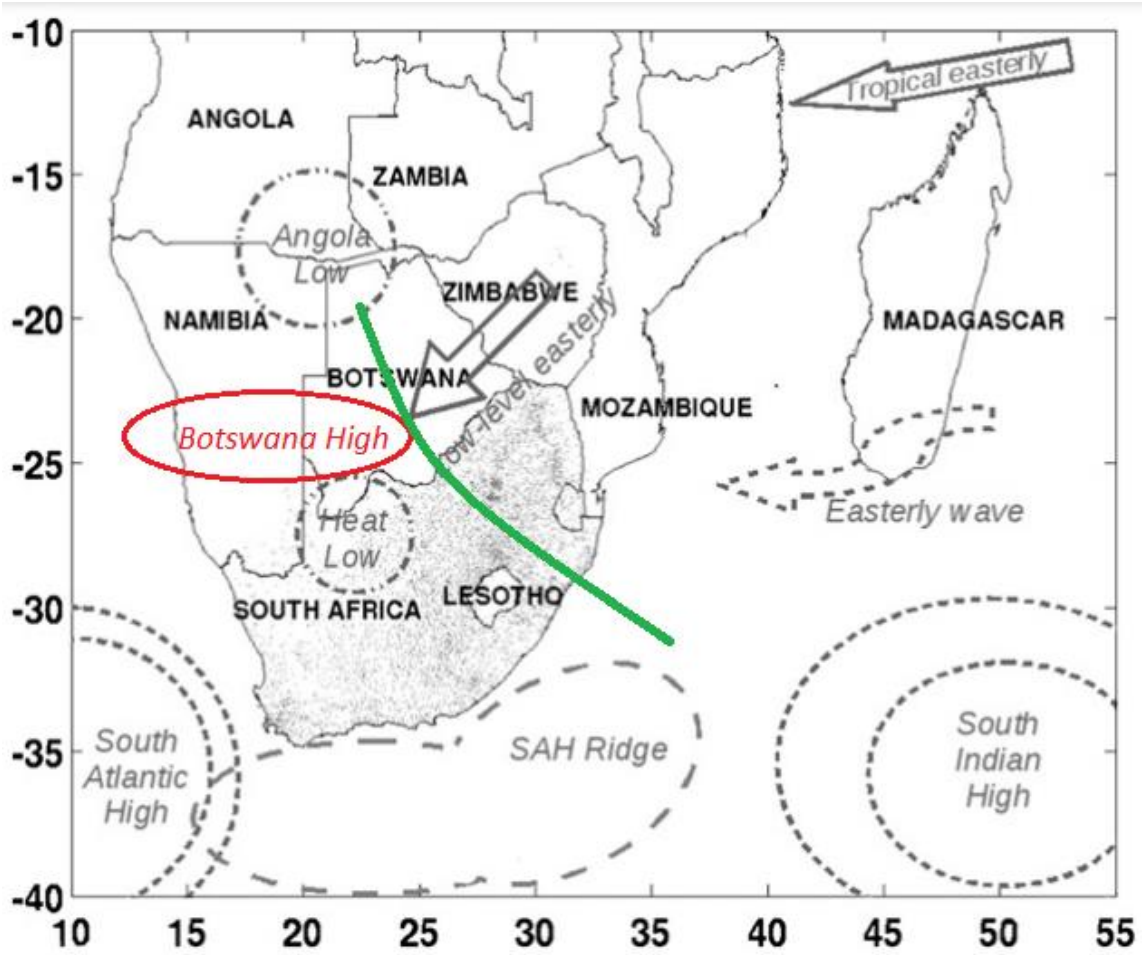

Fig 1. 10: Key Southern African synoptic features during austral summer. The green curve represents the mean position of TTT cloud bands over the region (source Hart et al., 2010, with some modification)

1.6 Ocean-Atmosphere Teleconnections over Southern Africa

1.6.1 El Niño Southern Oscillation

The El Niño Southern Oscillation (ENSO) is one of the most important coupled ocean-atmosphere phenomena affecting subtropical highs and interannual climate variability worldwide (Nicholson and Entekhabi, 1987; Lindesay, 1988; Nicholson and Kim, 1997; Reason et al., 2000; Cook, 2001; Reason and Jagadheesha, 2005; Gore et al., 2019). The Walker Cell (Lindesay,1988), a series of zonal cells stretching across the Southern Hemisphere, creates an atmospheric link between ENSO and the Southern African region's climate (Gore et al., 2019) (Fig 1.11). ENSO consists of three phases: El Niño (the warm or positive phase), the neutral phase and La Niña (the cold or negative phase). During El Niño's, anomalous west to east winds form and drive warm equatorial waters from the western Pacific towards the eastern Pacific and the northern parts of South America. This weakens the Walker circulation, resulting in strengthening the Southern Hemisphere subtropical high belt due to the Walker circulation's

descending limb. Furthermore, the strengthening of subtropical highs may increase subsidence over the region, reduce precipitation and lead to drought. On the other hand, during La Niña, the trade winds blow strongly westward on the ocean surface resulting in a westward current. This enhances the Walker circulation over Southern Africa as it experiences low pressure due to the Walker Circulation's ascending limb. This, in turn, weakens the subtropical belt over the region, resulting in increased convection over the region.

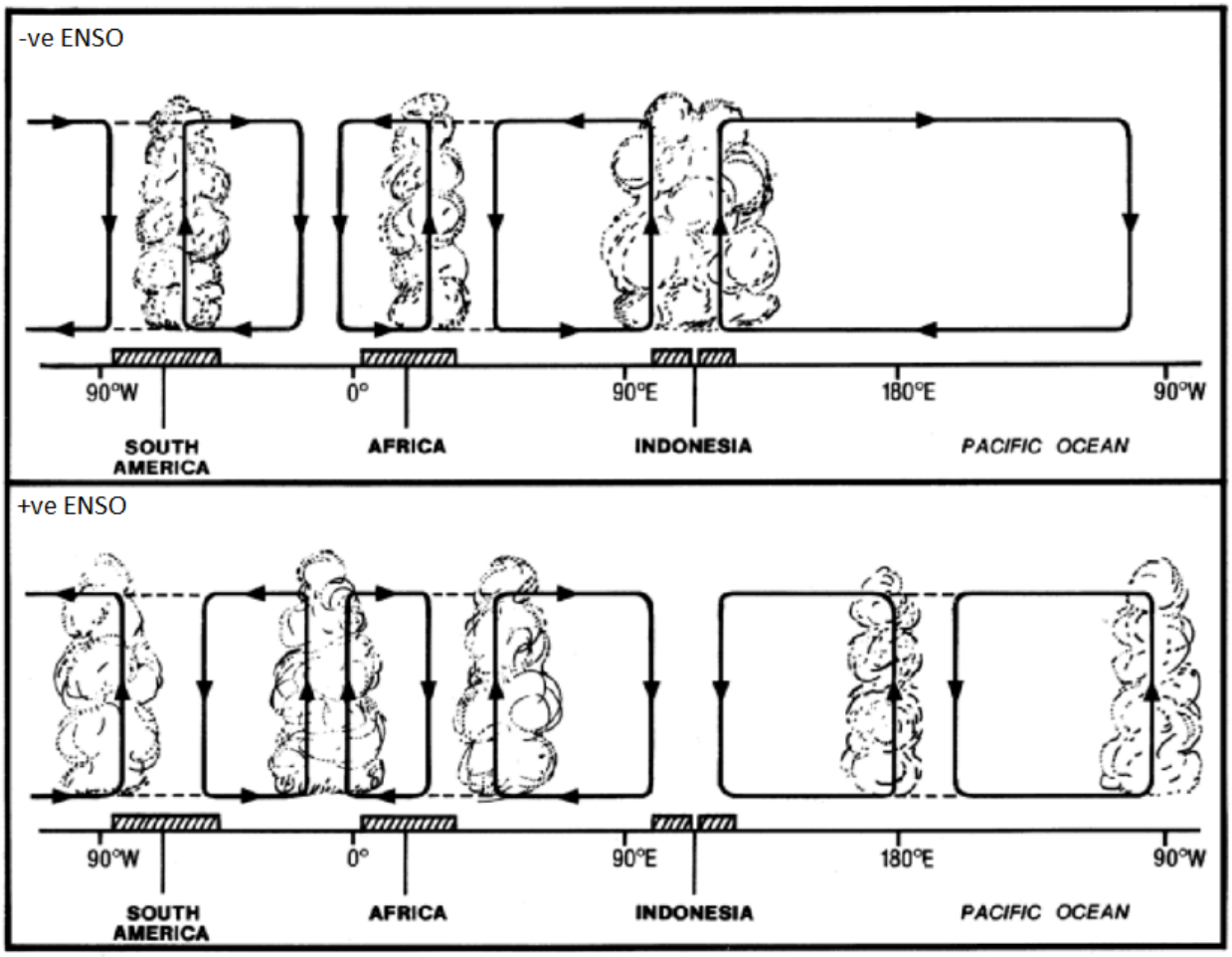

Fig 1. 11: The Walker Circulation cell. During a -ve ENSO event (top) and +ve ENSO event (bottom) (Source: Tyson and Preston-Whyte, 2000, with some modification)

1.6.2 Southern Annular Mode

The Southern Annular Mode (SAM), also known as the Antarctic Oscillation (AAO), is the dominant mode of variation in the Southern Hemisphere's high latitudes (Thompson and Wallace, 2000). It is distinguished by variations in atmospheric pressure between the mid-latitudes and the South Pole. The SAM is commonly represented by the Southern Annular Mode Index (SAMI) or Antarctic Oscillation Index (AOI), both of which can be calculated using two different methods. The SAMI is represented in the first approach by the leading Empirical Orthogonal Function (EOF) mode of the 850 hPa height anomalies poleward of 20°S (Reason and Rouault, 2005) (see Fig 1.12). In the second approach, the SAMI is calculated as the normalized difference of the zonal SLP between the Antarctic (65°S) and Southern Hemisphere mid-latitude (40°S). The SAM's negative phase is distinguished by high SLP anomalies around the Southern Polar region and low-pressure values over the Southern Hemisphere's mid-latitude region (Reason and Rouault, 2005; Bridgma and Oliver, 2006). During the positive phase of the SAM, a reversed situation is reported.

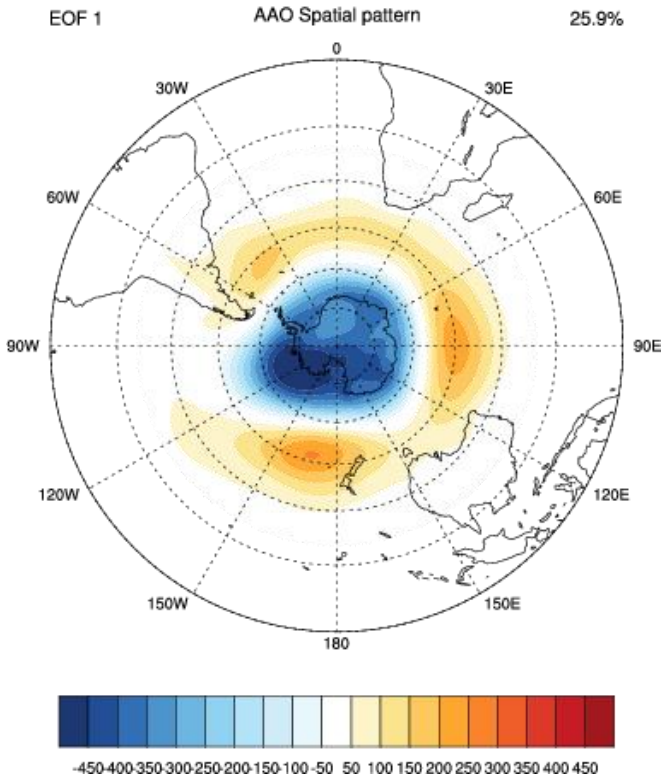

Fig 1. 12: Spatial pattern of the SAM for 1981-2010 (Source: National Oceanic and Atmospheric Administration, n.d)

1.6.3 Indian Ocean Dipole

The Indian Ocean Dipole (IOD) (Saji et al., 1999) is the Indian Ocean's counterpart to the Pacific ENSO. A dipole is defined as two "poles" or areas of difference. Given this, the IOD compares the SSTs of the Arabian Sea (western pole) and the eastern Indian Ocean south of Indonesia (eastern pole). Both poles are located within the Indian Ocean's equatorial belt (between 10°N and 10°S), but due to the physical configuration of the North Indian Ocean, they have a northwest-southeast diagonal orientation. The Arabian Sea lies north of the equator, while the Indian Ocean lies south of Indonesia. IOD, like ENSO, is an ocean-atmosphere coupled phenomenon. The shifting pools of warm/cold water contribute to variations in rainfall and storm activity in many of the Indian Ocean's surrounding countries. According to the Australian Government Bureau of Meteorology (AGBM, 2021), the IOD is thought to be linked to the Pacific ENSO via easterlies (considered as a limb/part of the Walker Circulation) and warm water transport from the Pacific into the Indian Ocean. During a positive IOD, warmer SSTs form over the western Indian Ocean (particularly the Arabian Sea). In contrast, the western Indian Ocean becomes cooler with higher air pressures during a negative IOD, forcing westerly winds to blow toward the Indian subcontinent (i.e., reversing the prevailing easterlies) (see Fig 1.13). Additionally, Positive IODs are frequently associated with El Niño, while negative IODs are associated with La Niña (AGBM, 2021).

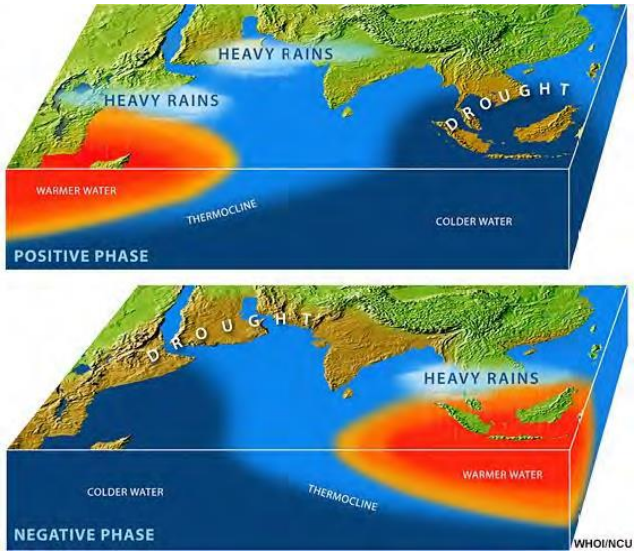

Fig 1. 13: Positive and Negative Phases of IOD (Source: Woods Hole Oceanographic Institution, 2021)

1.6.4 Subtropical Indian Ocean Dipole

Another factor influencing the Southern African climate, notably during the austral summer, is the Subtropical Indian Ocean Dipole (SIOD), sometimes known as the Indian Ocean Subtropical Dipole (IOSD) (Behera and Yamagata, 2001; Reason, 2001; Hansingo and Reason, 2009). A positive (negative) SIOD is characterised by warm (cold) SST anomalies south of Madagascar and negative (positive) anomalies along Australia's north-western coast (Morioka et al., 2010). The position of the Mascarene High-pressure Center has also been found to influence the development of the SIOD (Morioka et al., 2010). A positive SIOD phase, for example, is frequently connected with a strengthening Mascarene High-pressure centre, which leads to a stronger south-easterly flow pattern and, as a result, moisture flows inland. The SIOD index is calculated as a difference between the western and north-eastern SST anomalies (see Fig 1.14).

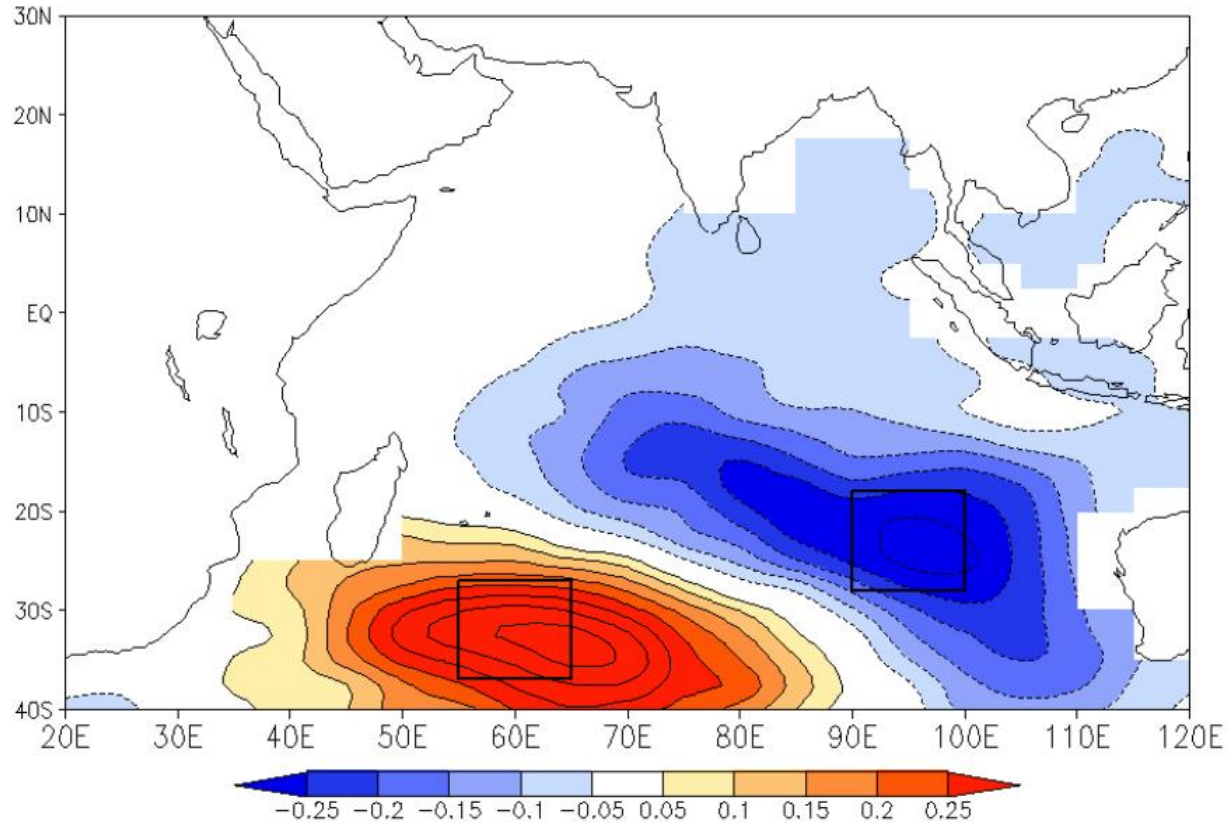

Fig 1. 14: Regressed SIOD on detrended Sea Surface Temperature from 1958-2007 (Source: Zhao, 2011, with some modification)

1.6.5 South Atlantic Subtropical Dipole

The South Atlantic Subtropical Dipole (SASD) is another dipole mode observed in the Atlantic Ocean (Venegas et al., 1997; Fauchereau et al., 2003; Hermes and Reason, 2005; Morioka et al., 2011; Morioka et al., 2012). A positive SASD event occurs when there are warm SST anomalies on the western side of the Atlantic Ocean's subtropical basin, as Hermes and Reason (2005) reported. The negative phase is the polar opposite. The SASD has a mechanism like the SIOD in that it is dependent on the strengthening or weakening of the St Helena subtropical high and is most common during the austral summer when it reaches its mature phase. The SASD is typically detected by the leading mode of either EOF analysis or Singular Value Decomposition (SVD). The SASD index is often calculated as the difference between southwestern and north-eastern sea surface temperatures (see Fig 1.15).

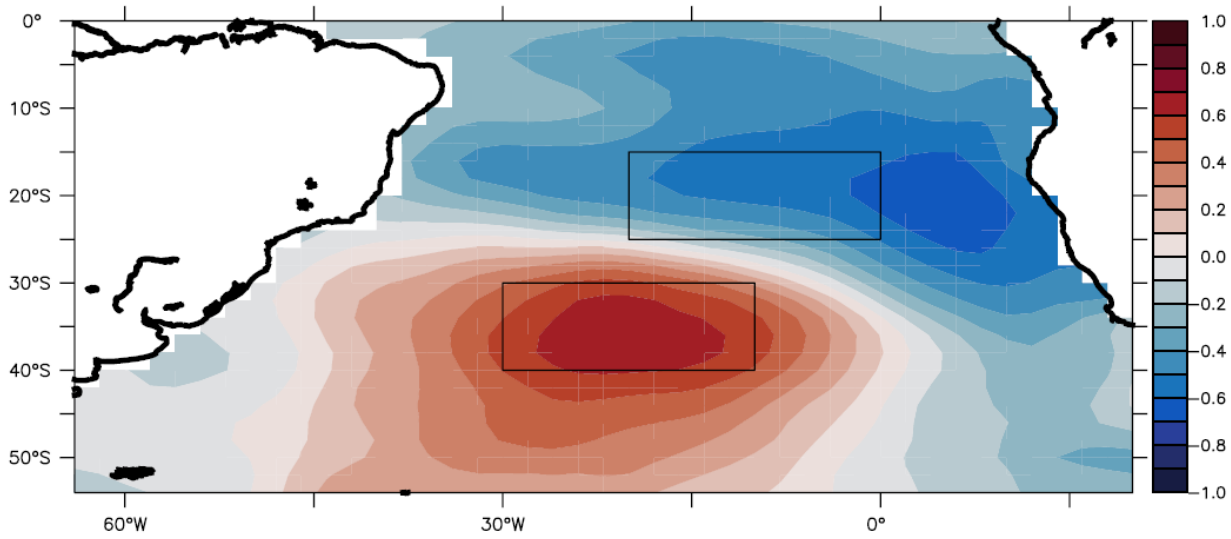

Fig 1. 15: Spatial structure of the SASD mode. The boxes indicate the areas of NE and SW SASD poles (Source: Wainer et al., 2020)

1.6.6 Benguela Niño

Benguela Niño is an El Niño-like phenomenon in the Atlantic Ocean (Shannon et al., 1986; Florenchie et al., 2003). It is distinguished by the anomalous warming of sea surface temperatures off the coasts of Angola and Namibia (Grimm and Reason, 2010). Unlike El Niño in the Pacific Ocean, Benguela Niño is a sporadic event in the Atlantic Ocean caused by the propagation of warm equatorial water towards Africa's west coast (Rouault et al., 2003) (Fig 1.16). The influx of warm waters disrupts the Benguela current, hence coastal upwelling, and results in a loss of fisheries due to insufficient nutrient availability in the ocean (Florenchie et al., 2003; Rouault et al., 2007). The Benguela Niño usually occurs during the austral summer, peaking around January-February-March (Grimm and Reason, 2010). However, an unusually cold event can sometimes occur over the same region, and it is commonly referred to as Benguela Niña (Florenchie et al., 2004; Reason et al., 2006).

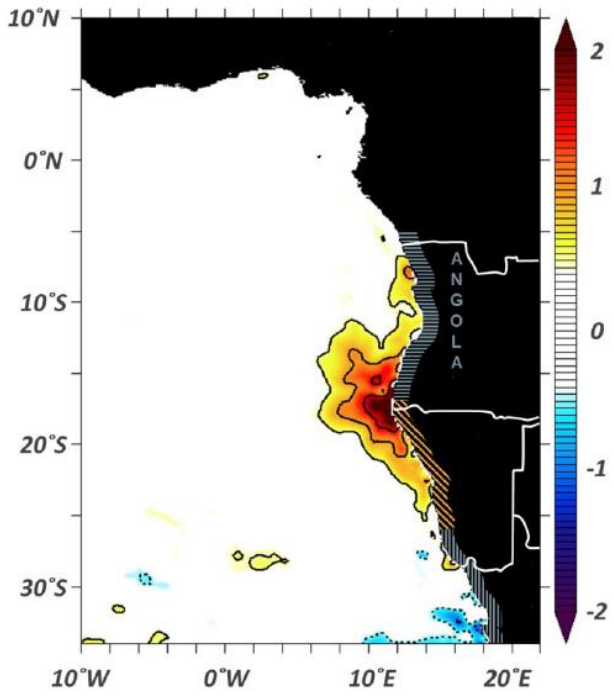

Fig 1. 16: Map of interannual Sea Surface Temperature averaged during the peak phase of the 2001 Benguela Niño event (Source: Bachèlery et al., 2020)

1.7 Southern African Droughts

1.7.1 Definition of Drought

There are different definitions of drought, but most agree that drought is a lack of precipitation in a particular region over an extended period (Meque, 2015). Drought is a brief period of dryness that can occur in various climate zones, as opposed to aridity, which is a permanent condition of dryness (Chikoore, 2016). Droughts are a common occurrence in Southern Africa, with Zimbabwe, Mozambique, and Tanzania being the most drought-prone countries in the region (Meque, 2015). For the period 1979-2012, seven drought events (extreme droughts of 1982 and 1992, severe droughts of 1983 and 1985, and moderate droughts of 1984, 1987 and 2003) impacted the SADC region (Chikoore, 2016). Furthermore, these extreme droughts of 1982 and 1992 occurred in the austral rainy seasons and threatened the rural population's livelihoods, who rely on rain-fed agriculture for income (Meque, 2015) (see Fig 1.17). Given this, identifying drought susceptible areas and probabilities of drought frequencies is essential for implementing programmes aiming to increase food security and better interpret the potential impacts of climate change in Southern Africa (Rojas et al., 2011).

Fig 1. 17: A man who might be facing hunger in Southern Africa because of a severe drought that has been exacerbated by the 2015/2016 El Niño. (Source: Muvuyani, 2016)

1.7.2 Drought Classification

Drought is generally classified into four main categories, which are: meteorological drought, agricultural drought, hydrological drought, and socio-economic drought. The last three types of droughts are caused by extended meteorological droughts and are defined according to their societal impacts (Lake, 2011). Droughts typically begin with a lack of precipitation accompanied by high temperatures, strong winds, and less cloud cover, as seen in Figure 1.18. If these conditions persist, it may result in agricultural drought followed by hydrological drought and eventually socio-economic drought.

- Meteorological drought is characterised by a lack of precipitation for long periods such as a season or year (Lake, 2011). In addition to that, meteorological drought is specific to different regions depending on the area's yearly average precipitation. For example, a reduction of 100 mm of precipitation over the semi-arid regions of Namibia would potentially put the region at risk of drought but would not have the same effect as in Mozambique's tropical regions.

- Agricultural Drought occurs when there is a deficiency in the soil moisture to sustain the growth of crops and forage, resulting in crop failure and a decrease in agricultural productivity. This type of drought also impacts livestock production due to a reduction in grazing. Therefore, the combined reduction in crops and livestock further impacts famine, malnutrition, epidemics, and displacement of people from one area to another (Rojas et al., 2011).

- Hydrological drought occurs when there is a significant decrease in surface or subsurface water supply, such as reservoirs, lakes, and groundwater (Heim, 2002; Meque, 2015; Chikoore, 2016). This type of drought is typically out of phase with the occurrence of meteorological or agricultural droughts (Heim, 2002). It typically takes longer for precipitation deficiencies to show up in the components of the hydrological systems, such as reservoir and groundwater levels, and as a result, the impacts are out of phase with other economic sectors. For example, low rainfall may decrease soil moisture, which will almost immediately impact the agriculture sector, but the impact on reservoir levels may not impact the hydropower sector for many months.

- Socio-Economic drought occurs when the demand for economic goods, which depend on water or rainfall (e.g. water, forage, food grains, fish, and hydroelectric power), exceeds supply due to weather-related water deficit (Heim, 2002). Because of climate variability, the water supply may be abundant in some years but unable to meet human and environmental needs in other years. In most cases, the demand for economic goods increases due to increasing population and per capita consumption.

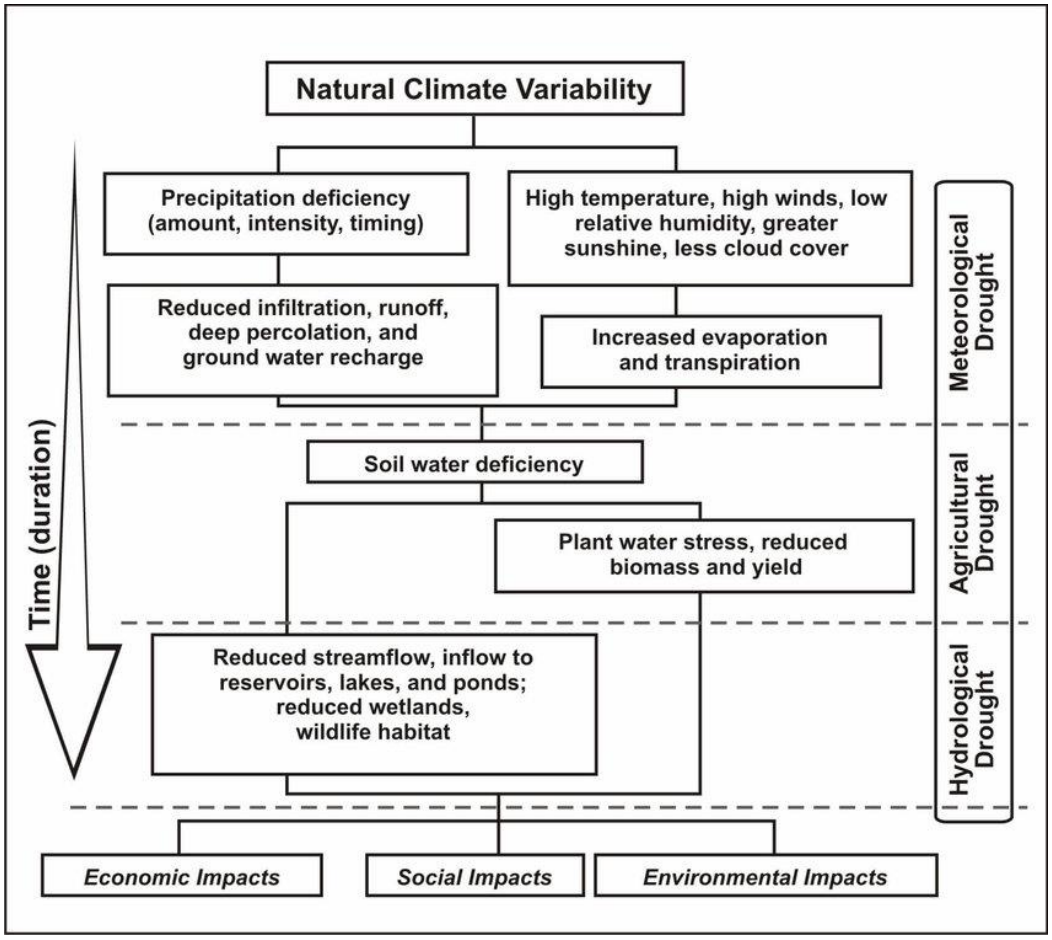

Fig 1. 18: Drought types and their associated impacts (Source: Wardlow et al., 2012)

1.8 Climate Modelling

Climate Models are tools for investigating climate variability and change (Rummukainen, 2010). Climate models are based on well-documented physical processes to simulate energy and materials transfer through the climate system. They use mathematical equations to characterise how energy and matter interact in different parts of the atmosphere, ocean, and land. Developing and running a climate model is a complex process of identifying and quantifying the earth's system processes, representing them with mathematical equations, setting the appropriate variables to represent the initial conditions and subsequent changes in the climate forcing, and repeatedly solving the equations using powerful computers. To reduce computational costs, climate models divide the earth's atmosphere into three-dimensional grid boxes, and each grid point represents the average condition of the atmosphere at a specific location (Dahan, 2010) (see Fig 1.19). The grid size defines the models' spatial resolution, and therefore the smaller the grid size, the higher the model's resolution and the higher computing power needed. In general, increasing the spatial resolution of a model by a factor of two will require ~10 times the computing power to run the model in the same amount of time. For processes that happen on scales higher than the grid cell, such as convection, the model uses approximations that simplify each process, called parameterisation (Crétat et al., 2011), and allows them to be included in the model. Climate models also include an element of time called a time step. The time step can be in seconds, minutes, hours, days or years, and like grid cells, the smaller the time step, the more detailed the results will be. However, this comes at an additional cost of computing power.

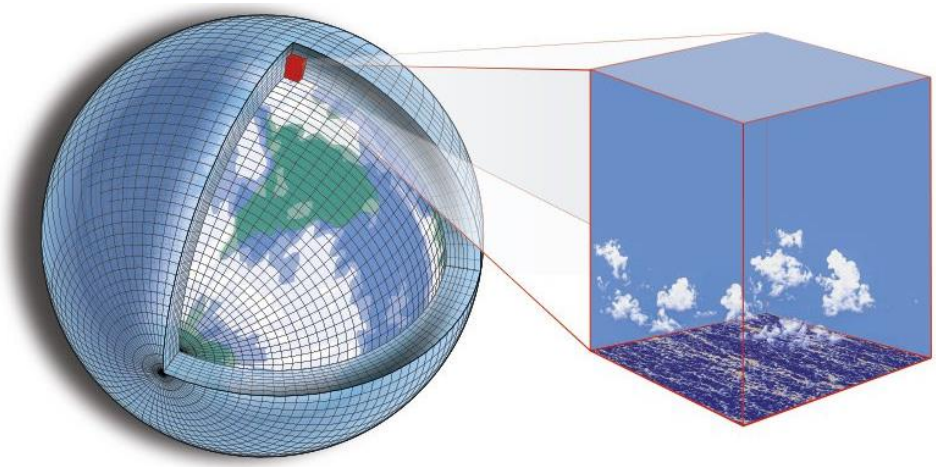

Fig 1. 19: Climate model grid (Source: Perkins, 2018)

There is a broad spectrum of climate models, and at the far end, in terms of complexity, are Global Climate Models (GCMs). GCMs can effectively provide information on large-scale climate features that include the general circulation of the atmosphere, ocean, and land (Rummukainen, 2010). Although GCMs can run at a very high resolution (e.g. 20km as in Mizuta et al., 2006), they are usually employed at lower resolution (~100 km) due to the higher computational costs required at higher spatial resolutions (Rummukainen, 2010), which is not ideal for the developing nations of SADC due to financial and resource constraints. To overcome the computational cost limitations, Regional Climate Models (RCMs) were developed to run at very high resolution with the added advantage of them being more computationally economical than high-resolution GCMs (Rummukainen, 2010). As the name implies, RCMs do not simulate the entire globe but only a portion thereof (see Fig 1.20). Because RCMs cover a smaller area, they can have higher resolution for the same number of grid points as a GCM. This allows for a better representation of small-scale processes such as convection, orography, and coastal areas. On the negative side, RCMs, because they do not span the entire globe, must rely on GCM output in the intermediary region close to the model domain's lateral boundaries to simulate climates for their model domain's interior. Because of the lateral boundary forcing, the large-scale circulations simulated by RCMs do not differ much from the GCMs forcing, especially in the middle and upper troposphere (Giorgi and Mearns, 1999).

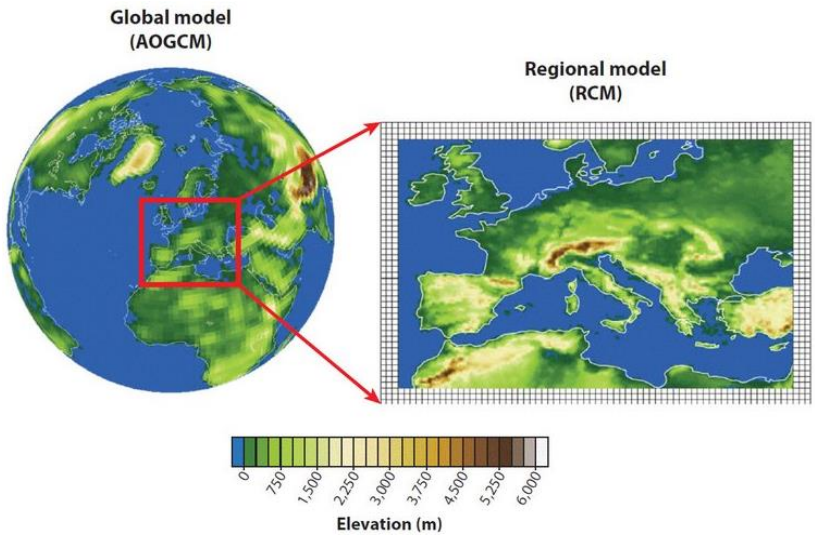

Fig 1. 20: RCM domain embedded in GCM grid (Source Giorgi and Gutowski, 2015)

In recent times, there has been a growing interest in using Variable-Resolution Global Climate Models (VRGCMs) for simulating regional climate over Southern Africa (Engelbretch et al., 2008; Engelbretch et al., 2012; Maoyi et al., 2017; Driver et al., 2018). Unlike uniform-resolution GCMs, VRGCMs are more computationally economical as they use a relatively coarse grid globally with enhanced resolution over a specific region (see Fig 1.21). Furthermore, compared to RCMs, VRGCMs are not dependent on lateral boundary forcing as they use a unified modelling framework rather than two separate models (GCM and RCM) and are free from the associated computational lateral boundary limitations (Fox-Rabinovitz et al., 2008), such as inconsistencies between global and regional scales and a lack of two-way interactions at the nested boundary. As a result, VRGCMs can be used for straightforward simulations as uniform-resolution GCMs and provide self-encompassing interactions between global and regional scales of motion as in traditional GCMs. Considering this, how well a VRGCM can simulate the interannual and seasonal climate of Southern Africa is a significant focus of this thesis.

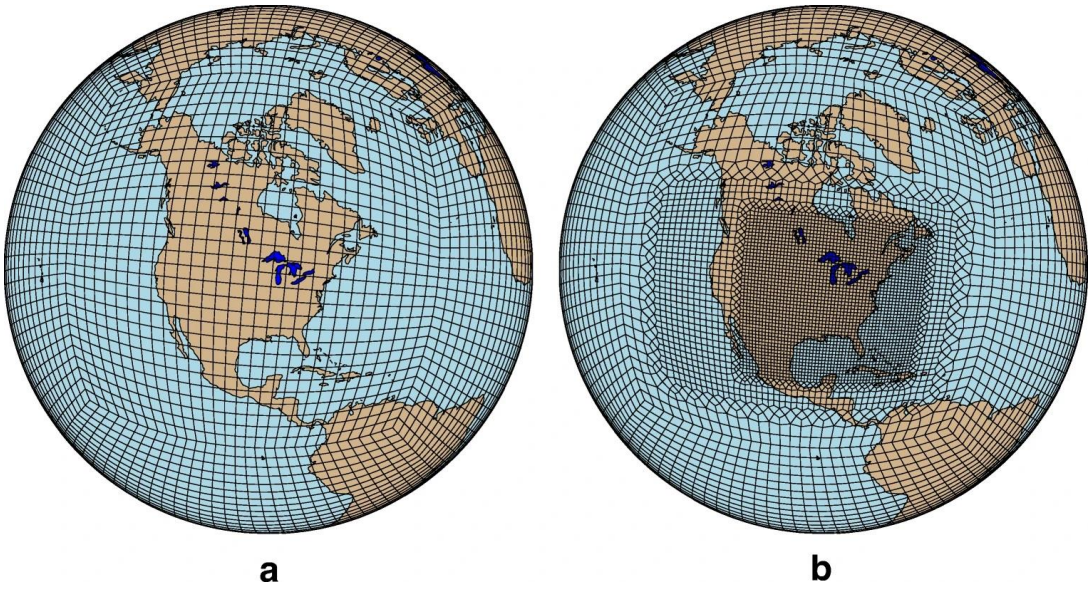

Fig 1. 21: Community Earth System Model (CESM) grids used in simulations: a uniform 1° grid and b variable-resolution CESM (VR-CESM) grid consisting of a 1° global grid with 0.25° refinement over North America (Source: Burakowski et al., 2019)

1.9 Empirical Orthogonal Functions

Empirical Orthogonal Function (EOF) analysis, one of the most commonly employed statistical techniques in climate science, is used to study spatial modes (i.e., patterns) of variability and how they change with time (Jolliffe, 2002; Wilks, 2011). In statistics, EOF analysis is referred to as Principal Component Analysis (PCA). However, unlike PCAs, the EOF method calculates both the time series and spatial patterns (Zhou, 2021). Furthermore, EOF analysis is not based on physical properties; instead, a field is partitioned into mathematically orthogonal (i.e., non-correlated or independent) modes, which may be interpreted as atmospheric and oceanographic modes. The first mode accounts for the largest variance in the dataset, the second mode accounts for the second largest variance and so on. The major shortcoming of EOF analysis is that physical systems are not necessarily orthogonal, and if the patterns depend on the region used, they may not exist if the domain changes. Still, even with these shortcomings, EOF analysis has proved to be helpful.

1.10 Motivation for the study

Previous research has shown that the Botswana High has a significant impact on summer rainfall variability over Southern Africa (Matarira, 1990; Unganai and Mason, 2002; Driver, 2014; Driver and Reason, 2017), with a stronger Botswana High typically associated with below-average rainfall. In addition to rainfall, Driver and Reason (2017) concluded that the Botswana High influences other important parameters affecting rain-fed agriculture in Southern Africa. These parameters include the frequency of dry spells during the austral summer, the maximum surface air temperature, and the number of days with maximum temperature extremes, which can lead to drought. However, the direct influence of the Botswana High on Southern African droughts has yet to be studied. Given the devastating effects of droughts on Southern African socio-economic activities, which rely primarily on rain-fed agriculture, it is critical to understand how the variability of the Botswana High influences the characteristics of Southern African droughts on a regional scale.

Past studies on summer droughts over Southern Africa have focused on characteristics of general drought patterns (Rouault and Richard, 2005; Meadows, 2006; Shongwe et al., 2009) with less emphasis on characteristics of drought modes (Ujeneza and Abiodun, 2014), which can reveal the drought dynamics and improve seasonal drought predictions. For instance, Rouault and Richard (2005) studied the spatial extent of droughts in Southern Africa between 1901 and 1999 and found that drought often occurs in Southern Africa in all climatic areas at all times of the year with different intensity spatial extent and duration. The only known study on drought modes over Southern Africa (Ujeneza and Abiodun, 2014) revealed the spatio-temporal characteristics of four drought modes or principal factors (hereafter PF1, PF2, PF3 and PF4) that accounted for about 50% of drought variability in Southern Africa and showed the influence of various atmospheric teleconnections. However, the study did not investigate the influence of Botswana High (a dominant mode of 500 hPa geopotential variability in summer over Southern Africa) on the drought modes. Therefore, understanding the link between Botswana High and drought modes is important for several reasons. For instance, the El Niño Southern Oscillation (ENSO) has a strong influence on the first two drought modes (PF1 and PF2) over Southern Africa during summer (Ujeneza and Abiodun, 2014) and is strongly correlated with the Botswana High (Reason, 2016; Driver and Reason, 2017). This strong association between ENSO and the Botswana High begs the question as to whether the Botswana High is a conduit pipe through which ENSO signals influence the droughts modes.

Furthermore, given that the relationship between ENSO and the Botswana High is not strictly linear (Driver and Reason, 2017), Ujeneza and Abiodun (2014) demonstrated that the influence of ENSO on drought over the PF3 and PF4 regions is weak, raising the question of whether or not the Botswana High influences PF3 and PF4 droughts. Hence, the present study extends the work of Ujeneza and Abiodun (2002) by investigating the link between Botswana High and drought modes in Southern Africa.

Over the years, several studies have been conducted to better understand the variability of the Botswana High, with some identifying ENSO as a major source of variability (Driver and Reason, 2017; Reason, 2018; Maoyi and Abiodun, 2021). However, the direct influence of ENSO on the high's variability remains unknown. Generally speaking, the Botswana High tends to intensify during El Niño summers over Southern Africa and weaken during La Niña events; however, the magnitudes of the Botswana High anomalies are not always proportional to the strength of ENSO events (Driver and Reason, 2017). For instance, Driver and Reason (2017) demonstrated that the anomaly in the high during the intense 1997/1998 El Niño event was less than the weaker 1986/1987 El Niño. Furthermore, summers over Southern Africa have also been unusually wet or dry but did not coincide with an ENSO event yet did correspond to significant anomalies in the Botswana High. As a result, a better understanding of the Botswana Highs variability may provide useful information and another metric for monitoring and evaluating rainfall over the subcontinent. Despite this, previous studies have used correlation and composite analyses to determine the relationship between ENSO and the Botswana High, which cannot determine cause-and-effect relationships. As a result, it is unclear whether the Botswana Highs variability is a response to ENSO. That is the motivation for this study.

1.11 Aim and objectives

This study aims to examine the capability of a GCM with variable-resolution (i.e., Model for Predictions Across Scale, MPAS) in understanding the characteristics of the Botswana High. To achieve this aim, the following objectives are addressed:

- Explore how well a Variable-Resolution GCM (MPAS) simulates the characteristics of the Botswana High.

- Identify the different drought modes over Southern Africa and their relationship with the Botswana High in observation, reanalysis and MPAS.

- To investigate the relationship between the Botswana High and El Niño Southern Oscillation using the MPAS model.

1.12 Thesis Outline

This thesis is divided into seven chapters, including this one (**Chapter 1**), which introduces the Botswana High, drought and the main factors that influence weather and climate over Southern Africa. The chapter also motivates why studying the impact of the Botswana High and drought is important in this region.

Chapter 2 reviews the literature on the formation of subtropical highs and the controversies surrounding the subject. A review of the impact of subtropical highs on droughts then follows. The chapter also discusses what other studies have found about the impact of ENSO on the Botswana High. A literature review on the simulation of drought and subtropical highs in GCMs is also presented. Finally, this chapter discusses various efforts by previous studies in identifying subtropical highs.

Chapter 3 describes the datasets and methods used to achieve the objectives of the study. MPAS, a fully compressible nonhydrostatic global climate model with variable-resolution capabilities, is presented. The chapter also describes how the Botswana High feature is identified.

Chapter 4 reports the results of MPAS in simulating the characteristics of the Botswana High and the influence of the high on Southern African droughts during the 1980-2010 study period. It also investigates whether the MPAS model, when compared to reanalysis, simulates the same spatial and temporal variability of the Botswana High. Furthermore, the chapter investigates whether and to what extent SSTs influence the Botswana High. Finally, the chapter discusses the Botswana High's influence on climate variables and drought in Southern Africa.

Chapter 5 discusses the characteristics of Southern African drought modes and their relationship to the Botswana High. Additionally, the chapter also compares how well MPAS simulates drought modes to observation. The Botswana High's influence on drought modes is also discussed, followed by a discussion of the atmospheric conditions associated with negative(-ve) and positive(+ve) drought modes.

Chapter 6 presents the results of a series of sensitivity experiments to understand the response of the Botswana High to the 1982/1983, 1991/1992, 1997/1998 and 2009/2010 El Niños and

1984/1985, 1988/1989, 1999/2000 and 2007/2008 La Niñas. Atmospheric dynamics associated with El Niños and La Niñas years are also presented.

Chapter 7 outlines and summarises the findings of this thesis. The chapter also points out the shortcomings of this study and provides suggestions to improve the work.

CHAPTER TWO: LITERATURE REVIEW

This chapter reviews the relevant literature pertaining to the study of the Botswana High and identifies gaps in the literature. It starts by reviewing past studies on the formation of subtropical highs (Section 2.1) and the impact of subtropical highs on drought (Section 2.2). Next, it discusses the literature on the impacts of ENSO on the Botswana High (Section 2.3), followed by section 2.4, which reviews the literature on simulating subtropical highs using Global Climate Models. Lastly, section 2.5 discusses the literature on identifying the spatial and temporal characteristics of subtropical highs in gridded datasets.

2.1 Formation of Subtropical Highs

The factors underlying the formation and persistence of subtropical highs are still being debated. Several studies have linked the formation of the subtropical highs to the subsidence in the descending limb of the Hadley Cell (Held and Hou, 1980; Choi and Kim, 2019; Fahad et al., 2020). According to these studies, the Hadley Cell is characterized by warm air rising near the equator, followed by cooling and poleward motion of the air in the higher troposphere. As the air advances poleward, the air cools and converges towards the 30° latitudes. This cold air mass convergence adds weight to local air columns near the subtropics, raising surface pressure and forming the subtropical high belt (Nguyen et al., 2015). However, Hoskins (1996) and Rodwell and Hoskins (2001) argued that the theory of zonally symmetric Hadley circulation theory predicts significantly weaker subtropical highs in the boreal and austral summer (Lindzen and Hou, 1988), which is unfavourable for maintaining strong summers subtropical highs. Furthermore, the Hadley Cell weakens throughout the austral summer, and there may be a weak or non-existent descent; so, the Hadley Circulation explanation does not appear to explain the occurrence of subtropical highs during the summer. Moreover, Miyasaka and Nakamura (2005) contended that observed summertime subtropical highs take the form of high-pressure cells rather than a zonally uniform high-pressure belt, implying that the dynamics of the highs may be better understood in the context of planetary waves rather than in the context of zonally symmetric circulation.

Over the last few years, the formation of the subtropical highs has also been linked to the impacts of monsoonal heating (Rodwell and Hoskins, 1996; Liu et al., 2001; Rodwell and Hoskins, 2001). For example, using a hydrostatic primitive equation global model, Rodwell

and Hoskins (1996) demonstrated that a portion of the summertime descent over the eastern Mediterranean and Sahara could be induced by forcing the atmospheric model with Asian monsoon heating. Furthermore, the authors hypothesised that the existence of other monsoon-climate regions around the world could explain the summertime strengthening of ocean-based subtropical highs and western continental deserts via the so-called monsoon-desert mechanism in a similar way (Rodwell and Hoskins, 1996). Rodwell and Hoskins (2001) later concluded that the summertime North Pacific subtropical anticyclone easterlies are primarily a planetary wave "response" to Asian monsoon heating, and the South Atlantic subtropical anticyclone is primarily a planetary wave "response" to South American monsoon heating. Furthermore, Rodwell and Hoskins (2001) showed that the combined effects of topography and monsoonal heating to the east are of primary importance for the generation of a surface subtropical anticyclone and subsidence aloft (e.g. the Indian, Mexican, and South American monsoons for subtropical anticyclones in the North Atlantic, North Pacific, and South Pacific, respectively), with the reinforcement by local cooling over the eastern oceans. However, Rodwell and Hoskins (2001) argued that the summer anticyclones forced by monsoonal heating are weak compared to observation. Given that, to bring the simulated subtropical highs up to observed strength, Rodwell and Hoskins (2001) appeal to “diabatic amplification”. On the other hand, Wu and Liu (2003) proposed that the combined impacts of sensible surface heating observed over the parched western regions of subtropical continents and lower-tropospheric radiative cooling along their west coastlines may play a role in the formation of subtropical anticyclones.

The summertime existence of subtropical highs has been attributed to air-sea interactions (Seager et al., 2003; Miyasaka and Nakamura, 2010). Using an Atmospheric General Circulation Model (AGCM) coupled with an ocean mixed layer model, Seager et al. (2003) demonstrated that monsoonal deep convective heating alone could not produce realistically intense subtropical highs. The authors suggested that air-sea interactions are critical in the intensification of subtropical highs. Based on their observations, once the subtropical highs have been forced by heating over land, the subsidence of dry air over the eastern subtropical oceans lowers SST, while poleward lower-tropospheric advection over the western subtropical oceans raises SSTs. As a result, the atmosphere is stabilised to deep convection in the east but becomes unstable in the west. According to Seager et al. (2003), this permits deep convection to move from land areas to surrounding areas of the subtropical oceans, enhancing air circulation forcing and strengthening subtropical highs. Miyasaka and Nakamura (2010) used a global primitive equation model to investigate the atmospheric response to low-level heating-

cooling in each ocean basin. The authors demonstrated that the formation of subtropical highs primarily results from the thermal effect of relatively low SSTs over the eastern ocean, with radiative cooling from marine stratus and heating from a sensible heating flux over a dry, heating landmass to the east. Furthermore, the study found that the strong radiative cooling associated with the marine stratus and stratocumulus could force the subtropical anticyclone. As a result, the cooling is maintained in the high, implying a local feedback loop in the atmosphere-ocean–land system in the summer subtropics.

2.2 Impact of Subtropical Highs on drought

2.2.1 North Pacific and North Atlantic High

Several studies have shown that Northern Hemisphere subtropical highs play a significant role in regional drought by affecting moisture transport between the mid-latitude and tropical regions (Chang et al., 2000; Lu, 2001; Zhou, 2005; Gamble et al., 2008; Li et al., 2011; Lee et al., 2013; Schmidt and Grise, 2019). In the North Pacific, the North Pacific High Subtropical High (NPSH) has been a significant component of the East Asian Monsoon (EAM) and has been shown to significantly influence East Asia's rainfall (Chang et al., 2000; Lu, 2001; Lee et al., 2013). Chang et al. (2000) showed that a stronger and westward extending NPSH blocks pre-Meiyu and Meiyu fronts from moving southward, causing droughts in southeast China during spring and early summer. In agreement with Chang et al. (2000), Lu (2001) asserted that the NPSH's position, shape, and strength dominate the large-scale quasi-stationary frontal zones across East Asia. Lee et al. (2013) showed that rainfall over the EAM region and Indian Ocean Monsoon (IOM) region had a significant correlation with the development of the NPSH. The high positive correlation between the NPSH and EAM rainfall implies that they mainly fluctuate in phase; however, since the correlation between the NPSH and IOM is much smaller than between NPSH and EAM, NPSH and IOM precipitation may fluctuate in-phase and sometimes out of phase. Schmidt and Grise (2019) examined how the variability in the location (i.e., longitude and latitude) and strength of the NPSH affect variability in precipitation over North America. The study showed that the northward movement of the NPSH reduced rainfall over the Gulf of Alaska and increased precipitation in the northern region of Hawaii. Zhou (2005) studied water vapour transport anomalies associated with typical anomalous summer rainfall patterns in China and found that the anomalous water vapour transports are determined by the western Pacific's position subtropical high as it dominates the water vapour transports for the typical anomalous rainfall patterns. This is consistent with an earlier study by Lu (2001),

who stated that the low-level circulation at the north-western edge of the NPSH transports large amounts of water vapour into East Asia.

A number of studies have shown that the North Atlantic Subtropical High (NASH), commonly referred to as the 'Azores' or the 'Bermuda High', has a significant influence on weather and climate over the eastern parts of the United States, western Europe and north-western Africa (Davis et al., 1997; Gamble et al., 2008; Li et al., 2011). Davis et al. (1997) developed the climatology of the NASH by examining its spatial and temporal changes from 1899 to 1990. The authors found that the blocking from the high has become less prevalent over the Atlantic, south-eastern United States and the British Isles but has increased over west-central Europe. These results are consistent with an earlier study by Stahle and Cleaveland (1992), who identified a trend of increasing spring rainfall over the south-eastern United States between 1887 and 1982 that was associated with the lack of ridging of the NASH off the coast. Gamble et al. (2008) studied the variability of the Caribbean mid-summer drought (MSD). They found out that the NASH was one of the dominant controls of MSD occurrence; however, compared to previous studies by Knaff (1997) and Gianini et al. (2000), the impact of the NASH is not spatially consistent and is manifested as different atmospheric processes at different times relative to MSD occurrence. Li et al. (2011) investigated the NASH's changes and impact on summer precipitation over the south-eastern United States. The authors found that the interannual variation of south-eastern United States summer rainfall decreases when the ridge moves north as the weather pattern is dominated by subsidence. Likewise, when the NASH moves southward, rainfall increases over the south-eastern United States, making way for winds along the NASH's western edge to transport warm and moist air from the Gulf of Mexico, which agrees with a more recent study by Schmidt and Grise (2019). Furthermore, Schmidt and Grise (2019) found that the northward shift of the NASH is associated with increased subsidence and drying over western Europe and the reverse in Greenland's vicinity.

2.2.2 South Pacific, South Atlantic and South Indian Highs

The Southern Hemisphere supports three subtropical highs over its subtropical ocean basins, namely the South Pacific High (SPH), South Atlantic High (SAH) and the South Indian High (SIH) (Miyasaka and Nakamura, 2010). Although they are well-known features, not much work has been done on these anticyclones and their direct impacts on drought. Over the South Pacific, an early study by Fuenzalida (1982) showed that the annual rainfall cycle (wet in winter and dry in summer) over central and southern Chile is sensitive to the seasonal migration (28°S

in winter and 35°S in summer) of the SPH. A more recent study by Barrett and Hameed (2017) showed that annual rainfall over central and southern Chile is negatively correlated to the intensity and longitude of SPH and positively correlated to the latitude of SPH. However, the negative correlations to SPH intensity were only seen in winter, spring, and autumn, and the negative correlations to SPH longitude were only seen in winter and autumn. Furthermore, the positive correlation to latitude was seen over land only in spring, summer, and autumn and largely absent in winter.

Over the Atlantic, Vigaud et al. (2008) studied the moisture exchange between the South Atlantic and Southern Africa through zonal moisture transport during summer. The authors found that the northward shift of the SAH and weakening of the Intertropical Convergence Zone (ITCZ) inhibited convection and resulted in below-average rainfall over subtropical Southern Africa, which might lead to drought. Using the Coupled Model Intercomparison Project Phase 5 (CMIP5) models, Mahlalela et al. (2018) attributed the dry winters over the southwestern tip of Southern Africa (i.e. Western Cape) to the poleward movement of the SAH, which may push fronts southward of the Southern African region leading to lesser rainfall. Similarly, Burls et al. (2019) studied the 2015-2017 Cape Town "Day Zero" drought and showed that the northward expansion of the Hadley Cell led to an increase in the SAH subsidence, which in turn led to the decrease in the number of rainfall days associated with the passage of frontal systems near the Western Cape. In South America, Reboita (2019) stated that the South Atlantic Subtropical High (SASH) seasonally contributes to drier conditions in winter and wetter conditions in summer over the south-eastern regions of Brazil. In winter, the SAH is more zonally expanded so that its western sector lies over south-eastern Brazil. This westward expansion of the anticyclone may hinder convective activity and precipitation over south-eastern Brazil (Reboita, 2019). On the other hand, in summer, the SAH is less expanded and located away from the Brazilian coast and contributes to the humidity transport from the Atlantic Ocean to the South America continent and favours precipitation in south-eastern Brazil (Reboita et al., 2010, 2015, 2017). However, in the summer of 2014, Coelho et al. (2015) showed that the SAH had an anomalous westward position which led to an intense drought in south-eastern Brazil.

Over the South Indian Ocean, the SIH or Mascarene High plays a significant role in the weather and climate of Southern Africa and Australia (Xulu et al., 2020). Using observational and reanalysis data, Manatsa et al. (2013) studied the variability of East Africa ‘short rains’ and

their link with the SIH and found that droughts in the eastern parts of Southern Africa are associated with the westward migration of the SIH eastern ridge. Similarly, Nkurunziza et al. (2019) found that a westward shift in the SIH resulted in October to December (OND) rainfall deficits over the East Africa region. Ogwang et al. (2015) found that the intensification and southeast-northwest orientation of the SIH inhibits the influx of moisture from the Indian Ocean into East Africa. Hameed et al. (2011) studied the relationship between the SIH as the immediate cause of drought over Western Australia and found that the east-west shifts in the position of the subtropical high significantly influences winter rainfall in western Australia. More specifically, when the SIH shifts to the east, rainfall in west Australia and southwestern Australia decreases and vice versa. In addition, rainfall over southwestern Australia is significantly and negatively correlated with the area-averaged pressure of the SIH. Xue and Wang (2004) analysed the interannual variability of the SIH and its influence on the East Asia Monsoon. The authors found that when the SIH intensified in March to May (MAM), the Meiyu / Baiu rainfall from the Yangtze River to south Japan tended to increase, while rainfall near the western tropical Pacific and mid-latitudes of East Asia near northern Japan tended to be less.

2.2.3 The Bilybara, Bolivian and Botswana High

Although the Bilybara, Bolivian and Botswana High are prominent climatic features at mid-levels (i.e., 500 hPa) during the austral summer (Reason, 2016), not much work has been done on the impacts of these mid-level subtropical highs. The first known study of the Bilybara High by Reason (2016) showed that the eastern two-thirds of Australia is drier than average when the Bilybara High is strong with enhanced subsidence over land. Later, Reason (2017) showed that variations in the strength and position of the Bilybara High are related to anomalies in the rainfall and temperature over tropical Australia and some areas in southern Australia. When the Bilybara High is shifted to its northwest and is stronger than average, weaker monsoonal north westerlies occur over the Timor Sea and the northern parts of Australia with decreased mid-level uplift leading to a deficit in rainfall. Simultaneously, there are reduced easterlies over the Tasman Sea, leading to drier conditions over south-eastern Australia. Furthermore, Reason (2017) asserted that such drier conditions are compounded by increased maximum temperatures and the occurrence of more days with temperatures exceeding the 90th percentile over Australia.

Numerous studies have noted a relationship between the seasonal variation in South American rainfall and the Bolivian High's position and intensity (Kousky and Kagano, 1981; Nishizawa and Tanaka, 1983; Horel et al., 1989; Reason, 2016). Kousky and Kagano (1981) examined the climatology of the tropospheric circulation for the period 1968 - 1976 over the Amazon region. The authors found that a decrease in rainfall over the Amazon River basin as a result of the north-westward shift of the main convective activity towards the Bolivian High. Horel et al. (1989) hypothesized that this north-westward shift of convective activity contributed to the formation of the Bolivian High. On the other hand, Nishizawa and Tanaka (1983) found that the position of the south-easterly return flow of the Bolivian High and the moist northwest flow of the Nordeste low (Lenters and Cook, 1997) contributed to the heavy rainfall in the Amazon River basin extending southeast towards Sao Paulo during austral summer. However, Reason (2016) pointed out that the impact of the Bolivian High on rainfall is complex due to the presence of the South Atlantic Convergence Zone (SACZ). The general conclusion offered by Reason (2016) is that the western and south-eastern regions of South America are drier when the Bolivian High is stronger; however, large areas of eastern Brazil are wet, which reflects a shift in the SACZ.

Several studies have documented the impact of the Botswana High on climate variables in Southern Africa (Matarira, 1990; Unganai and Mason, 2002; Reason, 2016; Driver and Reason, 2017; Reason, 2018), but there is a dearth of information on the impacts of the Botswana High on droughts over the region. Matarira (1990) and Unganai and Mason (2002) examined the relationship between the Botswana High and rainfall over Zimbabwe and showed that a strong Botswana High was behind the major droughts of 1982–1984 and 1991–1992. However, these studies used only rainfall to characterise drought (which depends on rainfall and potential evapotranspiration; Abiodun et al., 2018), and their focus was on Zimbabwe. Reason (2016) analysed the interannual variability of the Botswana High and droughts/floods over Southern Africa and found that the large areas over Southern Africa become drier than average when the Botswana High is strong. Similarly, Driver and Reason (2017) showed that the Botswana High variability impacts the frequency of dry spells during summer, the maximum surface air temperature, the daily surface air temperature range and days of maximum temperature extremes. Recently, Reason (2018) investigated the decadal variability in the Botswana High and showed that the high is associated with significant changes in regional rainfall and surface temperatures as well as changes in the onshore flow of moist marine and uplift over many parts of Southern Africa, all of which are strongly related to drought. However, the direct influence

of the Botswana High on droughts remains unstudied. Given the devastating impacts of droughts on socio-economic activities in Southern Africa (which mainly depend on rain-fed agriculture), it is essential to know how the variability of the Botswana High influences Southern African droughts at a regional scale. The present study will improve knowledge of the impacts of Botswana High on droughts.

2.3 Impacts of ENSO on the Botswana High

Several studies have been conducted to understand the summer variability of the Botswana High, some of which have identified the El Niño Southern Oscillation (ENSO) to be one major cause of the variability (Driver and Reason, 2017; Reason, 2018). In general, the high tends to intensify during El Niño associated summers over Southern Africa and weaken during La Niña events; however, the magnitudes of the Botswana High anomalies are not necessarily proportional to the strength of ENSO events. For example, Driver and Reason (2017) showed that the anomaly in the high during the intense 1997/1998 El Niño event was less than the weaker 1986/1987 El Niño event. Furthermore, summers over Southern Africa have also been unusually wet or dry but did not coincide with an ENSO event but did correspond to significant anomalies in the Botswana High. Therefore, in some instances, the variability of the Botswana High is still high during some neutral phases of ENSO. A study by Driver and Reason (2017) showed that the summer rainfall over Southern Africa correlates better with the Botswana High index than with the ENSO index. This suggests that the Botswana High may be useful in predicting Southern African rainfall, especially during neutral ENSO years. Given that, a better understanding of the Botswana High variability may provide useful information and another metric for monitoring and evaluating rainfall over the subcontinent. Despite that, we should note that previous studies have used analyses such as correlation and composite analyses in determining the relationship between ENSO and the Botswana High, which cannot determine cause-and-effect relationships. Therefore, it still remains unknown if the Botswana Highs variability is a response to ENSO. Therefore, this study presents the first known Global Climate Model (GCM) sensitivity experiment to demonstrate the causal relationship between ENSO and the Botswana High.

2.4 Subtropical High Simulation in Global Climate Models

The application of Global Climate Models in simulating subtropical highs has been minimal; however, past studies have shown that GCMs can reasonably simulate the spatial structure and

temporal variability of subtropical highs (Paek et al., 2015; Dong et al., 2017; He et al., 2017). For example, Paek et al. (2015) showed that the Central Weather Bureau AGCM gives a realistic simulation of the summer Western Pacific Subtropical High (WNPSH) variability in the high-frequency band (2-3-year) but underestimates it in the low-frequency band (3-5-year). Analysing the simulations of 22 GCMs from the Coupled Model Intercomparison Project 5 (CMIP5), Dong et al. (2017) showed that most CMIP5 models capture the sub-seasonal variability of the WNPSH and reproduce the influence of the high on sea level pressure and 850 hPa wind fields. A similar result was obtained by He et al. (2017) on the ability of 30 CMIP5 models in simulating subtropical anticyclones. However, despite the above, there is no study on the capability of GCMs in simulating the characteristics of the Botswana High. The present study intends to fill this gap by evaluating the capability of a GCM in simulating the Botswana High.

The MPAS model has been used in several sensitivity experiments (Skamarock et al., 2013; Zhao et al., 2016; Davis, 2016; Fowler et al., 2016; Judt, 2020). Skamarock et al. (2013) showed that the MPAS model could produce results similar to the state-of-the-art hydrostatic model at hydrostatic scales (dx > 10km) as well as nonhydrostatic structures (dx ~ few km) such as convective systems, similar to those produced by nonhydrostatic regional models. Zhao et al. (2016) used four different quasi-uniform resolution meshes (30, 60, 120 and 240 km) and a variable-resolution mesh (120-30km) in studying the impacts of resolution and physics (Community Atmosphere Model (CAM) version 4 vs CAM5) on the precipitation, clouds and large-scale circulation in an aqua-planet simulation. Using two configurations on MPAS, Davis (2016) compared a uniform 15 km mesh to a variable-resolution mesh (60km -15km) in simulating tropical cyclones in the eastern Pacific and found that the two configurations performed nearly identical to each other and performed comparably to the Global Forecasting System. Fowler et al. (2016) evaluated the performance of the Grell-Freitas parameterisation scheme using variable-resolution meshes, which varied between hydrostatic (50km) and nonhydrostatic (3km) scales and found that by increasing horizontal resolution, the subgrid-scale motions become increasingly resolved. Judt (2020) studied atmospheric predictability by using a set of twin experiments (Judt, 2018; Zhang et al., 2007) and found that tropics have longer predictability than mid-latitudes and polar regions. While the capability of MPAS to simulate different atmospheric features has been shown, no studies have shown how well MPAS reproduces the characteristics of the Botswana High. Hence, the present study examines how well the MPAS model simulates the Botswana High characteristics.

2.5 Identification of Subtropical Highs

A number of studies have used the EOF method in studying subtropical highs (Park et al., 2010; Wang et al., 2013; Xiang et al., 2013; Matsumuru and Horinouch, 2016; Reason, 2016; Reason, 2018). For example, Park et al. (2010) used EOF analysis to classify two spatial patterns of the WNPSH. The authors found that mode 1 of the WNPSH is associated with a Western North Pacific summer monsoon-related mode of rainfall variability and the SST warming in the equatorial eastern Pacific during the previous winter. This pattern of monsoon-ENSO connection is related to the principal mode after the mid-1990s. On the other hand, mode 2 of the WNPSH is associated with an ENSO-related mode, and equatorial SST warming shifted toward the dateline, which was the dominant mode before the mid-1990s. Xian et al. (2013) performed an EOF Analysis of June to August (JJA) 850 hPa geopotential height in the Asian-Australian monsoon domain (20°S–32.5°N, 30°E–180°E) that is similar to Wang et al. (2013). Xian et al. (2013) found that EOF-1 is highly correlated to the WNPSH index with r=0.86. Furthermore, EOF-1 was characterised by a southwest-northeast orientation over the Western North Pacific, which signifies an enhanced WNPSH (Wang et al., 2013). Matsumuru and Horinouchi (2016) conducted an EOF analysis for the period 1950-2005 using CMIP5 models. The authors showed that EOF-1 dominates the East Asian and Northwest Pacific summer climate, which is characteristic of the interannual variability of the Western Pacific Subtropical High (WPSH). In contrast, the simulated EOF-2 pattern captures the contrasting north-south SLP pattern of the WPSH and represents the decadal variability.

Previous studies have employed two approaches in identifying the spatial and temporal variability of the Botswana High to quantify its strength better. In the first approach, the Botswana High mode's spatial and temporal variability is identified by monitoring the 500 hPa geopotential height spatial averages and standardised anomalies in the so-called Botswana High core region (15^{o}-22^{o}E; 20^{o}-25^{o}S) as in Driver and Reason (2017). However, the deficiency of this method is that it cannot identify the Botswana High mode independently from the overall variability of the 500 hPa geopotential height. To overcome this deficiency, some Botswana High studies (i.e., Reason, 2016; Reason, 2018) have used EOF analysis to identify the High's spatial and temporal characteristics. That is because EOFs can partition a variable into mathematically orthogonal (i.e., non-correlated or independent) modes, which may be interpreted as atmospheric or oceanographic modes. For example, Reason (2016) used

EOF analysis of NCEP reanalysis 500 hPa geopotential height to study the Bilybara, Bolivian, and Botswana High's interannual variability. The EOF analysis showed that mode 2, which is not strongly related to ENSO, involved an in-phase modulation between the three subtropical highs, which is linked to the austral summer rainfall over Australia, South America, and Southern Africa. More recently, Reason (2018) employed EOF analysis to determine the dominant modes of variability in the Botswana High and their decadal variability between 1900-2011. The author found that the first mode accounts for 80% of the variance in 500 hPa geopotential height over the Southern Africa domain (5-60°E, 15-30°S) and represents a north-eastward shift of the Botswana High, while the second mode explains 9% of the variance and represents a weaker and slightly northward shifted Botswana High.

Despite these results, the EOF method is not always guaranteed to reveal physically interpretable modes. Nonetheless, in the Botswana High case, the EOFs temporal variability agrees well with the spatial average anomalies over the Botswana High core region, showing that the EOF mode is physically related to the temporal variability of the 500 hPa geopotential height over the core region. Less clear, however, is how the spatial and temporal variability of the Botswana Highs EOFs varies across different climate datasets since previous studies (e.g. Reason, 2016; Driver and Reason, 2017; Reason, 2018) only used a single dataset to classify the Botswana High. This present study will fill this gap by applying EOF analysis to multiple datasets to characterize the Botswana High.

CHAPTER THREE: DATA AND METHODS

This chapter provides a description of the data and methods used in the thesis. Section 3.1 details all the observation and reanalysis data. The model description and experimental setups are outlined in section 3.2, followed by section 3.3, which discusses the methods employed throughout the thesis.

3.1 Data

3.1.1 Observations

3.1.1.1 Climate Research Unit (CRU)

This thesis analysed monthly temperature and rainfall data from the Climatic Research Unit Version 4.03 dataset (hereafter CRU; Harris et al., 2014) for the study period 1980-2010. The CRU datasets are accessible from https://crudata.uea.ac.uk/cru/data/hrg/. The CRU dataset covers all land areas (excluding Antarctica) at a 0.5° resolution. The dataset is used to assess the skill of the Model for Prediction Across all Scales (MPAS) data in simulating the temperature characteristics (**Chapter 4**) and drought modes over Southern Africa (**Chapter 5**).

3.1.1.2 Global Precipitation Climatology Project (GPCP)

Monthly observed rainfall was obtained from the Global Precipitation Climatology Project Version 2.3 dataset (hereafter GPCP; Adler et al., 2003). The GPCP dataset combines global observations and satellite precipitation data into 2.5° × 2.5° global grids. The GPCP is used to evaluate the MPAS simulated rainfall over Southern Africa in **Chapter 4** and **Chapter 6**.

3.1.1.3 Climate Forecast System Reanalysis (CFSR)

Observed Sea Surface Temperatures (SSTs) and sea-ice data (6 hourly) were retrieved from the Climate Forecast System Reanalysis (CFSR; Saha et al., 2014) data products provided by the National Centers for Environmental Prediction
(NCEP; https://rda.ucar.edu/datasets/ds093.1).

The SST dataset has a grid resolution of 0.31° x ~0.31° and is used to evaluate how well the model simulates surface temperatures over the Southern African ocean basins and assesses the correlation between the Botswana High and global SSTs in **Chapter 4**. In addition to that, the SST dataset was used to force the MPAS model simulation in **Chapters 4-6** and calculate the El Niño Southern Oscillation (ENSO) index in **Chapter 6**.

3.1.1.4 SST Indices

Monthly SST indices were obtained from www.esrl.noaa.gov/psd/gcos_wgsp/Timeseries. The time-series data includes the Niño 3.4 and Dipole Mode Index and is used to evaluate the relationship between the Botswana High and SST modes over the Pacific and the Indian Ocean in **Chapter 4**.

3.1.2 Reanalysis

Monthly reanalysis temperature, rainfall, geopotential height, outgoing longwave radiation (OLR) and omega data were obtained from the Earth System Research Laboratory 20th Century reanalysis II (hereafter 20C; Compo et al., 2011), National Oceanic and Administration (NOAA; Lee, 2014) and the fifth-generation European Centre for Medium-Range Weather Forecasts (ECMWF) atmospheric reanalysis of the global climate (ERA5; Hersbach et al., 2018) dataset (https://climate.coper nicus.eu/climate-reanalysis). The study also used zonal and meridional wind components but from ERA5 and 20C only. All the reanalysis datasets have regular latitude-longitude grid resolution of 0.25°×0.25° and were used to evaluate the MPAS model simulation in **Chapters 4, 5 and 6**.

3.2 The MPAS Global Climate Model: Description and Experiments

The models evaluated in this study are the MPAS Global Climate Model version 5.2 and the most recent version 7.0. Both MPAS models are fully compressible nonhydrostatic global climate models with variable-resolution capabilities and use Advanced Research WRF (ARW) model physics. The MPAS model's variable-resolution uses Voronoi tessellation (Du et al., 1999), which is predominantly composed of hexagons, pentagons and heptagons that are occasionally present. The numerical schemes used in MPAS are like those in the ARW model, with the major differences in that ARW uses rectangular meshes and a hydrostatic vertical coordinate while the fully compressible nonhydrostatic equations in MPAS are derived in terms of a geometric-height vertical coordinate, and the solvers employ a split-explicit time-integration scheme which is described in Klemp et al. (2007). For meteorologically significant modes, the time-integration scheme uses a 3rd Order Runge-Kutta method with a large time step for meteorologically significant modes and a forward-backwards method with a smaller time step for acoustic modes.

In Chapters 4 and 5, the MPAS 5.2 model grid is set to a quasi-uniform resolution of 240 km (10242 grid cells) over the globe (Fig 3.1a). The model simulation uses 41 vertical levels with

an integration time step of 960 seconds and an output rate of 3-hourly data. The model simulation is initialised with NCEP CFSR data obtainable from https://rda.ucar.edu/datasets/ds093.1/ and, to give a more realistic simulation, the model was configured to update with 6 hourly CFSR SST and sea-ice data periodically. The model topography was obtained by interpolating the U.S. Geological Survey dataset into the MPAS grid (Fig 3.1b). The model simulation started from the 1st of January 1979 to the 31st of December 2011; however, the model results from 1979 were discarded as spin-up and only data from the 1st of January 1980 till the 31st of December 2010 was used for the study.

In Chapter 6, the MPAS 7.0 model grid is set to a variable resolution of 48 km over Southern Africa and 240 km worldwide (Fig 3.2). The variable-resolution grid contains 30210 grid cells and refines by a factor of 5 (from 240 km grid spacing to 48 km grid spacing), which satisfies the Caian-Geleyn condition of limiting the refinement factor to less than 8 in order to minimise pole-symmetric dilations (Caian and Geleyn, 1997). The prevailing advantage of using variable-resolution grids is applying higher resolution over an area of interest without requiring substantial computational power as with uniform high-resolution grids. The model simulation uses 41 vertical levels with an integration time step of 240 seconds and an output rate of daily data. The model topography was obtained by interpolating the U.S. Geological Survey (USGS) Global Multi-resolution Terrain Elevation Data 2010 (GMTED2010) dataset into the MPAS grid (Fig 3.3). A 32-year control integration and a set of SST perturbation experiments were performed in this study. The control integration (hereafter CTRL) runs from the 1st of January 1979 till the 31st of December 2010; however, the results from 1979 were discarded as spin-up and only data from 1980 till 2010 was considered. For the control run to give a more realistic simulation, the integration was configured to update with 6 hourly CFSR SST and sea-ice data (Gates, 1992). A series of August - April integrations with perturbed SST (hereafter NoENSO) were conducted for four El Niño (1983, 1992, 1998 and 2010) and four La Niña (1985, 1989, 2000 and 2008) years. In the 9-month integrations, the SST is the same as in the control run, except that monthly climatological SSTs are imposed over the entire Pacific Ocean to remove the influence of ENSO. For each 9-month integration, 10 ensembles were carried out with slightly different initial conditions to represent internal atmospheric variability. The initial conditions are taken from the previous years' August 20th - 29th snapshots (restart files) of the control run.

3.3 Methodology

3.3.1 Model Validation

To evaluate how well the model simulates the climate over Southern Africa, the simulated data (e.g. temperature and precipitation) are compared with the observed data. However, the known observational temperature datasets that were accessible have temperatures over either land or ocean. Therefore, the CRU data (which has observed surface temperature over the land only) was combined with CFSR SST (which has observed surface temperature over the ocean) data to have a complete observed temperature over the study area. In addition to that, we evaluated the model in simulating the climatology of the 500 hPa geopotential height over Southern Africa and compared the results to reanalysis data.

3.3.2 Identification of Botswana High

An Empirical Orthogonal Function (EOF) analysis of the 500 hPa geopotential height was performed on monthly reanalysis and model data to identify the Botswana High feature. The EOF analysis in this study was performed using the EOFSVD functions in NOAA Ferret (https://ferret.pmel.noaa.gov/Ferret/). The program code generates traditionally-scaled EOFs using a singular value decomposition routine. Traditionally-scaled means that the units of the EOFs are the units of the variable, while the principal components are dimensionless. The routine is based on numerical recipes routine svdcmp.f. The analysis was carried out for each dataset (ERA5, 20C, and MPAS) for the late summer season (JFM) over Southern Africa between 1980 and 2010. Because the Botswana High is often found in the southern parts of the continent, the Southern African domain was chosen for the regions spanning 10°E to 40°E and 0° to 33°S. Furthermore, this domain was chosen to concentrate on the core region of the Botswana High (15°–22° E; 20°–25° S), while minimising the effects of adjacent oceans and fluctuations in mid-latitude flow related to the Southern Annular Mode (Reason, 2016). To verify that the three datasets showed the same pattern, the reanalysis and model data were combined, and another EOF analysis was conducted on the combination of the datasets. Furthermore, we quantified the Botswana High index by taking a spatial average of 500 hPa geopotential height anomalies over the Botswana High core region (5^{o}-22^{o} E; 20^{o} -25^{o}S) to verify whether the EOF analysis is physically related to the temporal variability of the 500 hPa geopotential height over the Botswana High core region.

3.3.3 Performance Measures

In chapter 4, we performed a wavelet analysis to evaluate how well the model simulated the Botswana High periodicity compared to reanalysis. We also compared the model and reanalysis periodicities to ENSO periodicities to assess the annual variability between the Botswana High and ENSO. The wavelet analysis was performed using monthly SST time-series data (Sec 3.1.1.4) and Botswana High indices for the ERA5, 20C and MPAS data. The Botswana High indices were computed from the EOF time amplitude functions of the reanalysis and model data. Pearson correlation was used to measure the strength of association as well as the direction of the relationship between the MPAS simulation, reanalysis datasets, and SST data.

3.3.4 Drought Quantification

Chapters 4 and 5 used the 3-month Standard Precipitation Index (SPI, McKee et al., 1993) and Standard Precipitation Evapotranspiration Index (SPEI, Vicente-Serrano et al., 2010) Pearson III type distribution to characterize droughts over Southern Africa. SPI is a widely used index for characterizing meteorological drought across regions with markedly different climates (Keyantash and NCAR, 2018). SPI quantifies drought using only precipitation and can characterize drought or abnormal wetness at different time scales (e.g. 1-36 months), which correspond to the availability of different water resources at different times (e.g. soil moisture, snowpack, groundwater, river discharge and reservoir storage). However, SPI solely uses precipitation to characterize drought, meaning that it does not account for the influence of evapotranspiration on droughts. This limits the ability of SPI to capture the effect of increased temperatures on moisture demand and availability. To address this limitation, an alternative drought index (called SPEI) has been developed. SPEI is an extension of SPI designed to take into account both precipitation and potential evapotranspiration in quantifying drought, making it useful for climate change studies and may be a better way of characterizing drought risks (Vicente-Serrano and NCAR, 2015; Abiodun et al., 2018). Like the SPI, SPEI can be calculated on different timescales but has more data requirements than the precipitation-only SPI. To investigate the sensitivity of calculated drought characteristics to the choice of drought indices, both drought indices (SPI and SPEI) were employed in the present study. The indices were calculated from CRU observation, ERA5, 20C reanalysis and MPAS data. The values of SPEI and SPI typically range from −3 to 3 in depicting the intensity of dryness (drought; negative values) to wetness (positive values).

3.3.5 Identification of drought modes in different datasets

In Chapter 5, EOF analysis was applied to the SPEI and SPI data to obtain the spatio-temporal characteristics of drought modes over Southern Africa. The EOF algorithm was applied for the late summer season (JFM) between 1980 and 2010 over the Southern Africa domain. Several studies have utilised EOFs to extract usable information from large or complicated datasets by reducing the dimensionality of the dataset and uncovering hidden structures (i.e., Giannini et al., 2008; Manatsa et al., 2012; Richard et al., 2001). The EOF analysis was applied separately on the SPEI and SPI for each dataset (i.e., CRU, ERA5, 20C and MPAS). For each dataset, the first five principal EOF factors (i.e., EOF1-EOF5) were retained and discussed as the most significant drought modes (DMs) in the dataset.

3.3.6 ENSO Quantification

In Chapter 6, The ENSO index was quantified using the Oceanic Niño Index, which is the most common index used to monitor ENSO. We calculated the ENSO index as a 3-month running mean of SST anomalies in the Niño 3.4 region (5°N-5°S, 170°W-120°W). El Niño (La Niña) periods were defined when SSTs anomalies in the Niño 3.4 region are above (below) +0.5 (-0.5) for five consecutive months. For this study, the ENSO index was calculated using CFRS SST data for the period 1980-2010.

3.3.7 Assessing the response of Botswana High to ENSO

To assess the response of the Botswana High to ENSO in Chapter 6, two model experiments are conducted. The first experiment uses observed SSTs everywhere (CTRL), while the second experiment uses observed SST everywhere except over the Pacific Ocean, where monthly climatological SSTs are used. By prescribing monthly climatological SSTs over the Pacific, we essentially removed the ENSO signal and therefore referred to this experiment as NoENSO. These experiments are aimed to better understand the sensitivity of global and regional climatic features to ENSO events and how those impact the Botswana High.

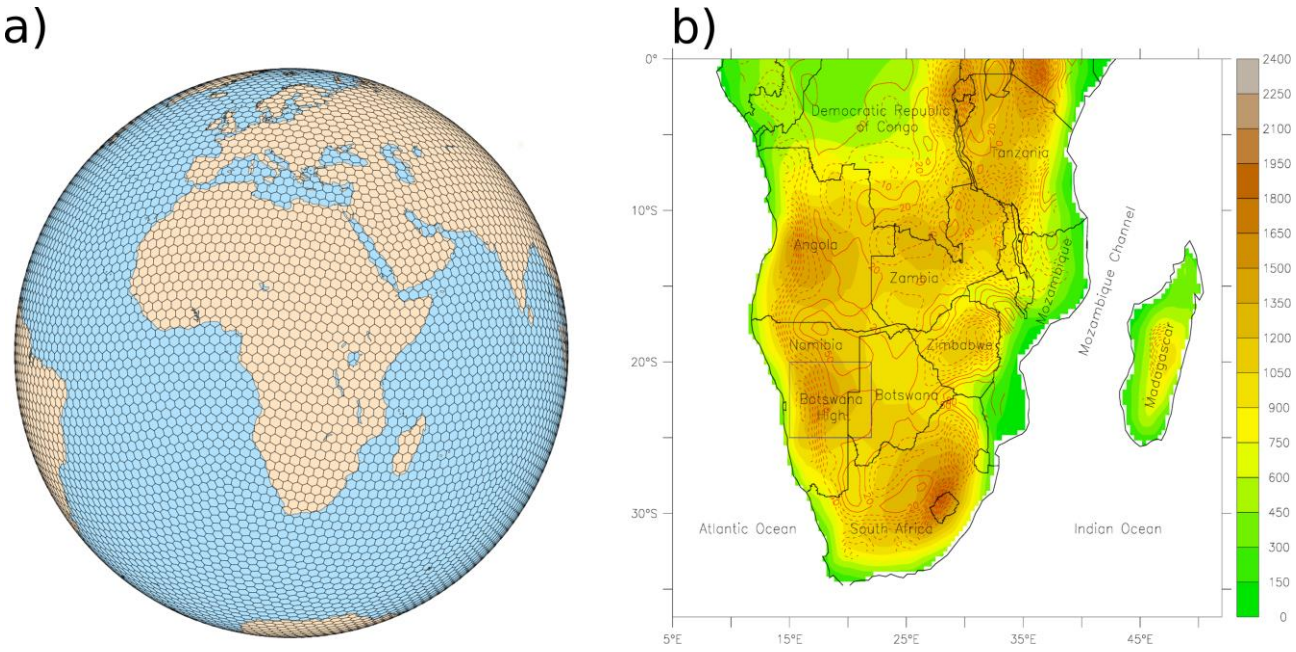

Fig 3. 1 : (a) The quasi-uniform mesh configuration (at 240km resolution with 10242 horizontal grid cells) used for MPAS simulation in the study. (b) The Southern African topography showing the Botswana High area (blue rectangle; 15°-22° E; 20° -25°S). Biases in representation of the topography in the MPAS simulation are shown in contours

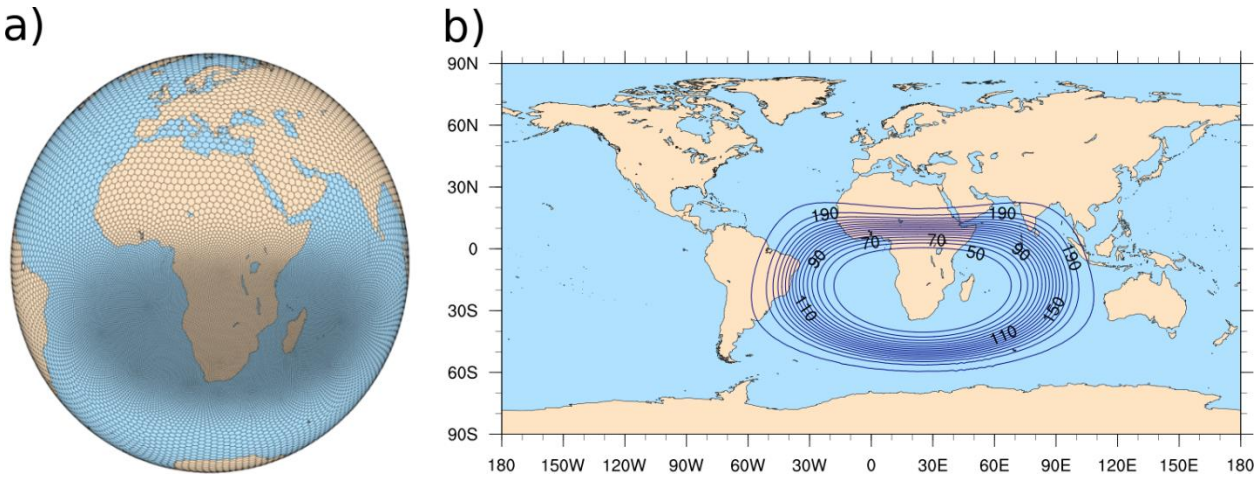

Fig 3. 2: The configuration of MPAS variable-resolution mesh used in Chapter 6, featuring the highest resolution (48 km) over Southern Africa and lower resolution (240 km) over much of the globe. The contours on (b) show the resolution from 50 km to 200 km in increments of 10 km

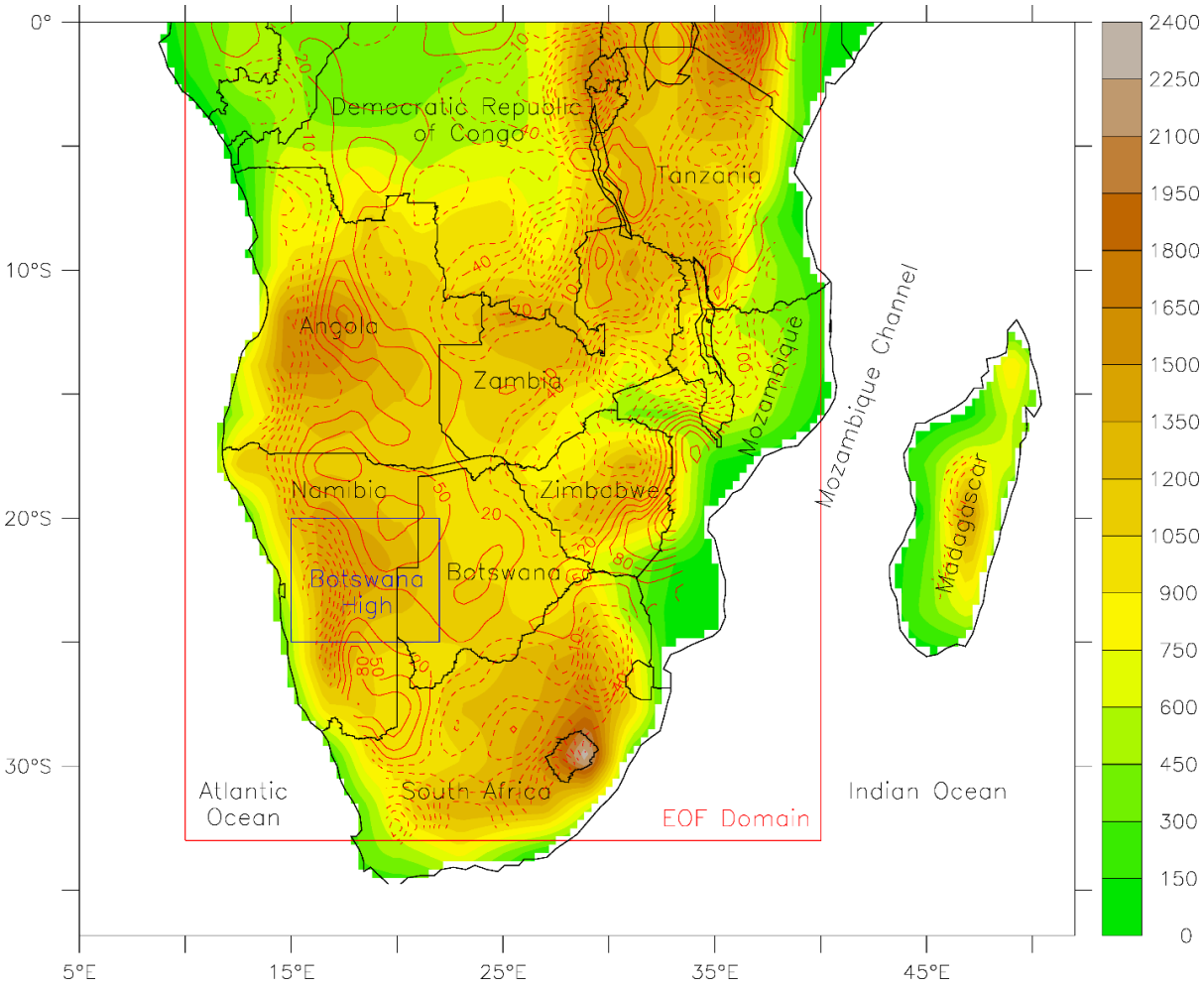

Fig 3. 3: The Southern African topography (in metres above sea level) as used in the Chapter 6 MPAS model simulation. The contours show the biases (i.e., MPAS minus original topography) of the topography. The blue box shows the Botswana High core region (15º-22º E; 20º-25ºS), while the red box shows the EOF domain (10º-40º E; 0º-33ºS)

CHAPTER FOUR: PERFORMANCE OF MPAS-ATMOSPHERE IN SIMULATING THE CHARACTERISTICS OF THE BOTSWANA HIGH

This chapter evaluates the Model for Prediction Across Scales version 5.2 (hereafter MPAS) in simulating the characteristics of the Botswana High and the influence of the High on drought over Southern Africa. Firstly, we evaluate how well MPAS simulates the climatology of temperature, rainfall and 500 hPa geopotential height over Southern Africa. Next, we evaluate the MPAS model's capability in simulating the spatio-temporal characteristics of the Botswana High. We then examine the influence of sea surface temperatures (SSTs) on the Botswana High, followed by an analysis of the impacts of the Botswana High on climate variables and drought over Southern Africa. Finally, we evaluate how well the MPAS model simulates the Highs impacts as compared to observation and reanalysis.

4.1 Climatology over Southern Africa

This section discusses how well MPAS reproduces the climatology over Southern Africa with a focus on the spatial distribution of temperature (Figs 4.1a, c and e), rainfall (Figs 4.1b, d and f) and 500 hPa geopotential height (Fig 4.2). Figure 4.1 shows that MPAS simulates well the spatial distribution of temperature over Southern Africa as compared to the observation and ERA5 reanalysis. The MPAS model has a strong spatial correlation ($r>0.9$) with the observation, indicating that it reproduces the dominating features in the observed temperature field. It captures the temperature gradient between the tropics and mid-latitudes and the relatively cold surface temperatures associated with the Benguela current near the western regions of the continent, and the warm surface temperatures associated with the Agulhas Current in the eastern parts of the continent. However, the model simulation shows a cold bias of about 2 °C over much of the Indian Ocean, which may be due to the coarser resolution in the model data (~ 240 km) as compared to the observation (~ 100 km). This bias suggests a weaker response of the MPAS atmosphere to SSTs over the Indian Ocean. The model shows a cold bias over the land, more especially over Botswana, Angola, Zambia, and western parts of Tanzania. This bias, which also features in ERA5 results, may be due to how the MPAS resolves the topography over these high-elevation areas (see Fig 3.1b).

The MPAS simulated rainfall field also has common features with GPCP observation (Fig 4.1b, d and f). GPCP shows an area of minimum precipitation over much of the Atlantic Ocean and

a band of maximum rainfall (associated with the South Indian Convergence Zone (SICZ)) over the Indian Ocean. The SICZ associated rainfall band shows a local maximum over the northern parts of the Indian Ocean (5–15° S; 60–80° E) and Madagascar (about 12 mm/day). MPAS reproduces the tropical rainfall band but with a wet bias of about±1 mm/day and fails to capture the local maximum rainfall over Madagascar in comparison to GPCP. The failure of the model to capture the local maximum over Madagascar may be attributed to the overestimation of deep convection over the Mozambique Channel, as the strong convection over the channel can suppress convection over the Malagasy Island, leading to a lack of local maximum rainfall. Additionally, the deep convection over the Mozambique Channel may be due to the dry bias in MPAS simulation over Mozambique and southern Tanzania. Despite that, MPAS shows good agreement with GPCP (r=0.89) over the Southern African continent, where all datasets show more rainfall in the tropics (6–8 mm/day) and lesser rainfall near the subtropics (about 2–3 mm/day). MPAS generally agrees with the two reanalysis datasets (ERA5 and 20C) on the spatial pattern of the 500 hPa geopotential height (Fig 4.2).

All the datasets show areas of high geopotential height over the tropics and low geopotential height poleward of 30°S. However, the MPAS model gives higher values of the 500 hPa geopotential height over much of the study area compared to the ERA5 reanalysis. The MPAS bias is more than 10 m for much of the area, but it is comparable with the difference between the two reanalyses (i.e., reanalysis uncertainty). There are also inconsistencies between the model simulation and the reanalysis over parts of Sub-Saharan Africa and over the Indian Ocean. For instance, the model shows a high-pressure centre (which resembles the Botswana High) farther east as compared to the reanalysis, which shows the high-pressure centre between Namibia and Botswana's border. Furthermore, MPAS struggles to capture the overall pattern of the 500 hPa geopotential height over the Indian Ocean as compared to the reanalysis. These inconsistencies may be due to the low 240 km resolution in the model simulation. Using a higher resolution may improve the model results. Regardless of that, MPAS features a high spatial correlation (r=0.98) with the ERA5 reanalysis.

4.2 Spatio-temporal distribution of the Botswana High

There is a good agreement between MPAS and reanalysis data on the variability of the pressure gradient over Southern Africa as well as the pattern and location of the Botswana High, although with some discrepancies (Fig 4.3). In each of the datasets, EOF analysis indicates that

mode 1 (EOF1) has a pattern reminiscent of the Botswana High, which is centred between 10° S and 25° S with an area of low pressure south of the ridge. Compared to the actual summer position of the Botswana High, EOF1 is displaced slightly equatorward, as in Reason (2018). Despite that, EOF1 in the MPAS model shows an area of high pressure centred between the borders of Botswana, Namibia, Angola and Zambia and accounts for approximately 80% in the variance of the 500 hPa geopotential height in the region, which is similar to ERA5 (85%) and 20C (83%). The 80% variance has also been found by Reason (2018). However, the MPAS high shows a broader centre located farther north in comparison to the reanalysis, whilst 20C shows a weaker and narrower centre which is located more eastward compared with the ERA5 and MPAS. Additionally, the combination of the model data and reanalysis EOF analysis (Fig 4.3d) shows a similar pattern to Figs 4.3a–c, but more comparable with the ERA5 high and explains 82% variance in the 500 hPa geopotential height over the region.

The time-series of EOF1 shows a strong agreement among the three datasets (MPAS, ERA5 and 20C reanalysis) in depicting the interannual variability of the Botswana High. However, the 20C reanalysis exhibits a weaker Botswana High in comparison to ERA5 and the MPAS results (Fig 4.4). In addition, even with the combination of the datasets (as in Fig 4.3d), the time-series results (Figure not shown) are comparable to Fig 4.4, indicating that EOF1 shows the same feature in both the model and reanalysis. In agreement with the previous studies by Reason (2016, 2018), Fig 4.4 shows a strong correlation between ENSO and the Botswana High Index during the study period. All three datasets indicate that the Botswana High was strongest in the years 1983, 1998 and 2010, which is consistent with Reason (2016). In addition, all three cases of the strongest Botswana High occurred during the mature phase of El Niño summers (1983, 1998 and 2010), while the majority of the weakest Botswana Highs occurred during La Niña summers except for 1994, which occurred in a neutral ENSO year. However, MPAS simulation indicates that the weak Botswana Highs occurred in 1985, 1986, 1989, 1999 and 2008, while ERA5 shows the weak high in 1985, 1986, 1989, 1996 and 2000. On the other hand, the 20C showed the highest number of weak highs (1985, 1986, 1989, 1994, 1996, 2000, 2001 and 2008), possibly due to the generally weaker high in the reanalysis. However, the time series shows that the MPAS results strongly correlated with that of ERA5 ($r=0.83$, $p<0.0001$), meaning that the MPAS model has a strong skill in simulating the interannual variability of the Botswana High.

A wavelet analysis of EOF1 in the reanalysis and model simulation indicates that the Botswana High is dominated by a strong 4–5-year cycle band before the early 1990s and a weak 2–3-year cycle band afterwards (Fig 4.5). All datasets show similarity in the 4–5-year cycle between 1981 and 1989; however, the power spectrum is stronger in the ERA5 than in 20C and MPAS. There are also some discrepancies between the MPAS and reanalysis on the 2–3-year cycle. For example, before the 1990s, the 2–3-year periodicity was weaker in MPAS than the reanalysis but stronger between 1995–2001 and 2007–2010. The dominance of the 4–5-year and 2–3-year periodicities of EOF1 compares well with the ENSO wavelet power spectrum (Fig 4.5d) and suggests that the Botswana High variability may be related to forcing from ENSO that also has leading periodicities in these two frequency bands.

4.3 The influence of SSTs on the Botswana High

The correlations between the JFM Botswana High index and SST anomalies in different seasons (OND, JFM, and AMJ) indicates a good agreement between MPAS, ERA5 and 20C (Fig 4.6). All the datasets feature a high correlation between the Botswana High index and global SST anomalies. During early summer (OND), the most significant correlations occur over the North Atlantic as well as parts of the South-West and North-East Pacific. However, during concurrent summer (JFM), the correlation becomes stronger over the tropical Pacific, tropical Atlantic, South-west Pacific, tropical Indian Ocean, Enderby Plain (60° S, 40° E), as well as over the Kerguelen Plateau (43° S, 72° E). In the Autumn (AMJ), the correlation decreases over the tropical Pacific as well as over the South-West Pacific and parts of the southern Indian Ocean. The decrease in correlation over the Pacific indicates that the Botswana High is highly correlated with the early development phase of ENSO and progressively becomes weaker during the mature phase.

To quantify the link between the Botswana High and ENSO, Table 4.1 shows the coefficient of correlation between the Botswana High and Niño 3.4 seasons. All datasets indicate a strong correlation between the Botswana High and ENSO in JFM; however, the correlation becomes rapidly weaker when negative lags are introduced, indicating a very weak relationship between the Botswana High and the decaying phase of ENSO. On the other hand, introducing positive month lags, the correlation becomes progressively weak but remains strong (0.61–0.69) at 95% significance up to a lag of 2, which is related to the ENSO development phase. At lag 3, which is indicative of the mature phase of ENSO, the correlation becomes weaker, heading to the

decaying phase of ENSO in lag 4 and 5. Despite the strong correlation between the Botswana High and the tropical Indian Ocean SST (as shown in Fig 4.6), there seems to be no link between the high and the Indian Ocean dipole index (Table 4.1).

To further assess the relationship between the Botswana High and ENSO, Fig 4.7 shows composite anomalies of JFM 200 hPa velocity potential and stream function (contours) during strong Botswana High Years (1983, 1998 and 2010) and weak Botswana High Years (1989, 1994 and 2008). The results show that +ve Botswana High years are characterised by anomalous upper tropospheric divergence (negative velocity potential) west of the prime meridian (i.e., 0° longitude) and anomalous upper tropospheric convergence (positive velocity potential) east of the prime meridian and vice versa during −ve years. This upper-level convergence-divergence pattern during the +ve (−ve) Botswana High years is reminiscent of the weakening (strengthening) of the Walker Circulation and typically forms during El Niño (La Niña) years. Furthermore, the increase (decrease) in upper-level convergence over Southern Africa may lead to increased (decreased) subsidence over the region and the strengthening (weakening) of the Botswana High. The 200 hPa eddy stream function during +ve (−ve) Botswana High years are characterised by anticyclonic(cyclonic) anomalies in the upper troposphere over the central and eastern pacific. This pattern is characteristic of a Gill-Matsuno type response, which typically occurs during El Niño (La Niña) Years due to warm (cold) SST anomalies in the tropical Pacific Ocean (Gore et al., 2019). This response indicates a weakening (strengthening) of the upper-level cyclonic flow in the eastern Pacific and a weakening (strengthening) of the Walker Circulation. During +ve (−ve) years, the upper-level stream function shows anomalous cyclonic (anticyclonic) flow over the Indian Ocean, Asia, and Southern Africa, which corresponds to the increase (decrease) in convergence over the area leading to lower-level subsidence (convection).

Figures 4.8 and 4.9 show the anomalous 500 hPa geopotential height and vertical cross-section of the geopotential height during +ve and −ve Botswana High years. In general, the position of the Botswana High varies between the datasets during +ve years (Figs 4.8a, c and e). The MPAS model shows a Botswana High located over northwestern South Africa and southeastern Botswana (Fig 4.8e), while ERA5 shows the high over much of Namibia (Fig 4.8a). However, the 20C reanalysis fails to adequately capture the net sinking motion ($\omega>0$) associated with the Botswana High over Namibia, Botswana, or South Africa (Fig 4.8c). The reason for this is that the 20C Botswana High is weaker (Fig 4.9c) as compared with ERA5 (Fig 4.9a) and MPAS

(Fig 4.9e). This may also explain why the 20C EOF 1 (Fig 4.3b) was weaker as compared to ERA5 and MPAS (Figs 4.3a and c). Nevertheless, all the datasets show sinking motion associated with the Botswana High, which is characterised by rising air to the west of the High, which sinks and manifests as upper-level convergence in the vicinity of the high, leading to increased subsidence in the mid-levels. Figures 4.8b, d and f also show variability in the position of the Botswana High during −ve years; however, the position of the Botswana High is more similar as compared to +ve years. Despite that, MPAS agrees well with ERA5 reanalysis on the depth of the −ve Botswana High mode (Figs 4.9b, d and f) and shows a −ve Botswana High that is characterised by lower divergence, which might lead to increased convection.

4.4 Impact of the Botswana High on climate variables and droughts

4.4.1 Positive phase of the Botswana High

Figures 4.10a, c, e and 4.11a, c, e show the anomalous 500 hPa geopotential height and anomalous surface temperatures, respectively, during +ve Botswana High years. The composite of standardised anomalies for 500 hPa geopotential height during +ve Botswana High years shows a good agreement between the MPAS simulation and reanalysis (20C, ERA5), in a sense that all datasets indicate enhanced geopotential height over the tropics and little to no change poleward of 30° S. Higher geopotential heights are typically associated with warm air masses and increased subsidence and may lead to an increase in temperature over the tropics. When an air mass descends, the pressure on the air mass increases. Because of the increase in pressure, the volume of the air mass decreases, increasing its internal energy, which manifests itself in the increase in temperature of that mass of air. This increase in the geopotential height agrees with Fig 4.11, which shows that +ve Botswana High years are generally characterised by warmer temperatures over the land surface as well as over the tropical Atlantic and the tropical Indian Ocean. During +ve Botswana High years, the observational data shows above normal temperatures mostly over the eastern parts of the continent (Zimbabwe, Zambia, and Mozambique) with slightly warmer conditions over the northeast regions of South Africa (Figs 4.11a, c, and e). The reanalysis shows a similar pattern; however, the warmer conditions extend throughout the eastern half of South Africa. On the other hand, the model simulation shows above-normal temperatures for much of the eastern parts of the continent as well as over South Africa. In addition to that, the positive anomaly extends along the coastline of Namibia and Angola as compared to the CRU CFSR and ERA5.

The above-normal temperatures in the MPAS simulation may be attributed to the anomalous local maximum in the geopotential height over the South African Development Community region (Fig 4.10e), which is stronger in MPAS as compared to the reanalysis (Figs 4.10a and b).

MPAS and reanalysis datasets indicate that +ve Botswana High years are typically characterised by neutral to positive OLR anomalies (Figs 4.12a, c, e), lesser convection (Figs 4.8a, b and c) and lesser rainfall (Figs 4.13a–c). Positive OLR anomalies indicate suppressed convection, lesser cloud coverage and more radiation emitted back into space, which is consistent with the increased subsidence in the area. However, there are notable discrepancies between 20C, ERA5, and the model simulation of OLR, especially over the ocean. The differences in OLR may be due to the Tiedtke convective parameterisation scheme used in the model, which removes convective instability before resolved-scale motions can respond to it. Another reason could be that the Tiedtke parameterisation is sensitive to entrained air from the free troposphere, and thus convection can be reduced by dry, free troposphere (Ali et al., 2015).

The discrepancies in the position of the Botswana High sinking motion may impact rainfall patterns in the datasets over Southern Africa (Fig 4.13). In actuality, there is poor agreement between the datasets on the +ve phase rainfall anomalies over land. GPCP shows below-average rainfall for much of the region and mildly wet conditions over South Africa, northern Angola, and Tanzania. The reanalysis shows an agreement with GPCP over Angola, northeastern parts of South Africa, and Tanzania but shows disagreement with the observation over Madagascar, Zambia, and the Democratic Republic of Congo (DRC). The MPAS model also shows disagreements with GPCP and ERA5 over Botswana and northern Namibia, where it simulates above-average rainfall, whereas the other datasets show below-average rainfall. The MPAS model's inability to adequately capture the precipitation anomalies may be due to the low resolution (240 km) used in the simulation. A higher resolution simulation could allow for a better representation of orography and surface fields vital for the initiation of convection in complex terrains (Hohenegger et al., 2008).

MPAS shows a broad agreement with reanalysis on drought patterns during the +ve Botswana High years, although with some discrepancies. Foremost, all datasets show a warm bias in Potential Evapotranspiration (PET) over much of the subcontinent (Figs 4.14a, c and e); however, the model shows higher anomalies than reanalysis. Higher PET anomalies indicate enhanced evaporation, leading to more severe drought conditions over the region in the absence of precipitation. Despite the good agreement among the dataset on the PET pattern, they disagree on the meteorological drought patterns (i.e., SPI and SPEI) during +ve Botswana High years (Figs 4.15a, c, e and 4.16a, c, e). For example, both MPAS and 20C show normal to wet conditions over Namibia, while ERA5 shows parched conditions. On the other hand, both reanalysis datasets show a relatively dry bias over Botswana, Zimbabwe, and the north-eastern regions of South Africa, while the model shows a wet bias. Despite that, some areas show agreement between the datasets, such as Angola, parts of Tanzania, and central parts of South Africa. However, MPAS shows better agreement with 20C in SPEI anomalies than with ERA5. For instance, both MPAS and 20C show +ve SPEI anomalies over central Namibia, Angola, and north-eastern South Africa, while ERA5 shows severe drought over much of the region.

4.4.2 Negative phase of the Botswana High

MPAS and reanalysis data show that −ve Botswana High years are characterized by a decrease in the geopotential height (Figs 4.10b, d, and f) which is typically associated with cooler air masses and is consistent with the decrease in the surface temperatures over land (Figs 4.11b, d, and f). During −ve years, the most obvious disagreement between the reanalysis and MPAS is the local minimum geopotential heights simulated over the Atlantic and the Indian Ocean as compared to the reanalysis. In addition to that, the reanalysis shows a slight increase in the geopotential height over the subtropics, whilst the MPAS simulation indicates a decrease in the geopotential height (Figs 4.10b, d, and f). In connection to the decrease in geopotential height over the region, both CRU CFSR and ERA5 show below-normal temperatures over much of the continent; however, the model simulation shows not much change in temperature except over Zambia, the DRC, Tanzania, and northern Mozambique. Despite this, the model shows a good comparison with observation and reanalysis regarding surface temperatures over the ocean. The datasets show two warm tongues over the Atlantic and a local minimum surface temperature south of Madagascar.

There is a better agreement in the OLR, omega, and rainfall patterns between the datasets during −ve Botswana High years as compared with +ve years. However, there are notable discrepancies between the model simulation and ERA5 reanalysis, especially over the ocean. In general, the datasets show negative OLR anomalies during −ve years are indicative of enhanced convection, which may lead to more cloud coverage and rainfall (Figs 4.12b, d, and f). More cloud coverage may increase the albedo effect leading to colder temperatures over the study areas, as shown by Figs 4.11b, d, and f; however, the effect of cloud cover on temperature is not singular as the role of horizontal advection is also important. Additionally, more convection implies higher and colder cloud tops that emit less radiation back into space. The 500 hPa Omega anomalies during −ve Botswana High years (Figs 4.8b, d and f) indicate areas of convection in the mid-levels (~ 500 hPa) in Namibia, southern Angola, Zambia, Botswana, and parts of the interior of South Africa. The anomalous convection in those areas is consistent with the increased rainfall over the region (Figs 4.13b, d, and f). Both GPCP and ERA5 show wetter conditions for much of the southern continent except for southern Mozambique, Zimbabwe, and parts of Angola. Similarly, MPAS simulates wetter conditions over much of the Southern African continent except over Namibia; however, these are weaker as compared to the observation and reanalysis. This result is consistent with the result of Fig 4.12f, which shows weaker negative OLR anomalies for MPAS as compared to Figs 4.12b and d).

The agreement between MPAS and reanalysis on drought patterns is better during the −ve Botswana High years than during the +ve years. As expected, the datasets generally show a cold bias in PET anomalies over the region, which is indicative of cool (Figs 4.11b, d, and f), cloudy (Figs 4.12b, d, and f) and rainy conditions (Figs 4.11b, d, and f). However, the MPAS model shows near-normal PET anomalies for South Africa, Botswana, and Namibia, which disagrees with the reanalysis results. This discrepancy may be due to the near-normal temperatures simulated by the MPAS model in Fig 4.11f, which the PET calculation is dependent on. The SPI also shows a good agreement between the datasets, especially over South Africa, Botswana, Angola, Zambia, southern DRC, northern Mozambique and much of Tanzania (Figs 4.15b, d, and f). However, the model fails to capture the wet (dry) spells near Namibia (Zimbabwe and southern Mozambique) as in the reanalysis. Nonetheless, SPEI also shows a better agreement between the MPAS and reanalysis data during −ve Botswana High Years. Again, the datasets indicate +ve anomalies over much of the region except over Angola and the southern coastline of South Africa (Figs 4.16b, d, and f).

4.5 Summary

This chapter has evaluated the capability of MPAS in simulating the characteristics of the summertime Botswana High. The global simulation covers a period of 31 years (1980–2010). Focusing on the Southern African domain, EOF analysis was used to extract the Botswana High feature from the 500 hPa geopotential height in the reanalysis and simulation datasets. To evaluate the skill of the model in capturing the spatial and temporal variability of the Southern African climate and the Botswana High, the simulated results were compared to the observed and reanalysis data. The results of the study can be summarised as follows:

- In general, MPAS performs well in simulating all the climate variables over Southern Africa. The simulated rainfall and temperature biases are about 1 mm/day (positive) and 2 °C (cold), respectively. However, the spatial variations in the 500 hPa geopotential height are larger in the 20C reanalysis (about − 16 to 18 m) and MPAS simulation (about − 9 to 10 m) as compared to ERA5 reanalysis.

- All the datasets agree that the Botswana High accounts for about 80% of the variability in the 500 hPa geopotential height over the Botswana area. However, the spatial pattern of the Botswana High simulated by MPAS features a better agreement with the ERA5 reanalysis than with the 20C reanalysis.

- MPAS reproduced the interannual variability of the Botswana High as in the reanalysis. The variability, which shows a strong connection with ENSO, suggests a link between the Botswana High and ENSO.

- MPAS captures the 500 hPa vertical velocity over Southern Africa with variations in the position of the Botswana High sinking motions. Despite that, the vertical cross-section of omega anomalies shows that the +ve Botswana High mode is characterised by upper-level convergence while the −ve mode is characterised by upper-level divergence.

- The MPAS model captures well the drought patterns over Southern Africa as compared to reanalysis; however, there is a better agreement during −ve Botswana High years than +ve years. In general, +ve Botswana High Years are characterised by increased evaporation, while −ve years indicate increased convection.

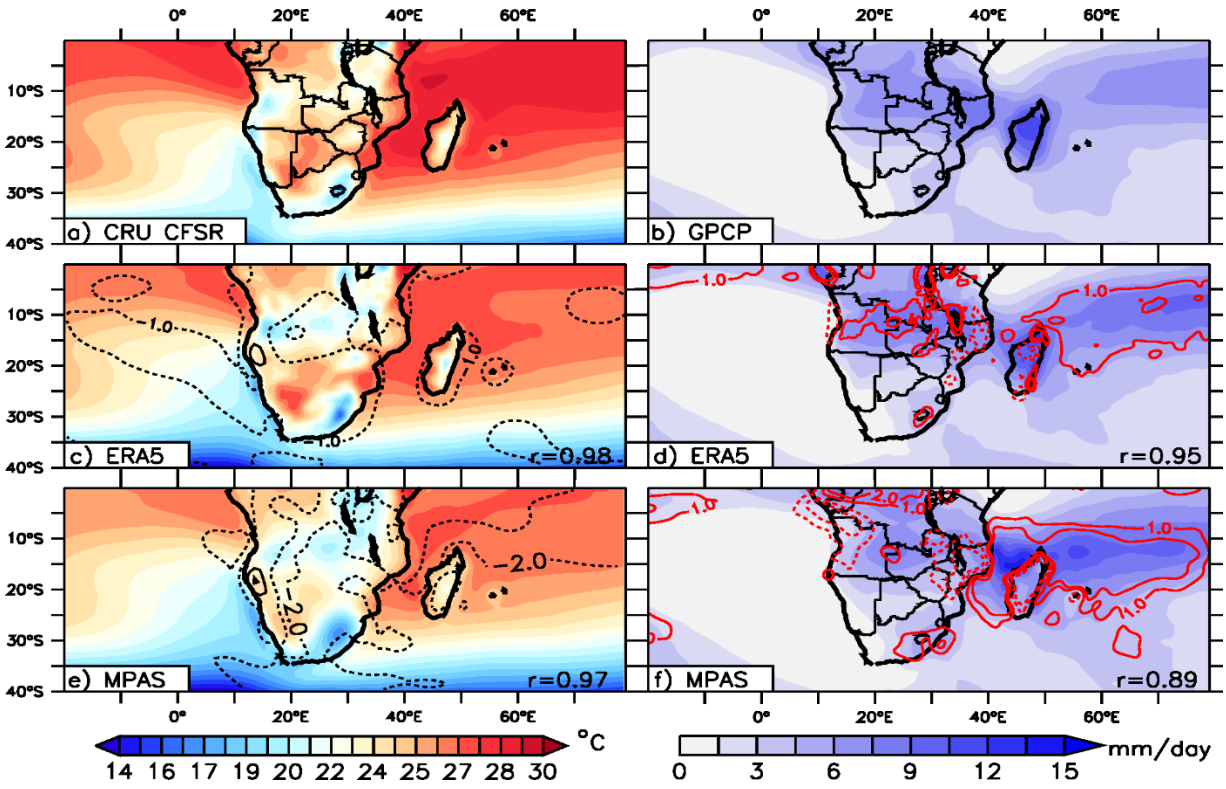

Fig 4. 1: The climatology of JFM surface temperature (°C) and precipitation over Southern Africa (1980–2010) (left and right columns, respectively), as depicted by CRU CFRS and GPCP (top panels), (b) ERA5 reanalysis (middle panels), and MPAS simulation (bottom panels). Biases in ERA5 data and MPAS simulation (with respect to CRU CFSR and GPCP) are indicated with contours. The corresponding correlation (r) of the spatial patterns is also indicated

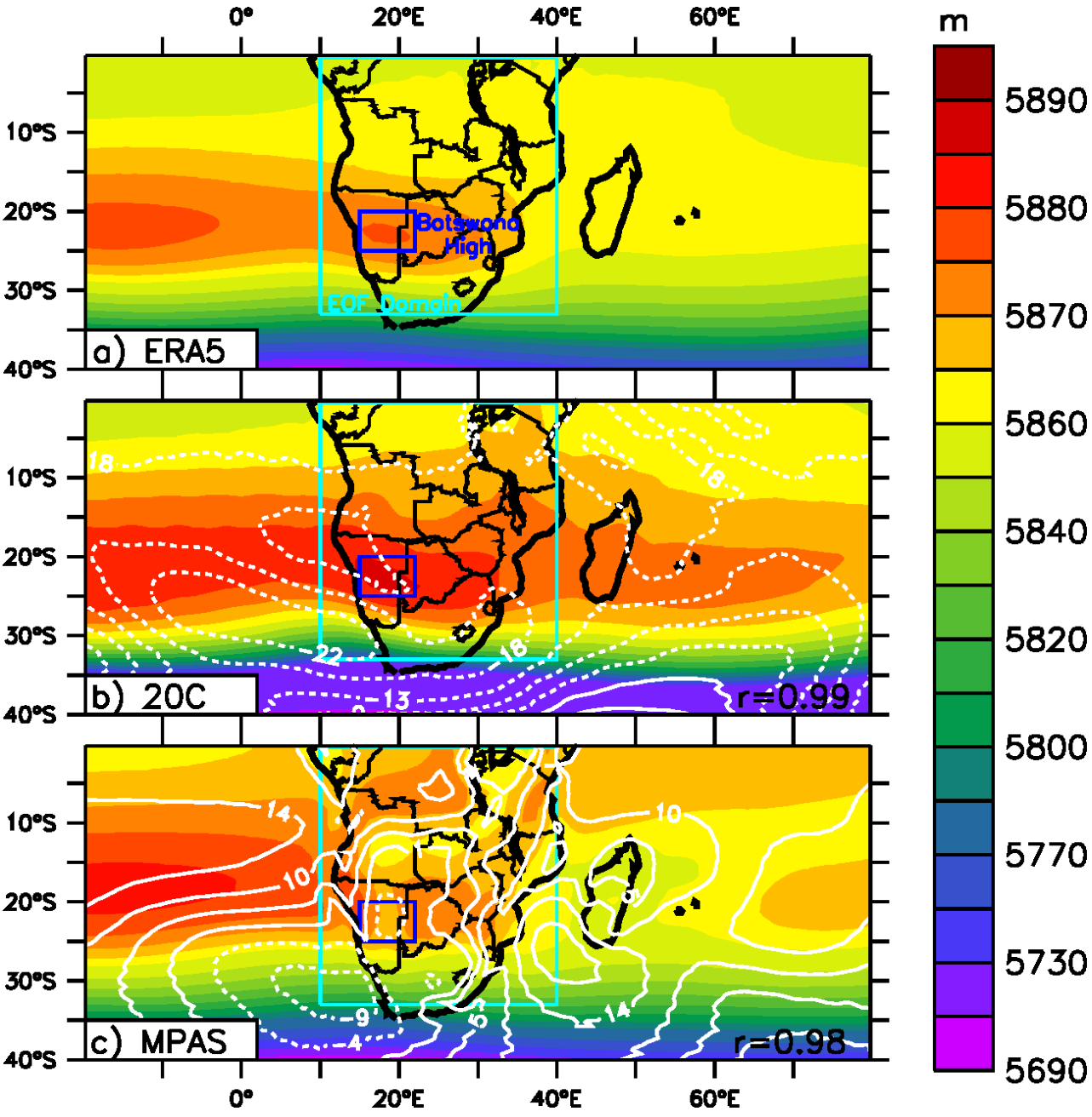

Fig 4. 2: The climatology of 500hPa geopotential height (m) over Southern Africa (1980–2010), as depicted by ERA5 (a) reanalysis, (b) 20C, and (c) MPAS simulation. Biases in the 20C data and MPAS simulation (with reference to the ERA5 Reanalysis) are shown with contours and the corresponding spatial correlation (r) is also indicated. The blue box shows the Botswana High area (15º-22º E; 20º -25ºS) while the cyan box shows the EOF domain (10º-40º E; 0º -33ºS)

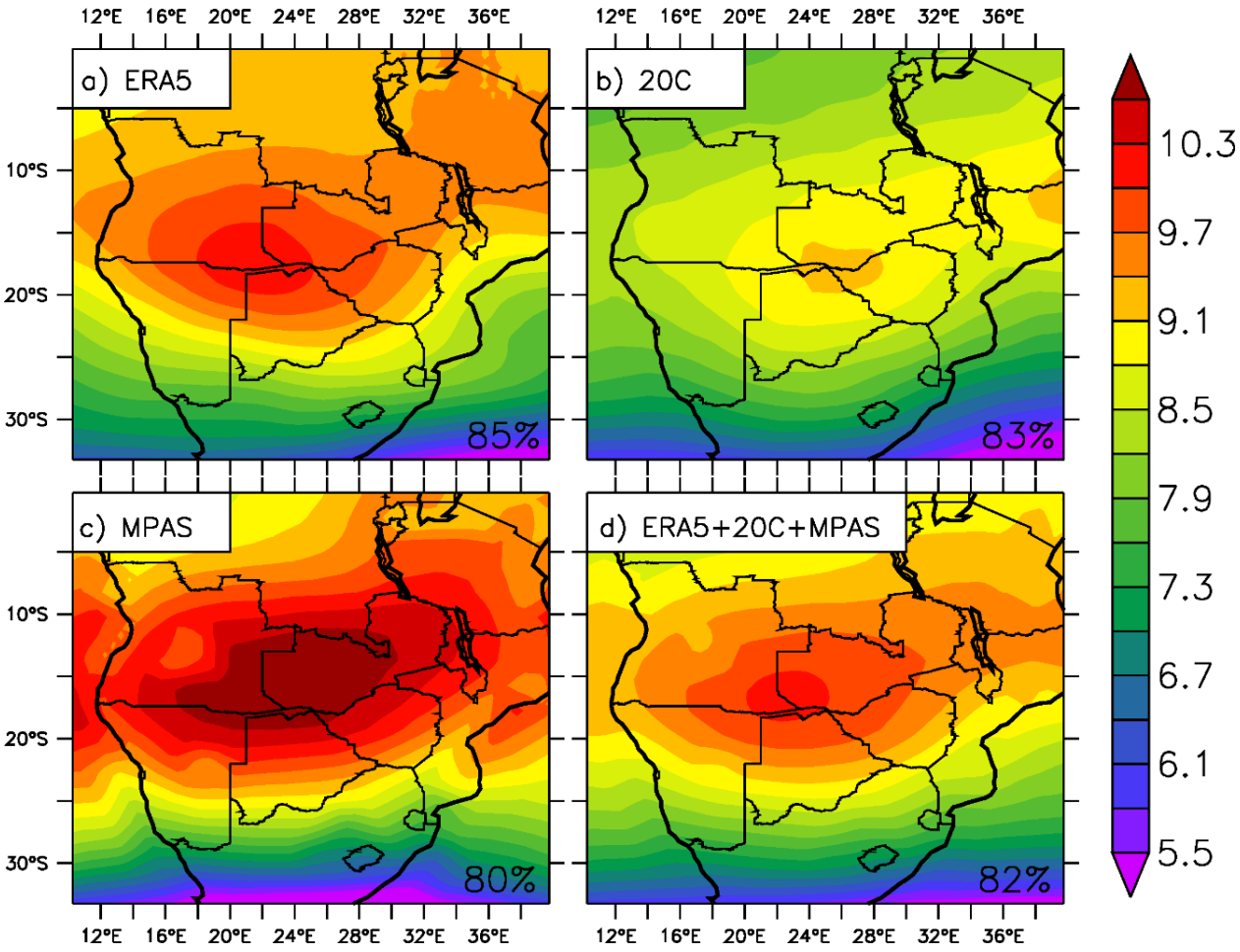

Fig 4. 3: The leading factor of EOF analysis (EOF 1) of JFM 500 hPa geopotential height using monthly (a) ERA5, (b) 20C reanalysis, (c) MPAS simulated data, and (d) the combination of the three datasets for 1980-2010. The numbers in the bottom right denote the percentage of variance explained by the leading factor

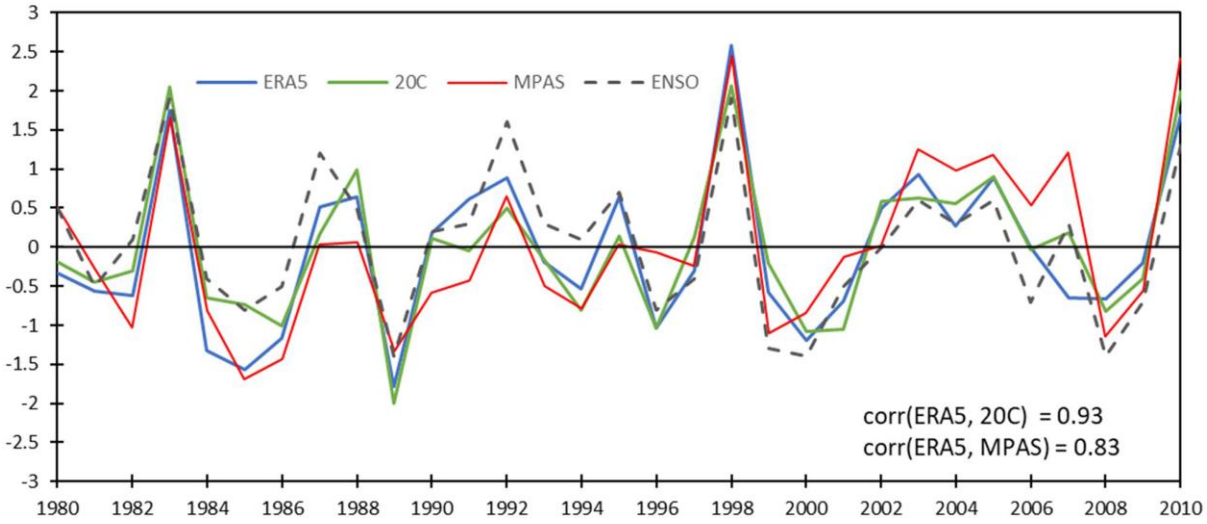

Fig 4. 4: Interannual variability of the Botswana High as shown by ERA5, 20C Reanalysis and MPAS datasets. The dashed line shows the Niño 3.4 index. The indices are derived from scores of the EOF 1 shown in Figure 4.3

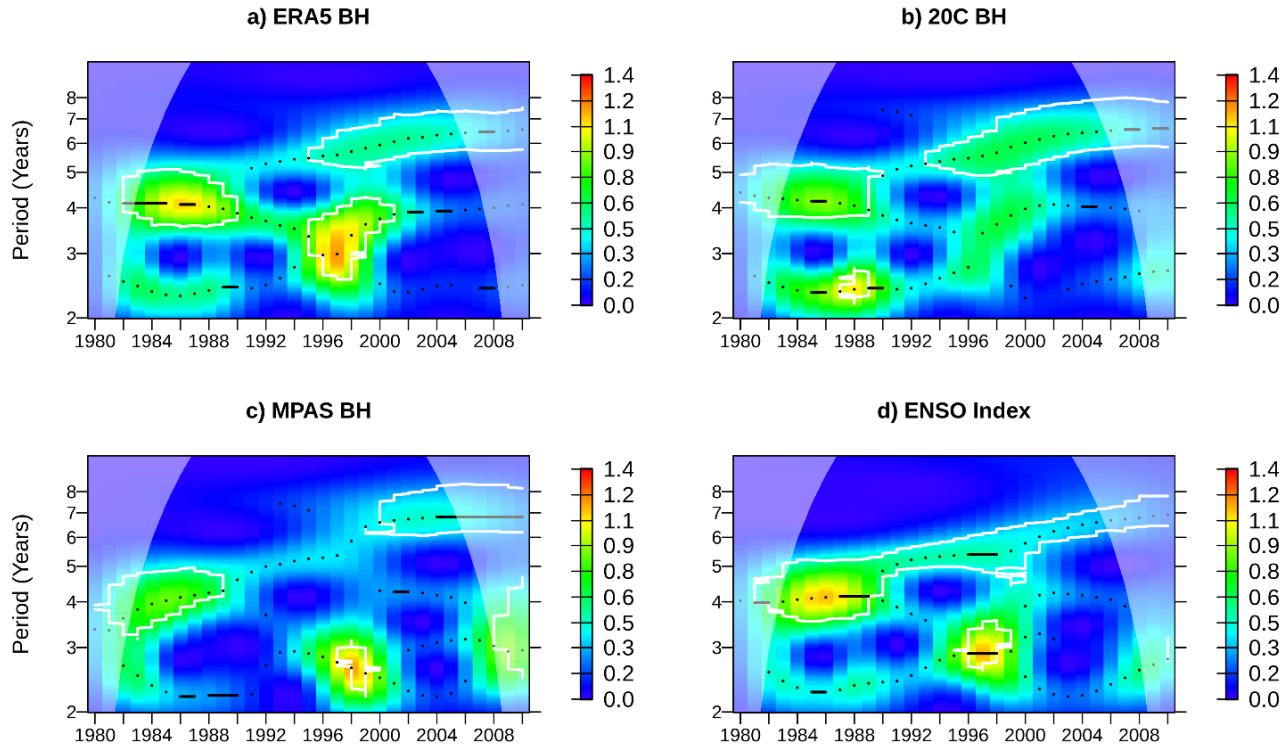

Fig 4. 5: Wavelet power spectrum of the Botswana High index in (a) ERA5, (b) 20C and (c) MPAS datasets for JFM 1980-2010. Panel d shows the wavelet power spectrum for the ENSO index

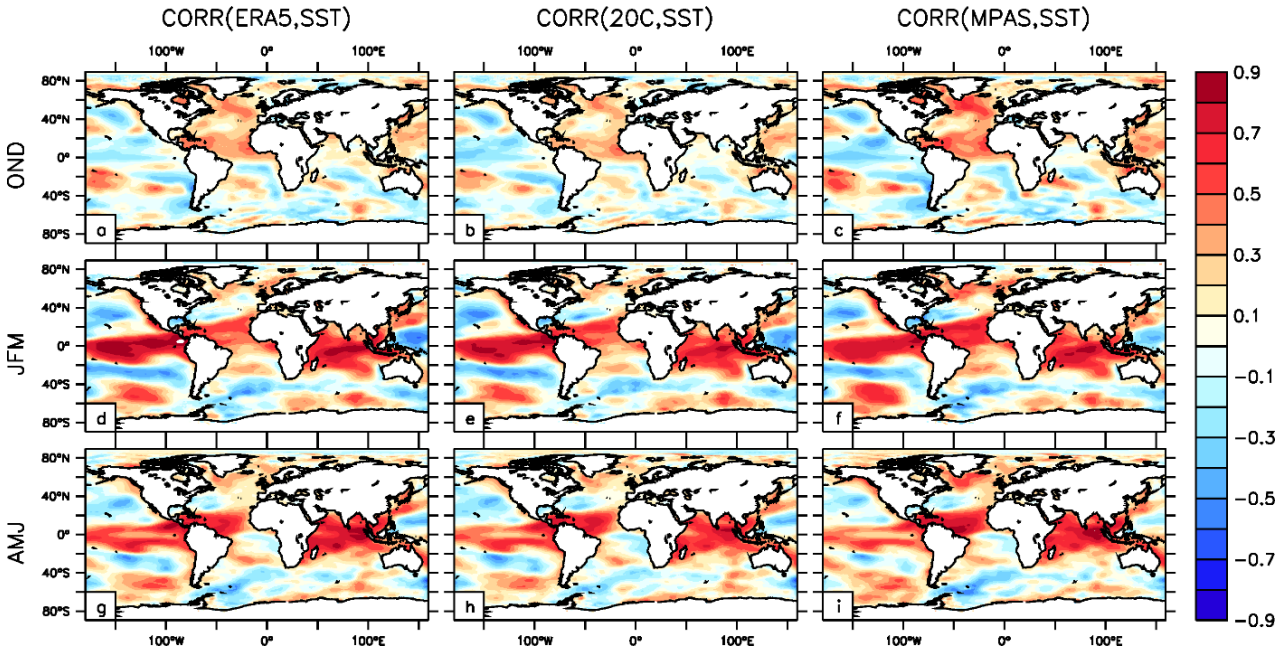

Fig 4. 6: Coefficient of correlation between the interannual variation of Botswana High Index and SST during early summer (OND), concurrent summer (JFM) and following Autumn (AMJ) for 1980-2010

Table 4. 1: Correlation between Botswana High JFM season, Niño 3.4 and IOD seasons 1980-2010.

	Niño 3.4			IOD		
Lag	**ERA5**	**20C**	**MPAS**	**ERA5**	**20C**	**MPAS**
-5	-0.14	-0.23	-0.28	-0.04	-0.02	-0.15
-4	-0.16	-0.26	-0.31	-0.10	-0.08	-0.22
-3	-0.16	-0.27	-0.31	-0.07	-0.06	-0.21
-2	0.26	0.15	0.07	0.08	0.09	-0.07
-1	**0.71**	**0.63**	**0.55**	0.24	0.17	0.15
0	**0.86**	**0.83**	**0.76**	0.13	0.08	0.15
1	**0.84**	**0.80**	**0.72**	0.00	-0.03	0.08
2	**0.76**	**0.69**	**0.61**	-0.01	-0.04	0.03
3	**0.40**	0.30	0.24	0.17	0.11	0.10
4	0.28	0.17	0.12	0.19	0.15	0.08
5	-0.05	-0.14	-0.17	0.11	0.12	0.00

Correlation coefficients significant at 95% or more are shown in bold

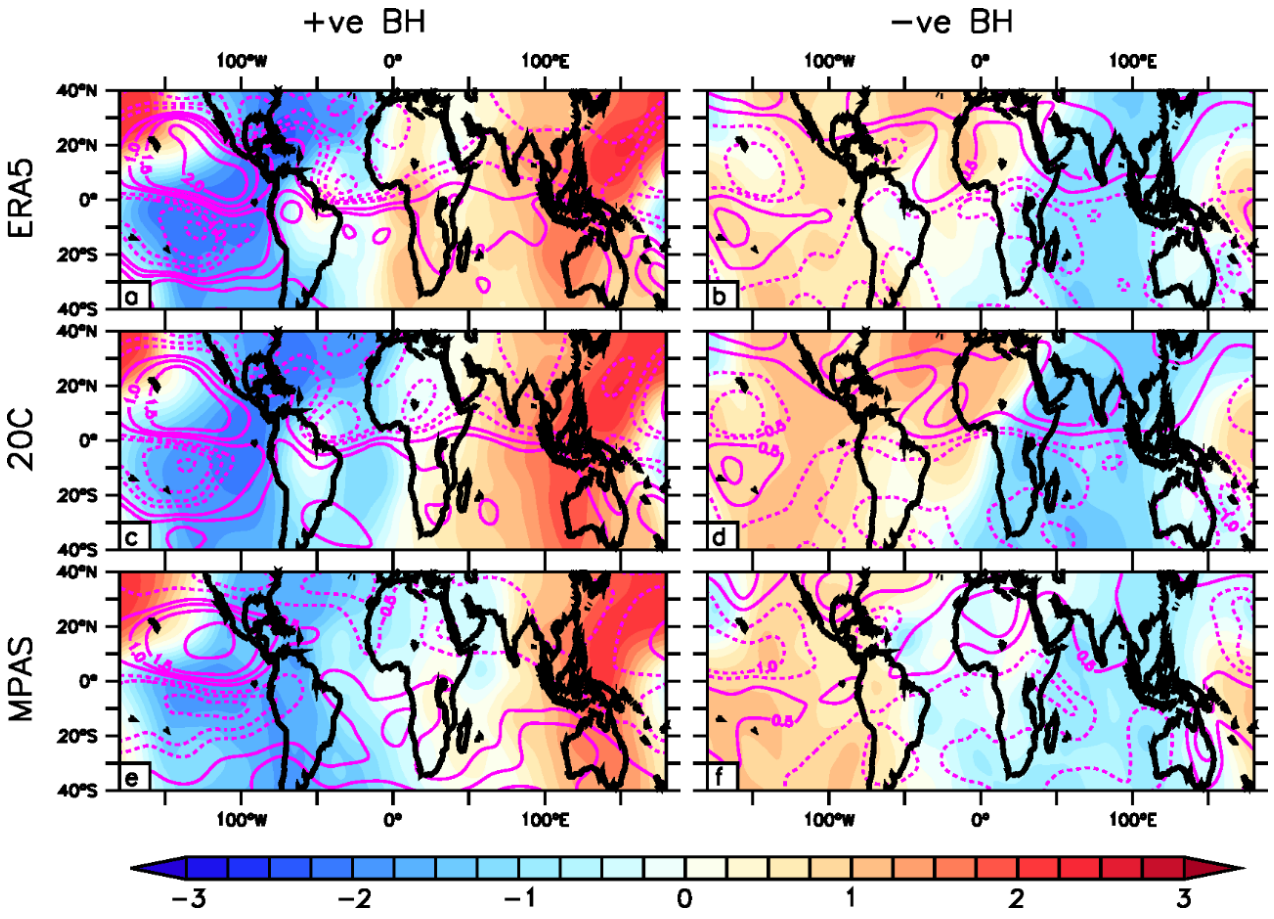

Fig 4. 7: Composite of the standardized anomalies of JFM 200hPa velocity potential and 200hPa stream function (contours) during +ve Botswana High Years (1983, 1998, 2010) and -ve Botswana High Years (1989, 1994, 2008). The mean and standard deviation used in calculating the anomalies were obtained using the 1980-2010 data

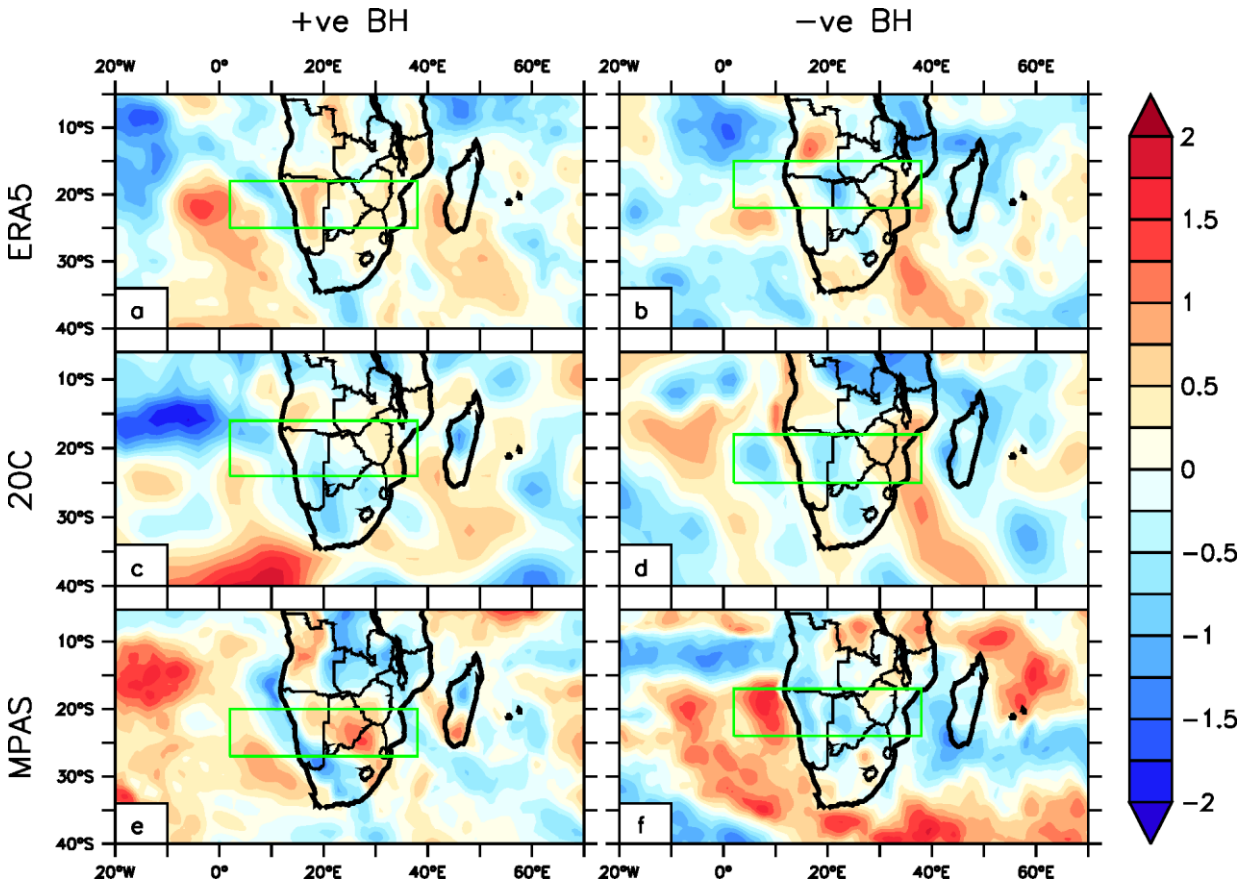

Fig 4. 8: Composite of the standardized anomalies of JFM 500hPa Omega during the +ve phase of Botswana High Years (1983, 1998, 2010) and -ve phase of Botswana High Years (1989, 1994, 2008). The mean and standard deviation used in calculating the anomalies were obtained using the 1980-2010 data. The green box shown in the region is used for the vertical cross-section plot in Figure 4.9

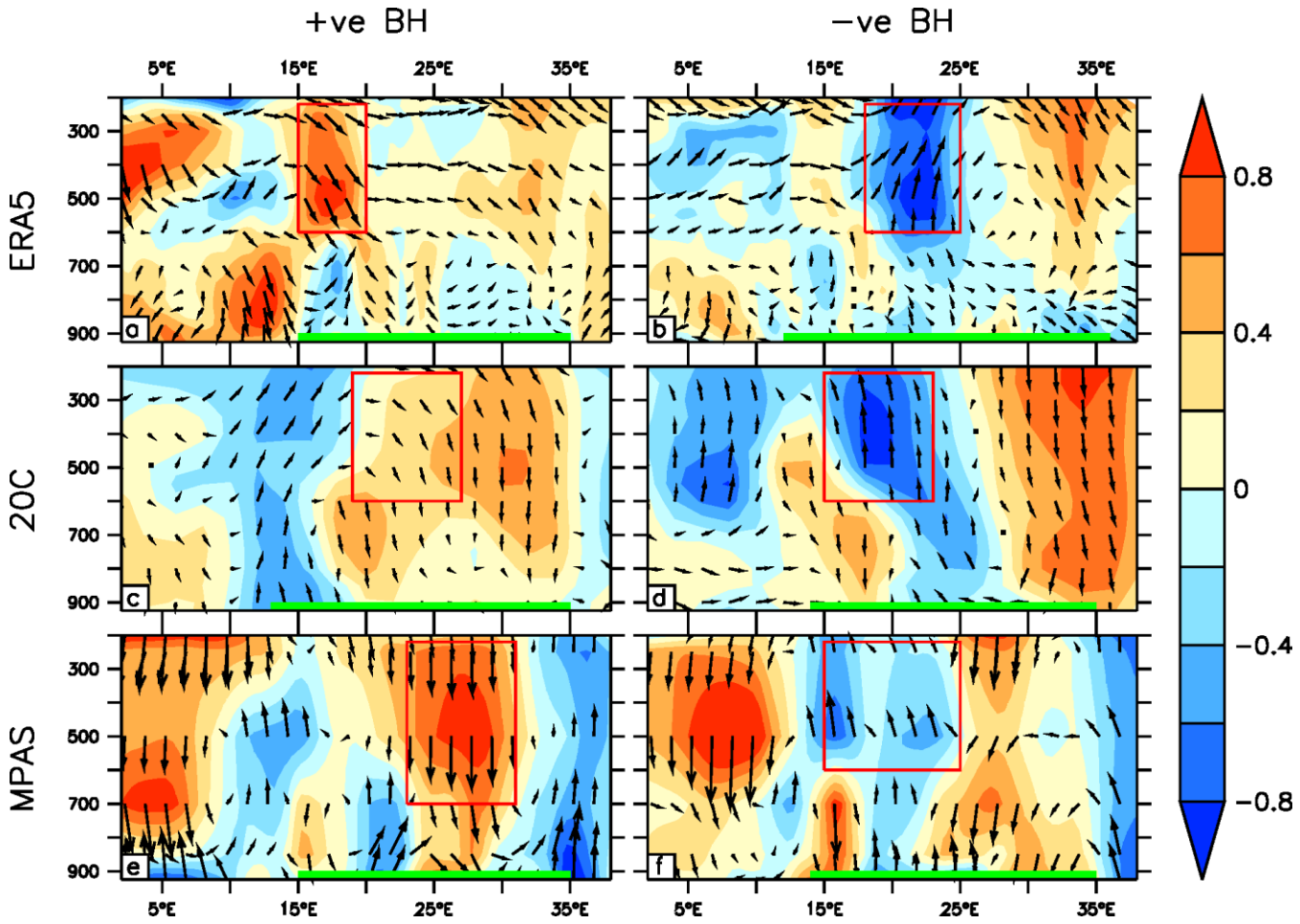

Fig 4. 9: Composite of the standardized anomalies of JFM Omega during +ve Botswana High Years (1983, 1998, 2010) and -ve Botswana High Years (1989, 1994, 2008). The mean and standard deviation used in calculating the anomalies were obtained using the 1980-2010 data. The green box shows the location of the continent while the red box shows the Botswana High

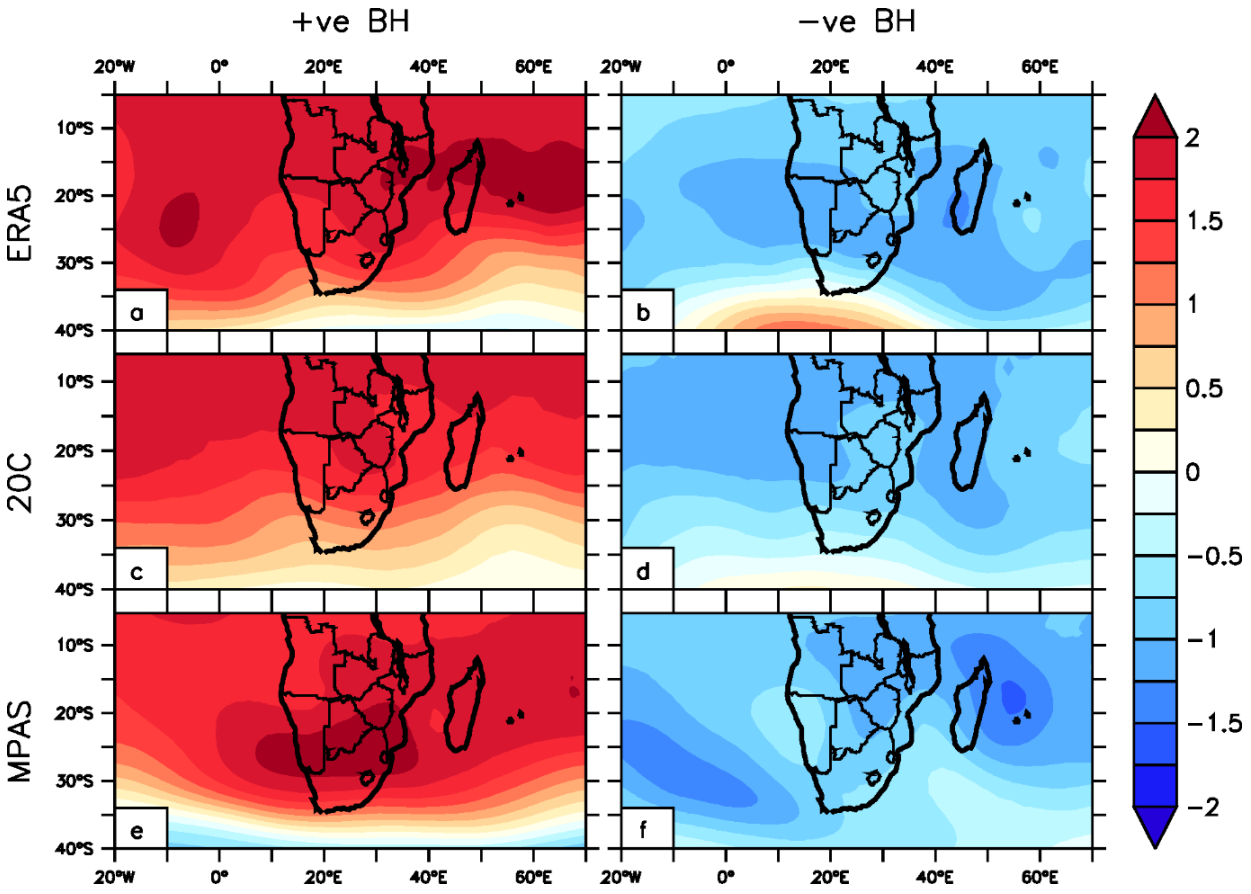

Fig 4. 10: Same as Figure 4.8 but for 500 hPa geopotential height

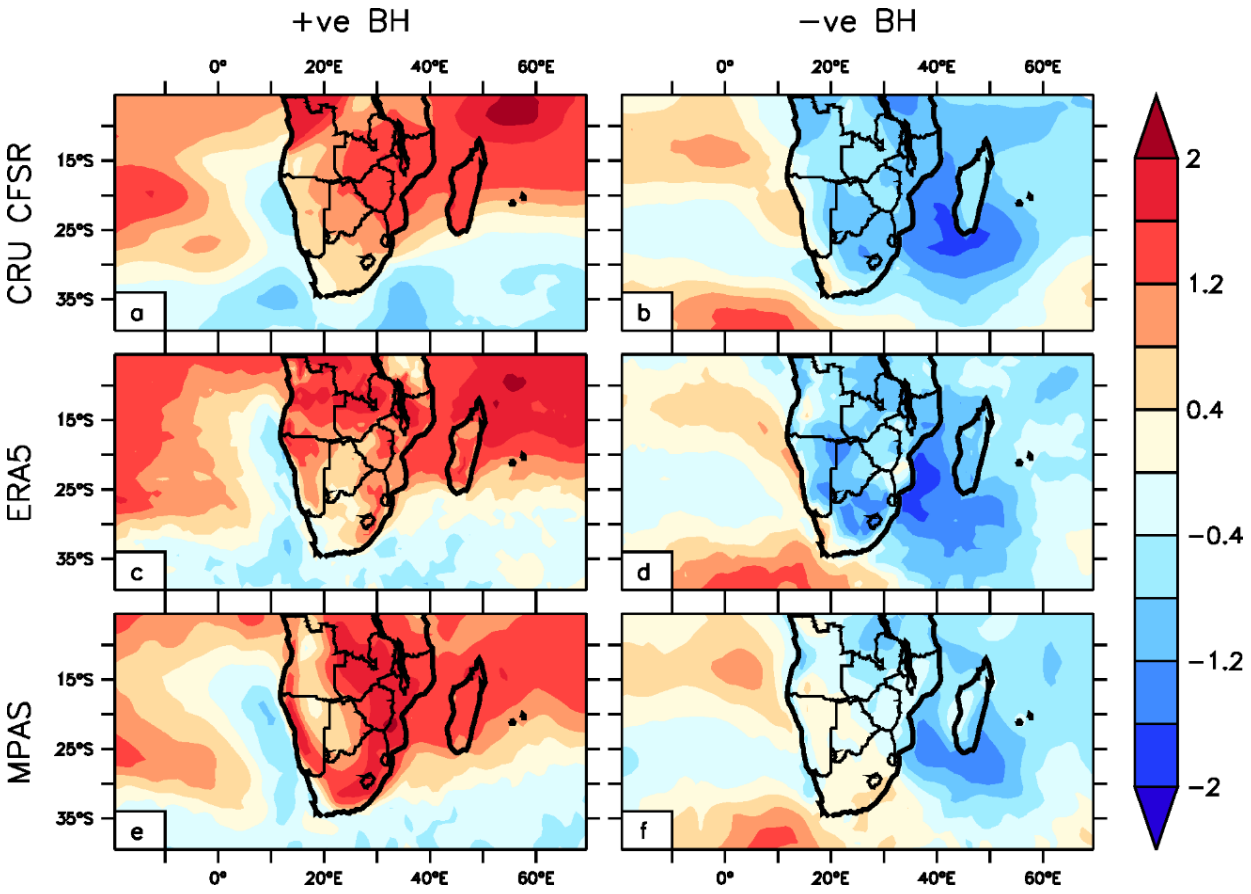

Fig 4. 11: Same as Figure 4.8 but for surface temperature

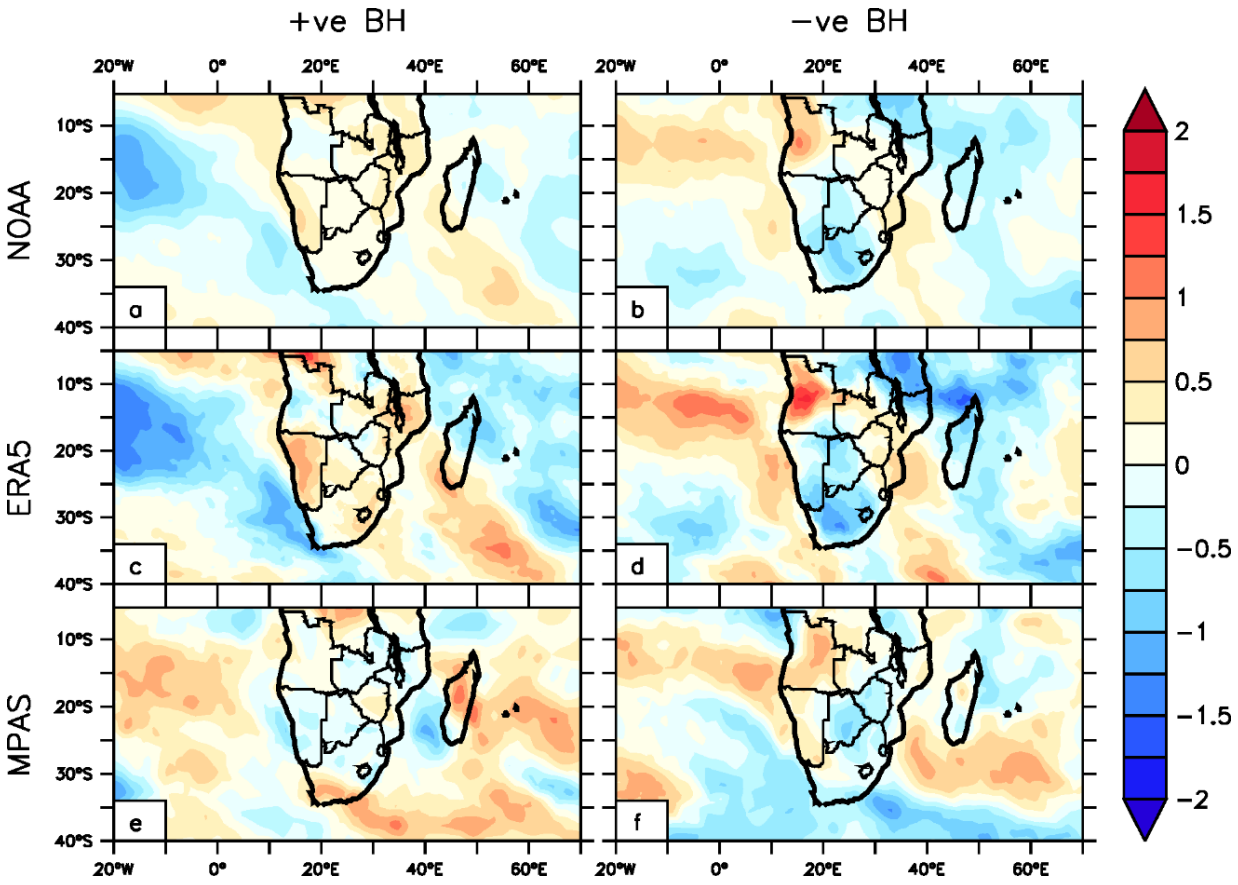

Fig 4. 12: Same as Figure 4.8 but for outgoing longwave radiation (OLR)

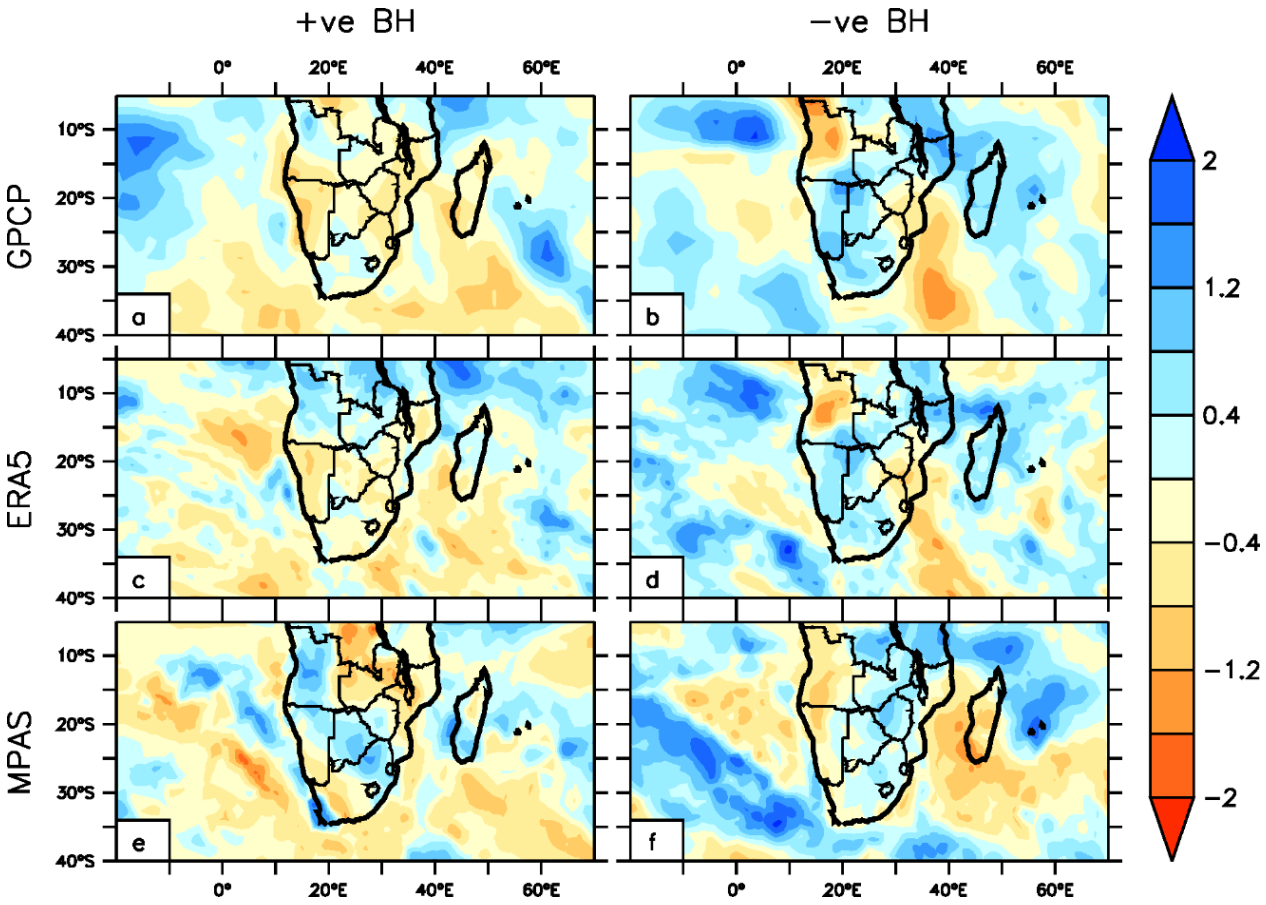

Fig 4. 13: Same as Figure 4.8 but for rainfall

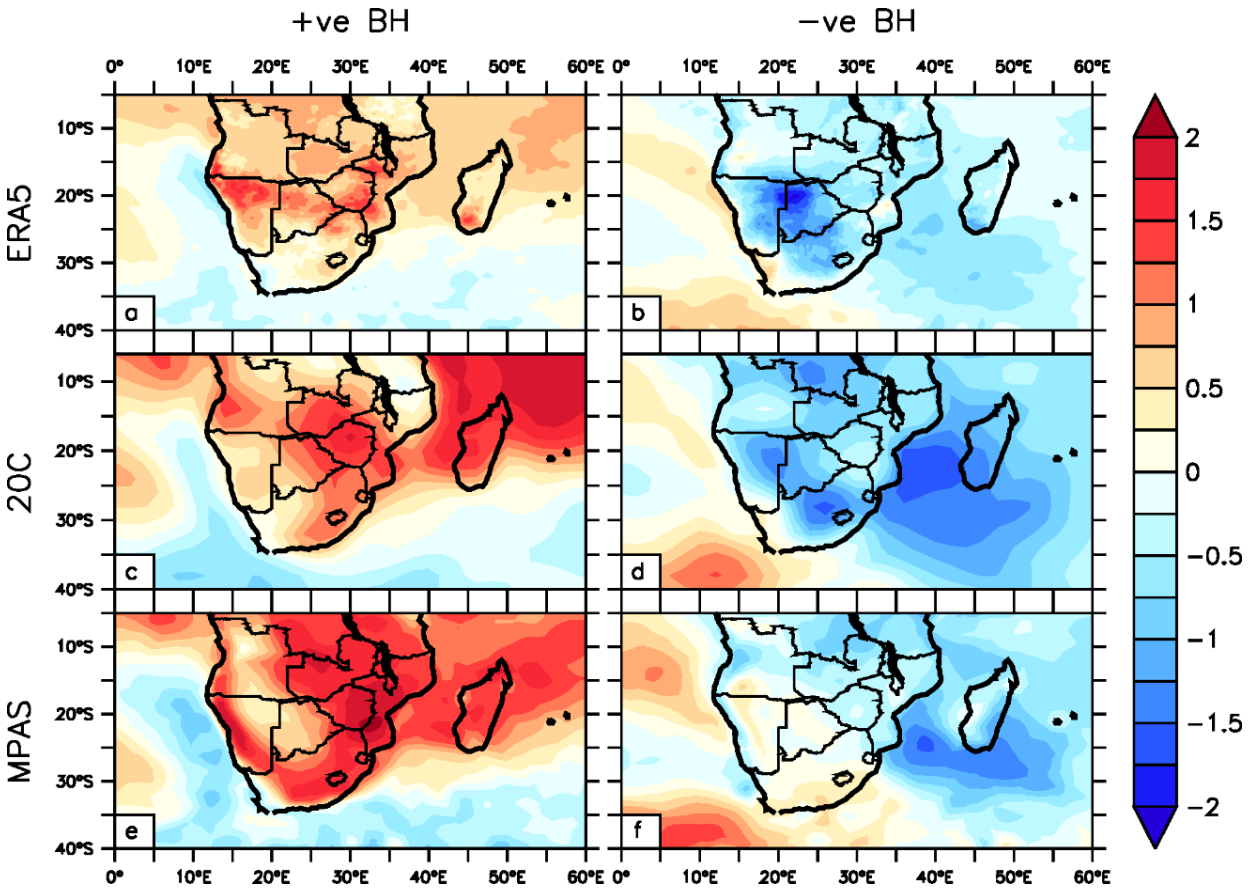

Fig 4. 14: Same as Figure 4.8 but for Potential Evapotranspiration (PET)

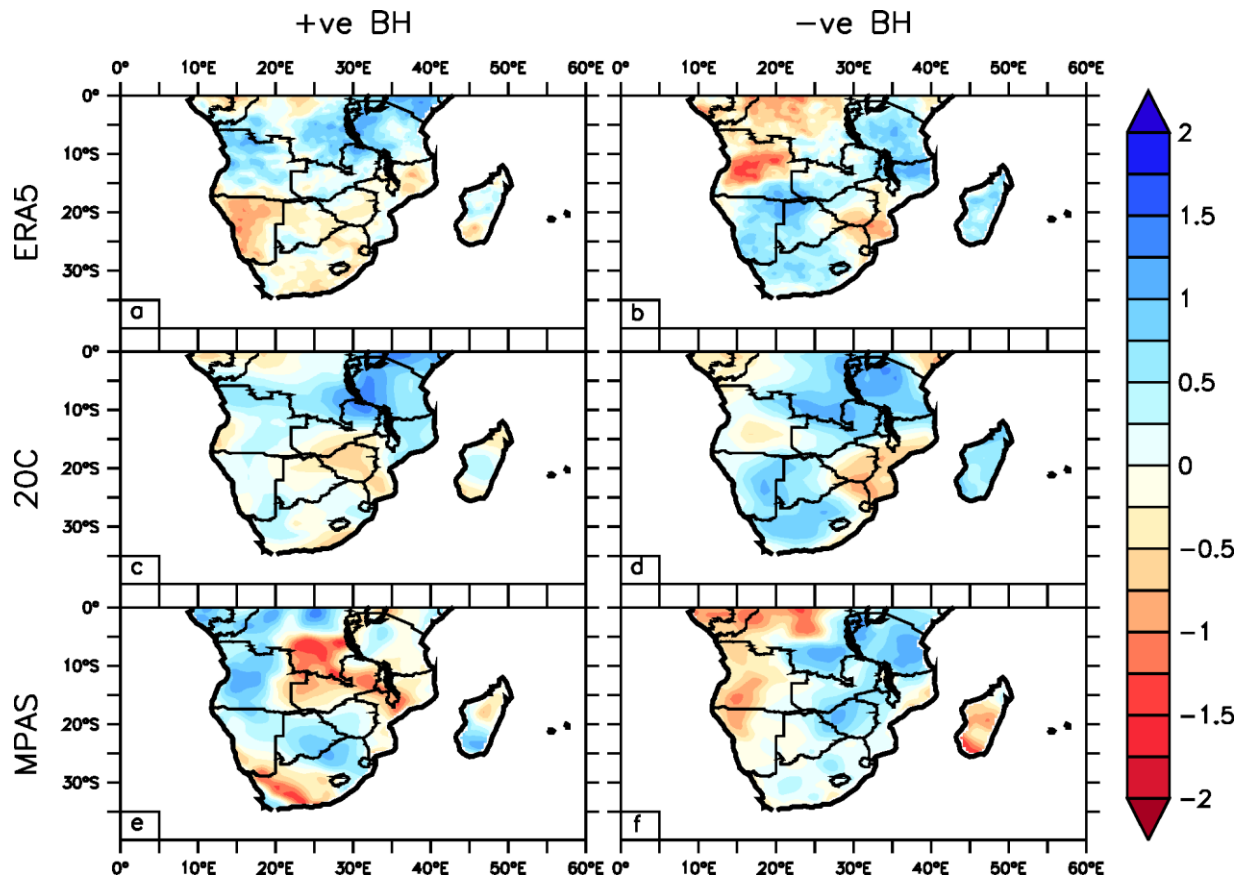

Fig 4. 15: Same as Figure 4.8 but for Standard Precipitation Index (SPI)

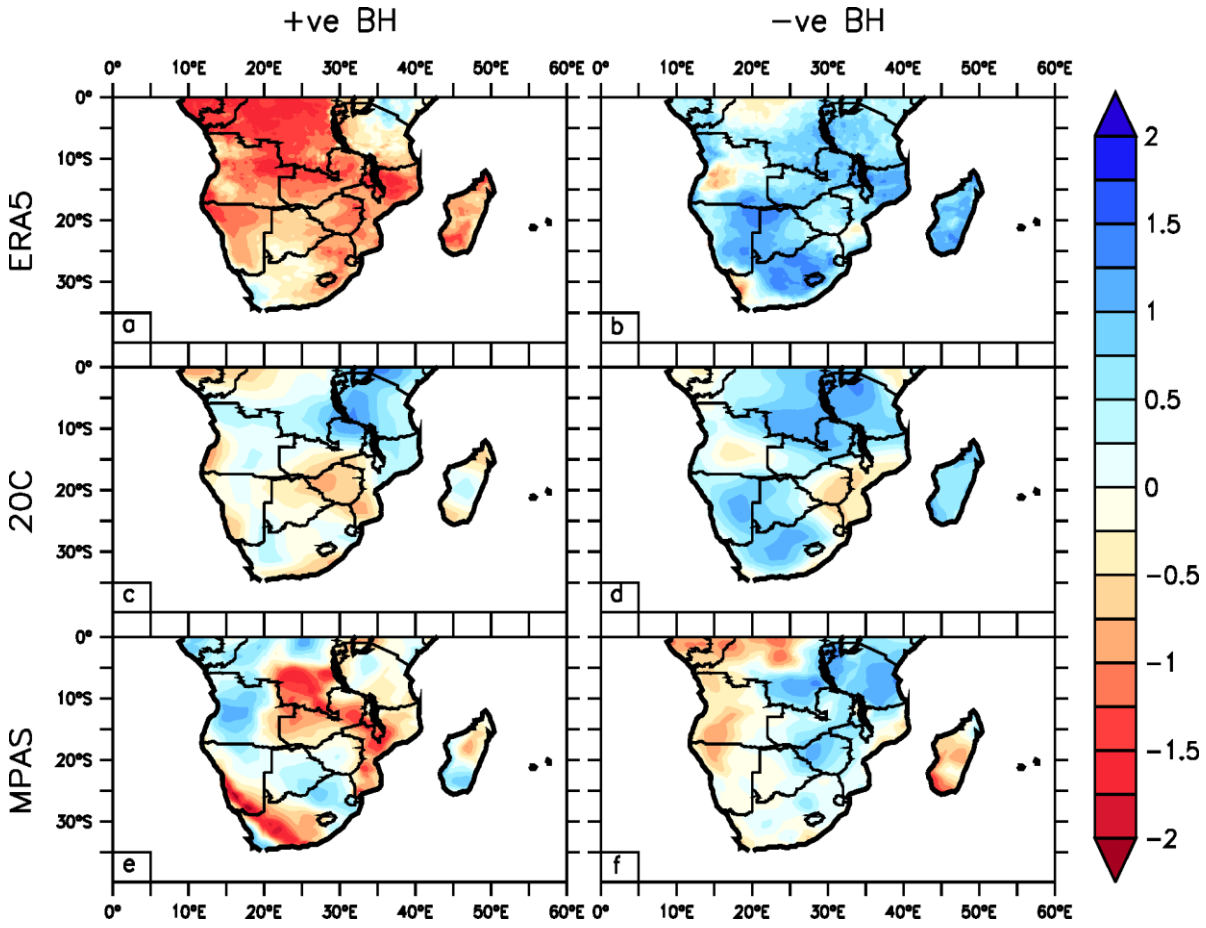

Fig 4. 16: Same as Figure 4.8 but for Standard Precipitation Evapotranspiration index (SPEI)

CHAPTER FIVE: THE INFLUENCE OF THE BOTSWANA HIGH ON DROUGHT MODES OVER SOUTHERN AFRICA IN OBSERVATION AND MPAS

This chapter examines the relationship between the Botswana High and drought modes over Southern Africa and investigates the capability of the Model for Prediction Across Scales version 5.2 (MPAS) model data in simulating the relationship. To analyse the spatio-temporal characteristics of drought modes over Southern Africa, this chapter applied Empirical Orthogonal Function (EOF) analysis on the Standard Precipitation Evapotranspiration Index (SPEI) and Standard Precipitation Index (SPI) data. The EOF algorithm was applied for the late summer season (JFM) between 1980 and 2010 over the Southern Africa domain (Fig 5.1). We present the results of this study in four phases. Firstly, we present the climatology of the 500 hPa geopotential height over Southern Africa and the spatial characteristics of the Botswana High as depicted by observation (reanalysis) and MPAS simulation. Secondly, we discuss the spatial characteristics of Southern African droughts. Thirdly, we discuss the influence of the Botswana High on drought. Lastly, we examine the atmospheric dynamics during the most frequent drought mode (DM) in observation and MPAS simulation.

5.1 Climatology of 500 hPa geopotential height and Spatial Distribution of Botswana High

Figure 5.2 (a, c and e) shows the late summer (JFM) climatology of the 500 hPa geopotential height (1980-2010) as depicted by reanalysis and model data. All datasets show a good agreement in the 500 hPa geopotential height, with a strong spatial correlation between 20C and ERA5 (r=0.99) and between MPAS and ERA5 (r=0.98). The reanalysis and model climatology show areas of high geopotential height in the latitudinal band between 10°S and 30°S and low geopotential heights poleward of 30°S, which is consistent with previous studies (Maoyi and Abiodun, 2021). Over the tropics, the ERA5 and 20C climatology show a strong anticyclone between the border of Namibia and Botswana (blue box), which resembles the centre of the Botswana High; however, MPAS does not capture this anticyclone well. The ERA5 and 20C Botswana High agree well with Reason (2016) and Driver and Reason (2017), who found a similar Botswana High pattern using the National Centres for Environmental Prediction (NCEP) reanalysis. In both the reanalysis and model data, the strong anticyclone

pattern extends from the Atlantic Ocean, covering much of Namibia, Botswana and the north-eastern regions of South Africa.

During the late summer season, all datasets show that the first EOF (EOF1) accounts for most of the variation (about ±85%) in the 500 hPa geopotential height over Southern Africa and exhibits a strong anticyclone pattern that is reminiscent of the Botswana High (Figs 5.2b, 5.2d and 5.2f). However, MPAS exhibits the strongest Botswana High pattern, while the 20C model shows the weakest. Note that the core of the Botswana High in the EOF1 analysis occurs north of its location in the geopotential height mean analysis (blue box Fig 5.2a). This is consistent with previous studies (i.e., Driver and Reason, 2017; Reason, 2018; Maoyi and Abiodun, 2021). The discrepancies between the EOF and mean analysis may be because the location of the Botswana High core in the mean analysis may be influenced by areas of strong high/low pressure near the core, resulting in a south-westward location of the core relative to the position in the EOF result.

5.2 Droughts modes

Figure 5.3 compares the spatial distribution of the SPEI drought modes (DMs: DM1, DM2, DM3, DM4, and DM5) in the datasets (CRU, ERA5, 20C, and MPAS). The five DMs (DM1 - DM5) jointly explain about 64%, 80%, 78%, and 74% of the total variance in the 3-month CRU, ERA5, 20C and MPAS SPEI, respectively. DM1 is the most dominant mode in all datasets and is characterised by widespread positive loadings over the subcontinent (Figs 5.3a, 5.3b, 5.3c and 5.3d). Among the datasets, MPAS features the best spatial correlation with CRU (r=0.64) in representing this drought mode, while 20C shows the worst correlation (r=0.16). DM2 (which is the second most dominant mode in CRU, third in ERA5 and MPAS, but fourth in 20C; Table 5.1) shows positive loadings over Zimbabwe, Mozambique, Zambia and parts of Namibia and Angola (Figs 5.3e, 5.3f, 5.3g and 5.3h). However, there are some inconsistencies among the datasets on the DM2 pattern, especially over South Africa. For instance, CRU and ERA5 show a negative loading over much of South Africa, while 20C and MPAS show a dipole loading pattern. The datasets feature a better agreement on the DM3 pattern, which is characterised by widespread negative loading over much of Namibia, Botswana and South Africa, while positive loading is found equatorward of 18°S. In CRU, the DM4 shows a negative loading over the eastern two-thirds of the subcontinent and positive loading over parts of Namibia and Angola. Both ERA5 and MPAS feature the same level of agreement with the

CRU (with r=0.43 and r=0.44, respectively) on the DM4 pattern, while 20C shows a poorer correlation (r=0.27). In all the datasets, DM5 is characterised by negative loadings over much of Namibia, southern Angola, northern Zambia and southern parts of Tanzania, except that the magnitude of the loading over northeast South Africa is stronger in 20C and MPAS. However, the presence of these drought modes (DM1 - DM5) in all the datasets indicates that they are unique and robust features over Southern Africa.

The characteristics of CRU DMs (DM1-DM4) described here agree with the four drought patterns (PF1-PF4, respectively) reported in Ujenzena and Abiodun (2014). However, there are some discrepancies (Fig 5.3). For instance, DM1 shows widespread positive loadings over much of the Southern African region (except over parts of Angola), Tanzania and northern Mozambique, while the PF1 shows positive loadings poleward of 10°S (Ujenzena and Abiodun, 2014). Another discrepancy is that while DM2 and PF2 agree on positive loading over Zimbabwe and Mozambique, DM2 features a negative loading over much of South Africa while PF1 limits it over the south-west tip of the country (i.e., Western Cape). DM3 agrees very well with PF3 in drought patterns except over Namibia, where DM3 shows a strong negative loading (about -0.6) while PF3 shows weak loading (about ±0.2). Likewise, the DM4 and PF4 patterns are similar, except that the magnitude of the negative loading is stronger in DM4 than in PF4. Another discrepancy between the DMs and PFs is that DMs (DM1 - DM4) explain a higher total variance (58%) than the PFs (PF1 - PM4; 46%; Ujeneza and Abiodun 2014). All these discrepancies may be due to the shorter analysis period (i.e., 1980-2010) used in the present study than the period (i.e., 1940-2009) used in Ujeneza and Abiodun (2014).

As indicated earlier, we investigate the sensitivity of drought patterns to the choice of drought indices by repeating EOF analysis using SPI. Figure 5.4 presents the results of SPI DMs, showing that the five SPI DMs jointly explain about 64%, 73%, 76%, and 75% of the total variance in the 3-month CRU, ERA5, 20C and MPAS SPI. In general, there is a good agreement between the SPEI and SPI DMs. For example, with both SPEI and SPI, DM1 explains the highest variation in all datasets. In addition, the correlation between the spatial distribution of SPEI and SPI DMs is generally high, especially in CRU and MPAS ($r > 0.95$ for all DMs) and 20C ($r > 0.82$ for DM1 and DM2), suggesting these DMs can be identified with either SPEI and SPI. However, the similarity between SPEI and SPI DMs is weaker in the reanalyses (ERA5 and 20C) than in CRU and MPAS. For example, in CRU and MPAS, the total variance of the DMs is the same for SPEI and SPI, but in ERA5 and 20C, it is lower

for SPI. This decrease may be due to SPI using only rainfall to classify drought, as some of the SPEI variability might be due to variation in potential evapotranspiration, which is not included in the SPI variability. Furthermore, in some cases, the correlation between spatial patterns of SPEI and SPI DMs is poor in ERA5 and 20C ($r < 0.2$ for DM4 and DM5), indicating that these two DMs are not the same in SPEI and SPI results.

5.3 Influence of the Botswana High on Drought Modes

Figure 5.5 shows the interannual variability of the Botswana High and the corresponding SPEI DMs. For CRU, we used the ERA5 Botswana High since the CRU dataset does not contain 500 hPa geopotential height; however, every other dataset used its own realisation of the Botswana High. The correlation between the Botswana High and DMs varies across the datasets. For instance, the Botswana High features its strongest correlation with DM1 in CRU ($r = -0.35$) and ERA5 ($r = -0.85$), but with DM2 in 20C ($r = -0.30$) and MPAS ($r = -0.47$). While its weakest correlation is with DM2 in CRU ($r = -0.10$) and ERA5 ($r = -0.02$), it is with DM4 in 20C ($r = -0.05$) and MPAS ($r = -0.00$). The discrepancies among the datasets on the correlation between the Botswana High and DMs may be due to the differences in the characteristics of each DM across the datasets, as discussed in Section 5.2. However, DM1 negatively correlates with the Botswana High in all the datasets. Although the correlation is very strong in the ERA5 result ($r = -0.85$), it is weak in CRU ($r = -0.35$) and MPAS ($r = -0.42$) and very weak in 20C ($r = -0.10$). In ERA5, the correlation explains more than 70% of the variability in DM1 at the 95% confidence limit (Fig 5.5b). The negative correlation implies that the positive phase of DM1 (wet years; e.g. 1981, 1989 and 2000) is associated with a weak Botswana High while the negative phase of DM1 (drought years; e.g. 1983, 1992 and 2003) is characterised by a strong Botswana High. This is consistent with previous studies (Driver and Reason, 2017; Maoyi and Abiodun, 2021) that linked the Botswana High with droughts over Southern Africa because DM1 features high loadings over most parts of the subcontinent. Furthermore, Maoyi and Abiodun (2021) showed that the weak (i.e., 1981, 1989 and 2000) and strong (i.e., 1983, 1992 and 2003) Botswana High years correspond to the negative and positive phases of ENSO, respectively, while Ujeneza and Abiodun (2014) showed that ENSO has the most significant influence on PF1 droughts, which correspond to DM1 in the present study. Hence, these results suggest that the Botswana High might be a conduit pipe through which ENSO signals influence the DM1 over Southern Africa.

In CRU and ERA5, DM2 does seem to have a relationship with the Botswana High ($r < 0.01$). The poor relationship between DM2 and the Botswana High may be due to the more substantial influence of the Indian Ocean Dipole (IOD) than ENSO (Ujeneza and Abiodun, 2014). Ujeneza and Abiodun (2014) showed that PF2, which roughly corresponds to DM2 in this study, is influenced more by IOD than ENSO. Also, Maoyi and Abiodun (2021) showed that IOD does not influence the Botswana High and therefore, the ENSO signal feeding into the Botswana High might be too weak to influence DM2 droughts.

There are some relationships between the Botswana High and other DMs (i.e., DM3-DM5, especially in CRU and ERA5), but the R2 values indicate that the Botswana High does not explain the variabilities in the DMs. Ujeneza and Abiodun (2014) demonstrated that the Tropical North Atlantic (TNA) has a more significant influence on PF3 than ENSO (which roughly corresponds to DM3 for this study). Again, the influence of the ENSO signal feeding into the Botswana High in influencing DM3 drought may be too weak compared to the TNA signal. Ujeneza and Abiodun (2014), on the other hand, demonstrated that none of the teleconnections had a significant and persistent influence on PF4 drought modes (which roughly corresponds to DM4 for this study).

Figure 5.6 presents the Botswana High temporal variability and corresponding SPI DMs. The results are similar to those obtained from the SPEI drought modes (Fig 5.5). However, for most of the datasets (i.e., ERA5, 20C and MPAS), the DM1 and the Botswana High correlations are lower in the SPI results (Fig 5.6). This implies that the Botswana High correlates better with the DMs when the temperature is accounted for (i.e., using SPEI). This is consistent with Meque and Abiodun (2014), who found that ENSO correlates better with SPEI droughts than with SPI droughts over Southern Africa.

5.4 Atmospheric conditions with associated positive and negative phases of DM1

The previous sections (Sections 5.2 and 5.3) revealed that DM1 is the most dominant DM in Southern Africa and the most correlated DM with the Botswana High. Hence, this section presents the atmospheric dynamics associated with DM1 in the ERA5 dataset (Fig 5.3b) and examines how well MPAS reproduce the dynamics (Fig 5.3d).

5.4.1 ERA5 analysis

Figure 5.7 shows the 500 hPa geopotential height anomalies during wet years (column 1). The results show that wet years are generally characterised by low geopotential heights, which indicate cold air masses and enhanced convection. However, the geopotential height patterns vary from year to year. For example, 1981 and 1989 are characterised by strong troughs over the subcontinent, while 1989 and 2000 have strong closed lows (-ve Botswana High) centred near the Botswana High mean core. The -ve Botswana patterns produced the lowest PET anomalies (~-30 mm/month) (Figs 5.8g and 5.8i), which resulted in more intensive and widespread rainfall over the region (Figs 5.9g and 5.9i). However, more interesting is that the different tilts of the 1981 and 1986 troughs form dipole patterns over Namibia and Botswana. For example, the 1981 (Fig 5.7c) trough is oriented in the southeast-northwest (positive tilt) direction and forms a +ve PET over Namibia and -ve PET over Botswana. In contrast, the 1986 (Fig 5.7e) trough is tilted in the southwest-northeast (negative) direction and forms -ve PET over Namibia and +ve PET over Botswana (Fig 5.8e). The +ve tilt is consistent with the dryness over Namibia and wetness over Botswana (Fig 5.9c), while the opposite is true for the -ve tilt (Fig 5.9e). In connection to the low 500 hPa geopotential heights, PET shows a local cold bias over much of Botswana for wet years, except for 1986, which shows a local maximum near Botswana and a local minimum between Namibia and Angola's border. The discrepancy in the 1986 PET as compared to other years may be due to the -ve tilt (southwest-northeast) of the 500 hPa geopotential height trough (Fig 5.7g), which may result in severe thunderstorms westward of the trough and dry conditions to its east (Fig 5.9e). These severe storms may result from colder air on top of warmer air feeding from or near the surface and allowing for instability and convection westward of the trough. However, more research on the impact of -ve vs +ve tilted troughs over Southern Africa's climate is needed to confirm the veracity of the result.

Figure 5.7 (column 2) shows that drought years are characterised by high 500hPa geopotential heights, which may also increase surface temperatures over the region. Furthermore, just like the wet years, the drought's geopotential patterns vary by year. For instance, 1983 (Fig 5.7d) and 1992 (Fig 5.7f) have a similar pattern which is characterised by a closed anticyclone (+ve Botswana High) over the subcontinent as well as a low south of the continent. On the other hand, 1998 (Fig 5.7h) is characterised by a trough south of the continent, while 2005 (Fig 5.7j) is characterised by a ridging high south of the continent that pushes the trough eastward into the Indian Ocean. The +ve Botswana High pattern produces the highest and broadest PETs

(Figs 5.8d and 5.8f) over the subcontinent, resulting in drought over much of Southern Africa (Figs 5.9d and 5.9f). In the trough patterns (i.e., 1998 and 2005), PETs were mostly -ve over South Africa while some areas north of the country had +ve PET. In turn, this led to wet conditions over much of South Africa and drought north of the country (Figs 5.9h and 5.9j). Based on these results, one could argue that even though the 1998 Botswana High was one of the strongest on record, the trough pattern was stronger than the +ve Botswana High pattern (closed anticyclone), and instead of drought, it led to the unexpected wet weather over South Africa as mentioned by previous studies (Reason, 2016; Driver and Reason, 2017).

5.4.2 MPAS analysis

MPAS shows a good agreement with ERA5 on the 500 hPa geopotential heights for wet DM1 years (Fig 5.10 Column 1). All wet years show a decrease in the geopotential height over much of the subcontinent, which is consistent with the ERA5 results. In addition to that, MPAS can reproduce some of the geopotential height patterns as in ERA5. For example, the years 1980 (Fig 5.10c), 1988 (Fig 5.10e), and 2000 (Fig 5.10i) have a closed low pattern that is reminiscent of the -ve Botswana High. Furthermore, the MPAS year 2000 (Fig 5.10i) is comparable to the ERA5 year 2000 (Fig 5.7i) in the sense that both have a -ve Botswana High centre and anomalously +ve geopotential heights south of the continent. The -ve geopotential heights are consistent with the widespread -ve PETs as in Figures 5.11a, 5.11c, 5.11e, 5.11g and 5.11i, which correspond to the +ve rainfall anomalies. On the other hand, the 1988 PET (Fig 5.11e) shows a local maximum near the Botswana and Namibia border, consistent with the lack of rainfall in those areas (Fig 5.12e).

The MPAS 500 hPa geopotential height anomalies during drought years show a good agreement with ERA5 because all years indicate enhanced geopotential height over the tropics. In addition, the +ve Botswana High pattern is clearly visible in the MPAS composite (Fig 5.10b) as in the ERA5 (Fig 5.7b). 1991 and 1995 are dominated by a strong trough south of the continent (Figs 5.10d and 5.10f) which is responsible for the local PET minimums between Namibia and South Africa (Figs 5.11d and 5.11f). However, the localised -ve PET resulted in anomalous rainfall between southern Botswana and northern South Africa in 1995 (Fig 5.12f); however, it was not strong enough to cause anomalous rainfall in 1991 (Fig 5.12d). 2004 and 2010 (Figs 5.10h and 5.10j) are characterised by strong +ve geopotential heights, +ve PET (Figs 5.11h and 5.11j) and are consistent with dry climate over much of Southern Africa (Figs 5.12h and 5.12j)

5.5 Summary

This chapter has investigated the spatio-temporal structures of Southern African drought patterns, shown how the temporal variability of the Botswana High influences the drought modes and examines the capability of the MPAS in simulating the influences. The skill of the model in capturing the spatial variability of the 500 hPa geopotential heights and the Botswana High is quantified by comparing the simulated results with the ERA5 reanalysis. SPEI and SPI were used to characterize droughts over Southern Africa, while EOF analysis was applied on the 500 hPa geopotential height to extract the Botswana High feature and the drought indices to extract the drought modes. The relationship between the Botswana High and drought modes was quantified with correlation. The findings of the studies can be summarized as follows:

- The MPAS simulation captures the summer (JFM) 500 hPa geopotential height patterns over Southern Africa as in ERA5 during the study period (1980-2010). The spatial correlation between the MPAS simulation and ERA5 reanalysis is very high ($r > 0.90$).

- All the datasets (MPAS, ERA5 and 20C) agree that the Botswana High accounts for about 80% of the variability in the 500 hPa geopotential height over Southern Africa. However, the spatial pattern of the Botswana High simulated by MPAS features a better agreement with the ERA5 reanalysis than with the 20C reanalysis.

- In all the datasets (CRU, ERA5, 20C and MPAS), the most dominant five DMs (DM1-DM5) over Southern Africa jointly explain more than 60% of the interannual variability in the 3-month summer droughts for SPEI (64%, 80%, 78%, 74%, respectively) and for SPI (64%, 73%, 76%, 75%, respectively).

- ERA5 and MPAS agree that the Botswana High influences the interannual variability of DM1. However, the influence is strong in ERA5 ($r = -0.85$) and moderate in MPAS ($r = -0.42$). Wet years are characterised by a weak Botswana High, and drought years by a strong Botswana High. Also, the wet and dry years correspond to the -ve and +ve phases of the El Niño Southern Oscillation (ENSO), respectively. These results suggest that the Botswana High might be a conduit pipe through which ENSO signals influence DM1 over the region.

- In both ERA5 and MPAS, during the positive phase of DM1, the core area of the drought mode is characterized by negative anomalies in 500 hPa geopotential height (i.e., weaker Botswana High), cooler temperature, weaker PET, net cyclonic flow, stronger moisture convergence and positive anomalies in precipitation. The reverse is the case for the negative phase of DMI.

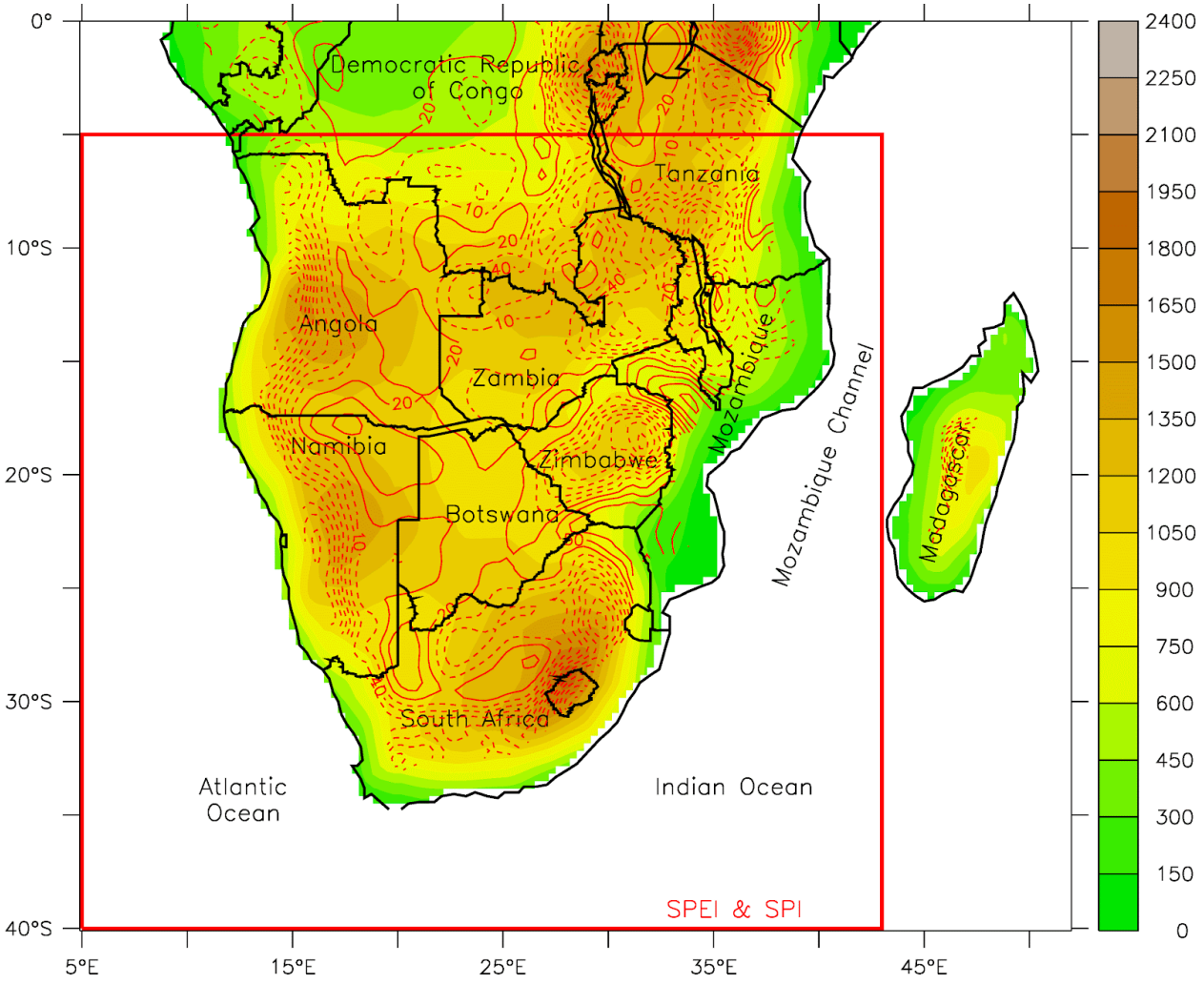

Fig 5. 1: The Southern African topography (in metres above sea level) as used in the MPAS model simulation. The contours show the biases (i.e., MPAS minus original topography) in the topography. The red box shows the SPI and SPEI EOF domain (5º-43º E; -5º -40ºS)

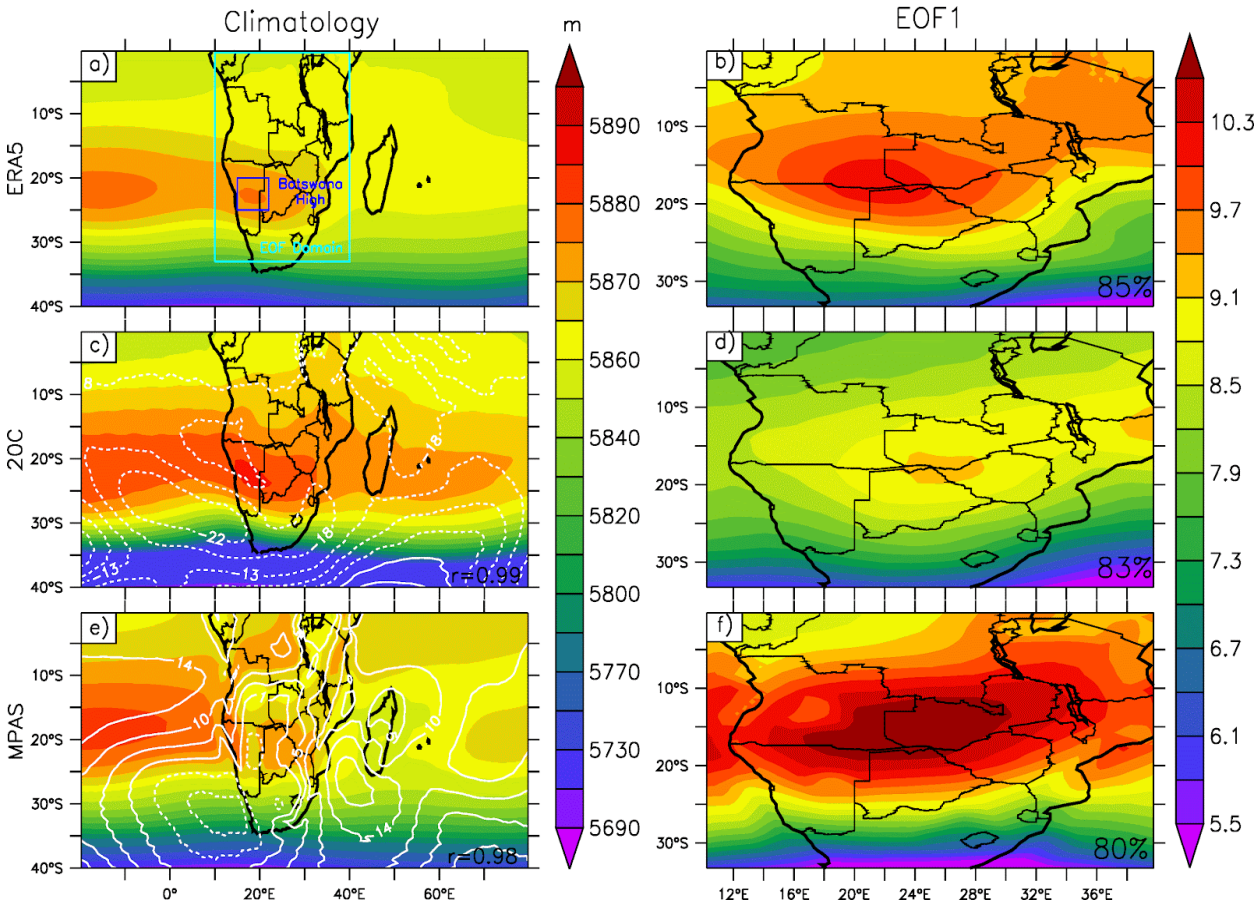

Fig 5. 2: The climatology (left column) and EOF1 (i.e., Botswana High; right column) of 500hPa geopotential height as depicted by ERA5, 20C and MPAS over Southern Africa (1980-2010). In the left column, the contours show the biases in the 20C and MPAS (with reference to the ERA5); the corresponding spatial correlation (r) is indicated at the bottom right corner. In panel (a), the green box indicates the area used for the EOF analysis, while the blue box shows the mean core area of the Botswana High (15°–22° E; 20°–25° S). In the right column, the percentage of variance explained by the EOF1 (Botswana High) is shown at the bottom right corner

Table 5. 1: The matching of the SPEI drought modes (DMs or EOFs) in CRU dataset with the closest EOFs mode in ERA5, 20C and MPAS datasets using correlation and root mean square errors with respect to CRU drought modes. In each cell, the three numbers in the first line represent the correlation coefficient for ERA, 20C and MPAS (respectively), while the three numbers in the second line show the corresponding RMSE. For each DM, the bolded values indicate the EOF chosen for the DM

DM CRU	EOF1 ERA5, 20C, MPAS	EOF2 ERA5, 20C, MPAS	EOF3 ERA5, 20C, MPAS	EOF4 ERA5, 20C, MPAS	EOF5 ERA5, 20C, MPAS
DM1	**0.54**, **0.16**, **0.64** **0.30**, **0.45**, **0.29**	0.75, 0.57, 0.13 0.55, 0.69, 0.80	0.19, 0.41, 0.34 0.56, 0.47, 0.57	0.11, 0.24, 0.27 0.57, 0.46, 0.57	0.16, 0.28, 0.16 0.56, 0.56, 0.56
DM2	0.26, 0.30, 0.10 0.63, 0.58, 0.57	0.35, 0.59, 0.04 0.64, 0.33, 0.56	**0.43**, 0.13, **0.56** **0.50**, 0.45, **0.58**	0.34, **0.17**, 0.29 0.31, **0.43**, 0.49	0.32, 0.29, 0.14 0.42, 0.30, 0.34
DM3	0.20, 0.06, 0.06 0.63, 0.54, 0.54	**0.72**, 0.26, **0.65** **0.67**, 0.45, **0.39**	0.51, **0.79,** 0.03 0.28, **0.62**, 0.47	0.06, 0.48, 0.08 0.36, 0.29, 0.37	0.06, 0.48, 0.08 0.36, 0.32, 0.42
DM4	0.17, 0.18, 0.30 0.64, 0.49, 0.61	0.11, **0.27**, 0.30 0.53, **0.46**, 0.59	0.18, 0.27, 0.23 0.35, 0.51, 0.47	0.37, 0.07, 0.30 0.27, 0.38, 0.31	**0.43**, 0.29, **0.44** **0.22**, 0.36, **0.38**
DM5	0.07, 0.27, 0.09 0.67, 0.47, 0.58	0.10, 0.42, 0.29 0.52, 0.57, 0.45	0.03, 0.13, 0.40 0.31, 0.50, 0.34	**0.46**, 0.03, **0.23** **0.36**, 0.38, **0.38**	0.01, **0.37**, 0.25 0.32, **0.25**, 0.28

Table 5. 2: Same as Table 5.1 but for SPI

CORR	EOF1 ERA5, 20C, MPAS	EOF2 ERA5, 20C, MPAS	EOF3 ERA5, 20C, MPAS	EOF4 ERA5, 20C, MPAS	EOF5 ERA5, 20C, MPAS
DM1	**0.87**, **0.29**, **0.65** **0.22**, **0.38**, **0.31**	0.11, 0.60, 0.19 0.65, 0.74, 0.80	0.24, 0.20, 0.24 0.60, 0.58, 0.56	0.03, 0.30, 0.35 0.58, 0.46, 0.59	0.20, 0.05, 0.10 0.50, 0.61, 0.55
DM2	0.33, 0.17, 0.06 0.63, 0.53, 0.57	0.02, **0.43**, 0.01 0.47, **0.38**, 0.56	**0.77**, 0.30, **0.44** **0.56**, 0.40, **0.57**	0.11, 0.07, 0.38 0.37, 0.39, 0.29	0.14, 0.43, 0.05 0.37, 0.31, 0.37
DM3	0.49, 0.36, 0.03 0.63, 0.57, 0.54	**0.75**, 0.36, **0.64** **0.57**, 0.42, **0.39**	0.15, **0.68**, 0.03 0.40, **0.59**, 0.47	0.30, 0.42, 0.12 0.43, 0.29, 0.42	0.13, 0.14, 0.46 0.33, 0.36, 0.42
DM4	0.17, 0.19, 0.31 0.59, 0.48, 0.62	0.27, 0.44, 0.42 0.35, 0.41, 0.61	0.12, 0.20, 0.26 0.40, 0.49, 0.49	**0.66**, 0.04, 0.37 **0.44**, 0.39, 0.42	0.20, **0.30**, **0.45** 0.28, **0.42**, **0.38**
DM5	0.07, 0.12, 0.12 0.56, 0.50, 0.58	0.30, 0.33, 0.32 0.45, 0.57, 0.45	0.16, 0.26, 0.29 0.35, 0.52, 0.37	0.41, **0.16**, **0.19** 0.27, **0.29**, **0.36**	**0.05**, 0.16, 0.26 **0.31**, 0.29, 0.29

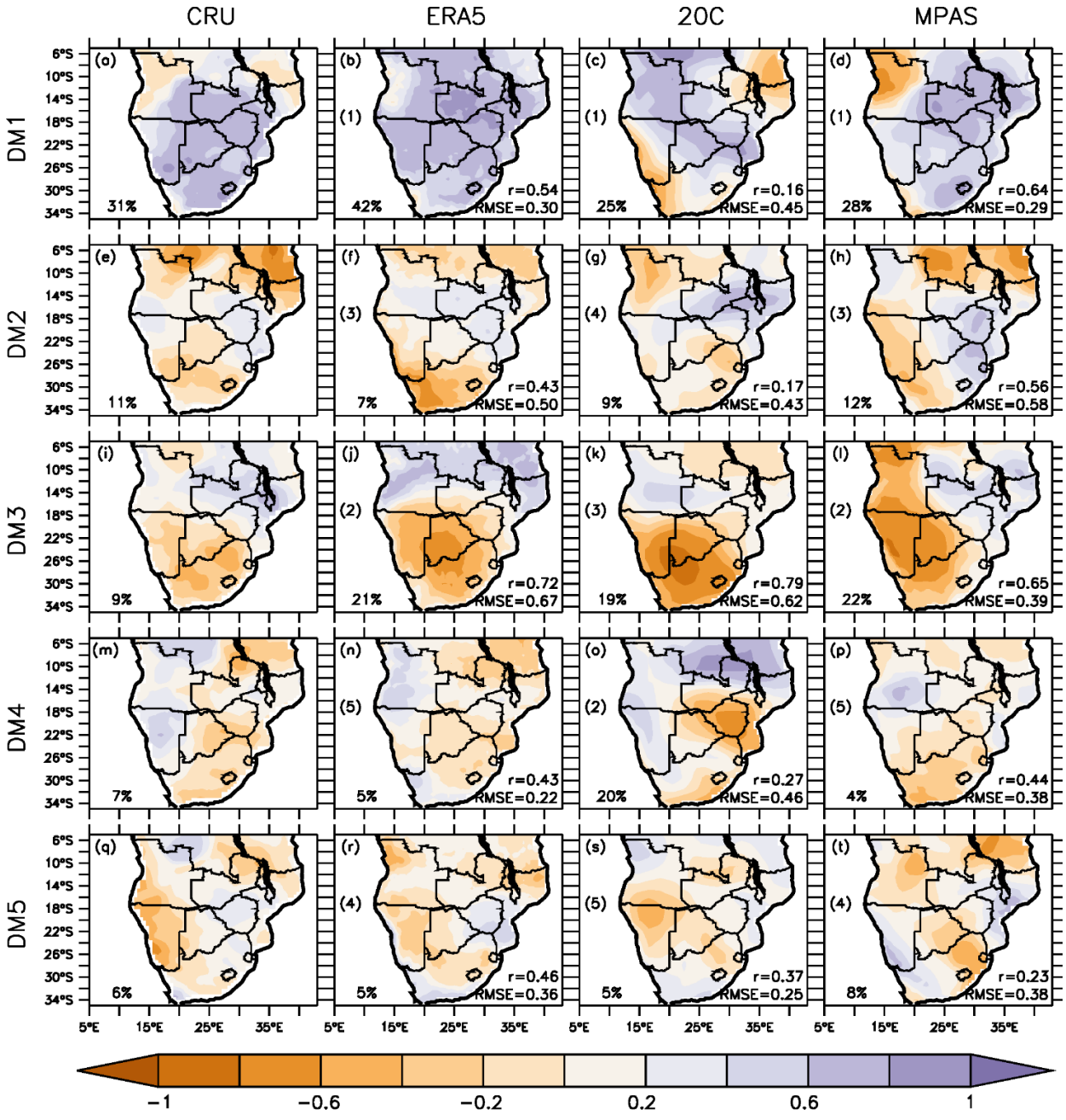

Fig 5. 3: The spatial variability of SPEI EOFs (at a 3-month scale) over Southern Africa. The number in the centre-left shows the EOF mode, while the number in the bottom left denotes the percentage of variance explained by the corresponding EOF mode. The spatial correlation (r) and root square mean (RMSE) error of each EOF mode with respect to CRU drought modes is shown in the bottom right

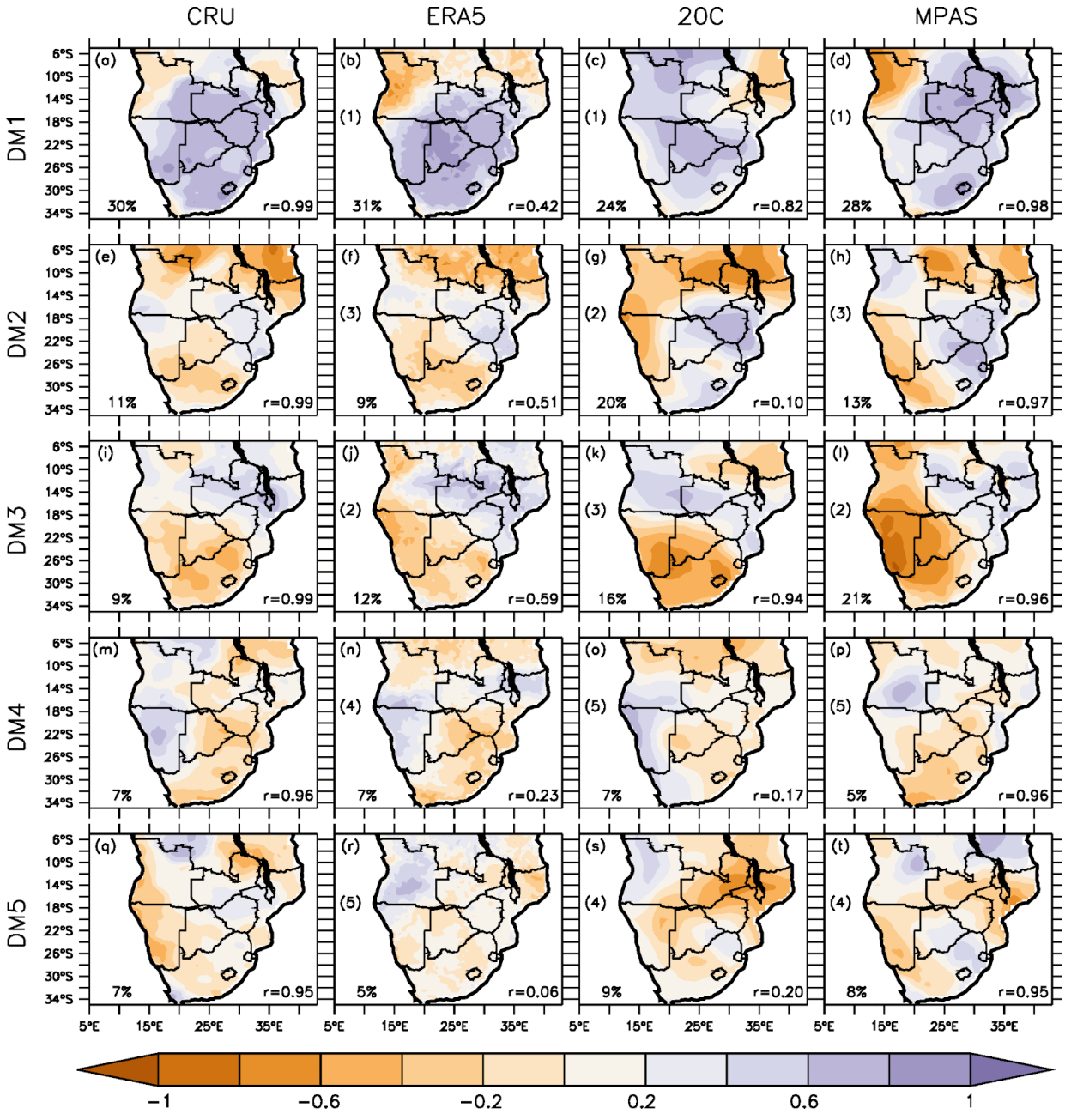

Fig 5. 4: The spatial variability of SPI EOFs (at a 3-month scale) over Southern Africa. The number in the centre-left shows the EOF mode, while the number in the bottom left denotes the percentage of variance explained by the corresponding EOF mode. The correlation between each DM for SPI and SPEI (in Fig. 5.3) is indicated in the lower right corner

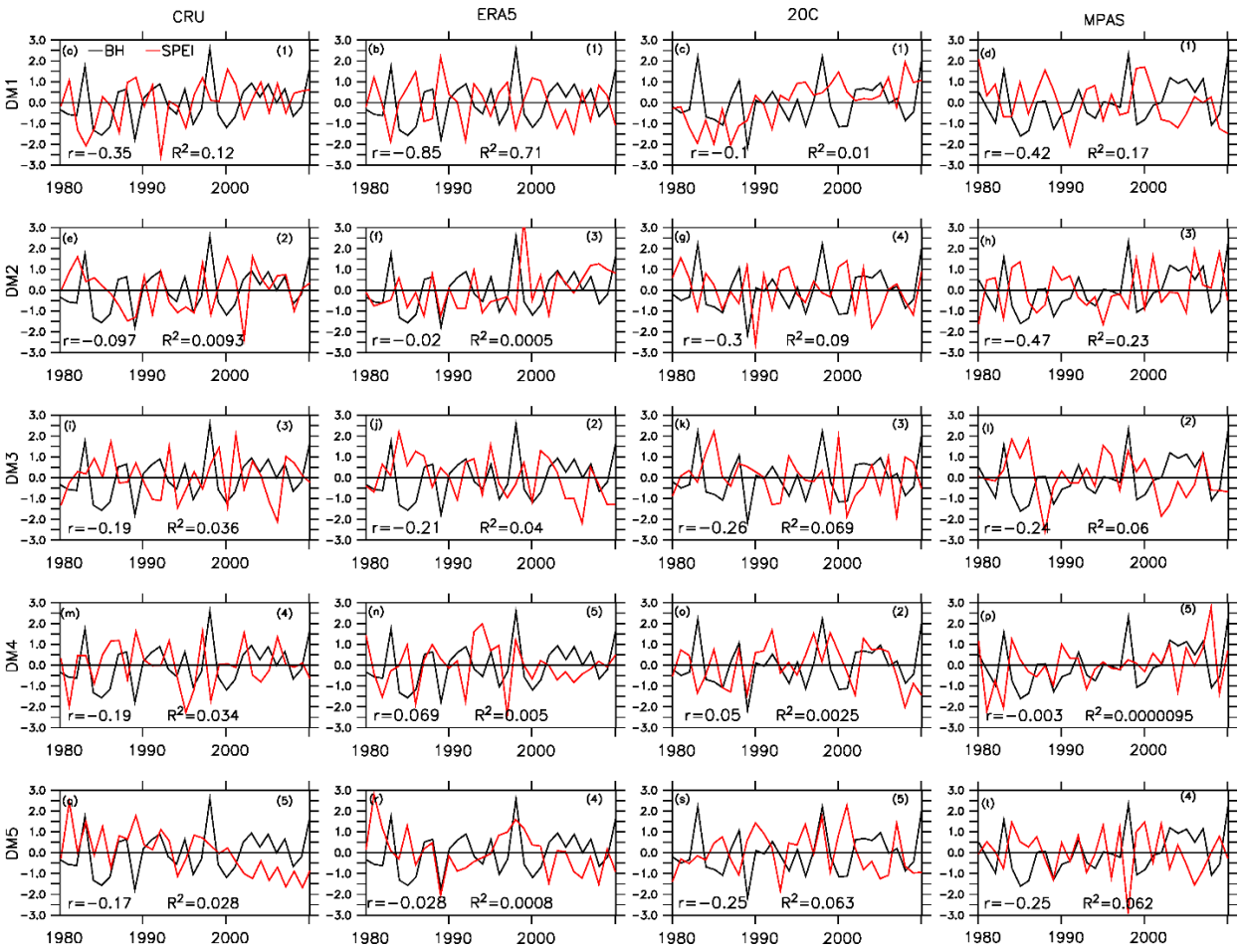

Fig 5. 5: The Interannual variability of SPEI EOFs (at a 3-month scale) and Botswana High over Southern Africa. The numbers on the top right indicate the SPEI EOF modes corresponding to Fig. 5.3. In addition, the correlation (r) and R-Square (RSQ) between SPEI and the Botswana High are indicated

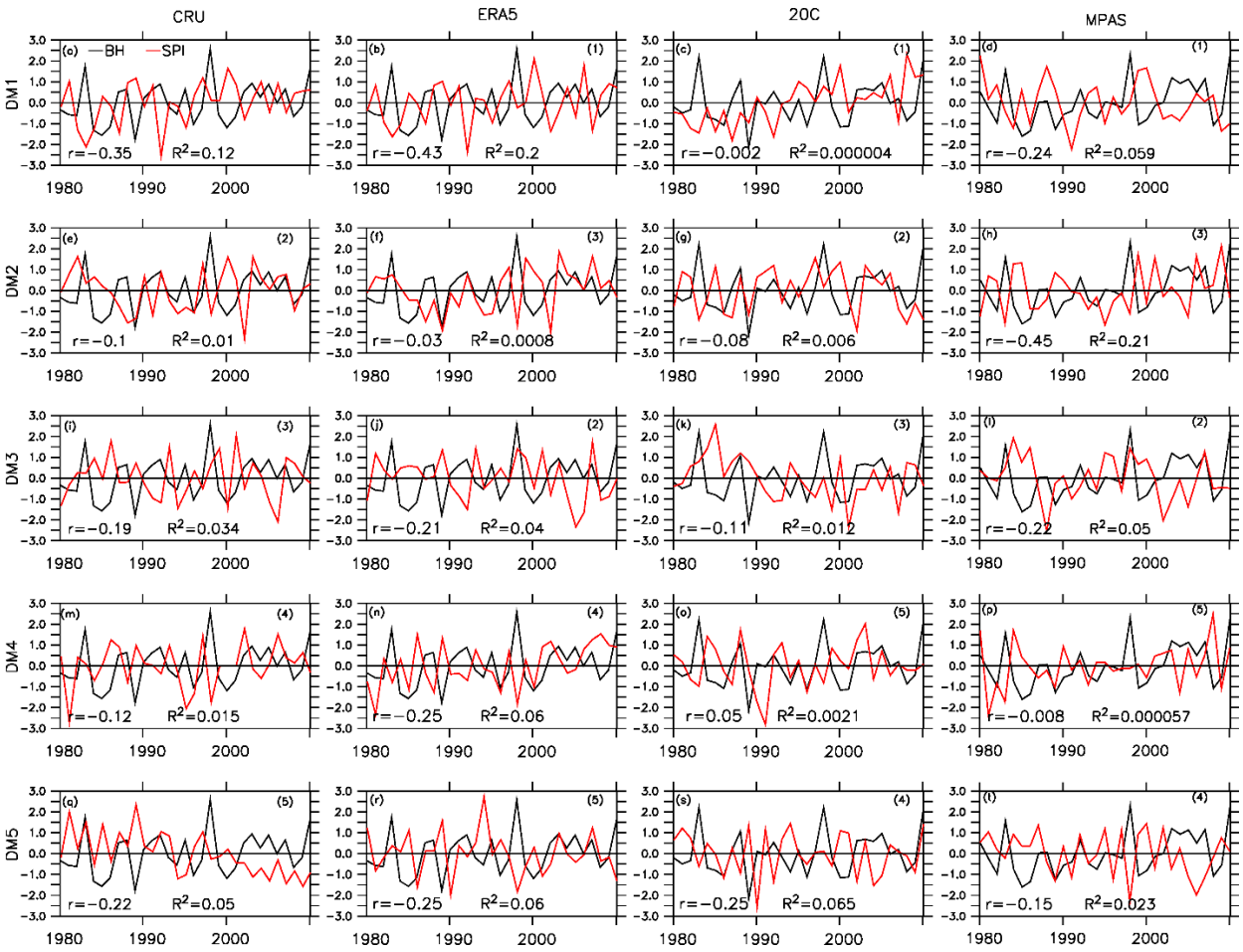

Fig 5. 6: Same as Fig. 5.5 but for SPI

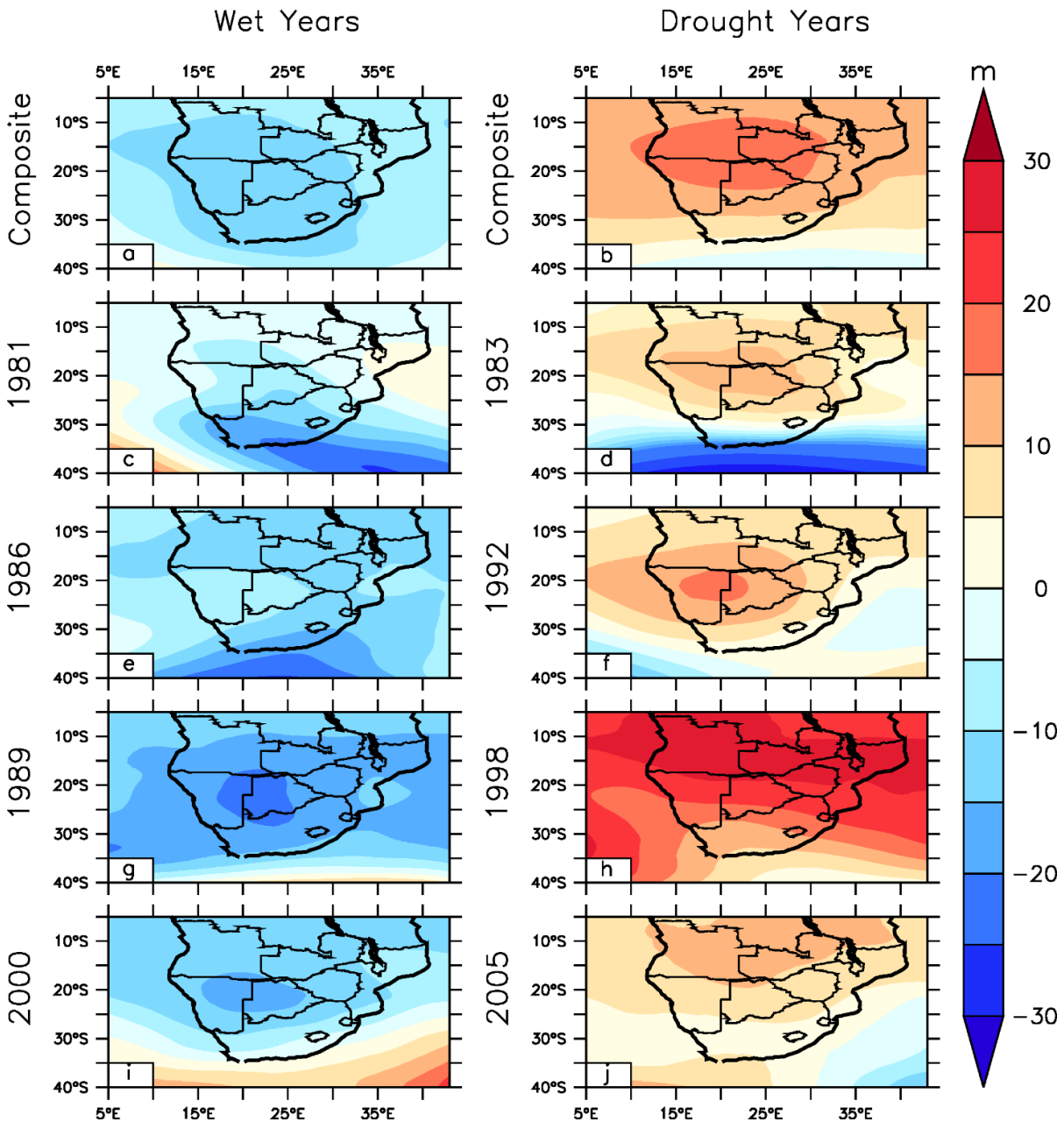

Fig 5. 7: Anomalies of JFM 500 hPa geopotential height during wet and drought years based on ERA5 SPEI EOF 1 (Fig. 5.5b). The mean used in calculating the anomalies was obtained using the 1980–2010 data

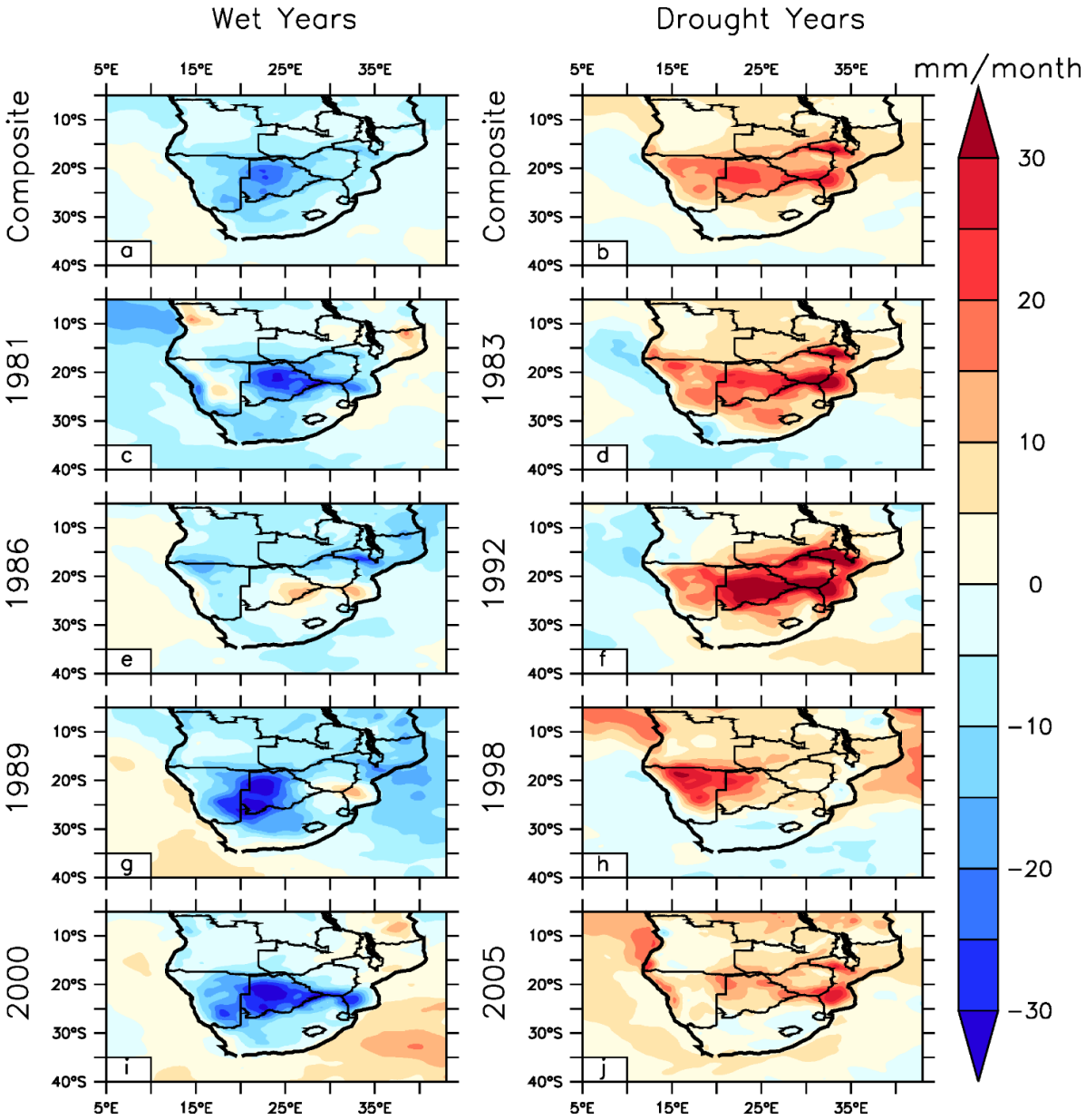

Fig 5. 8: Same as Fig. 5.7 but for PET

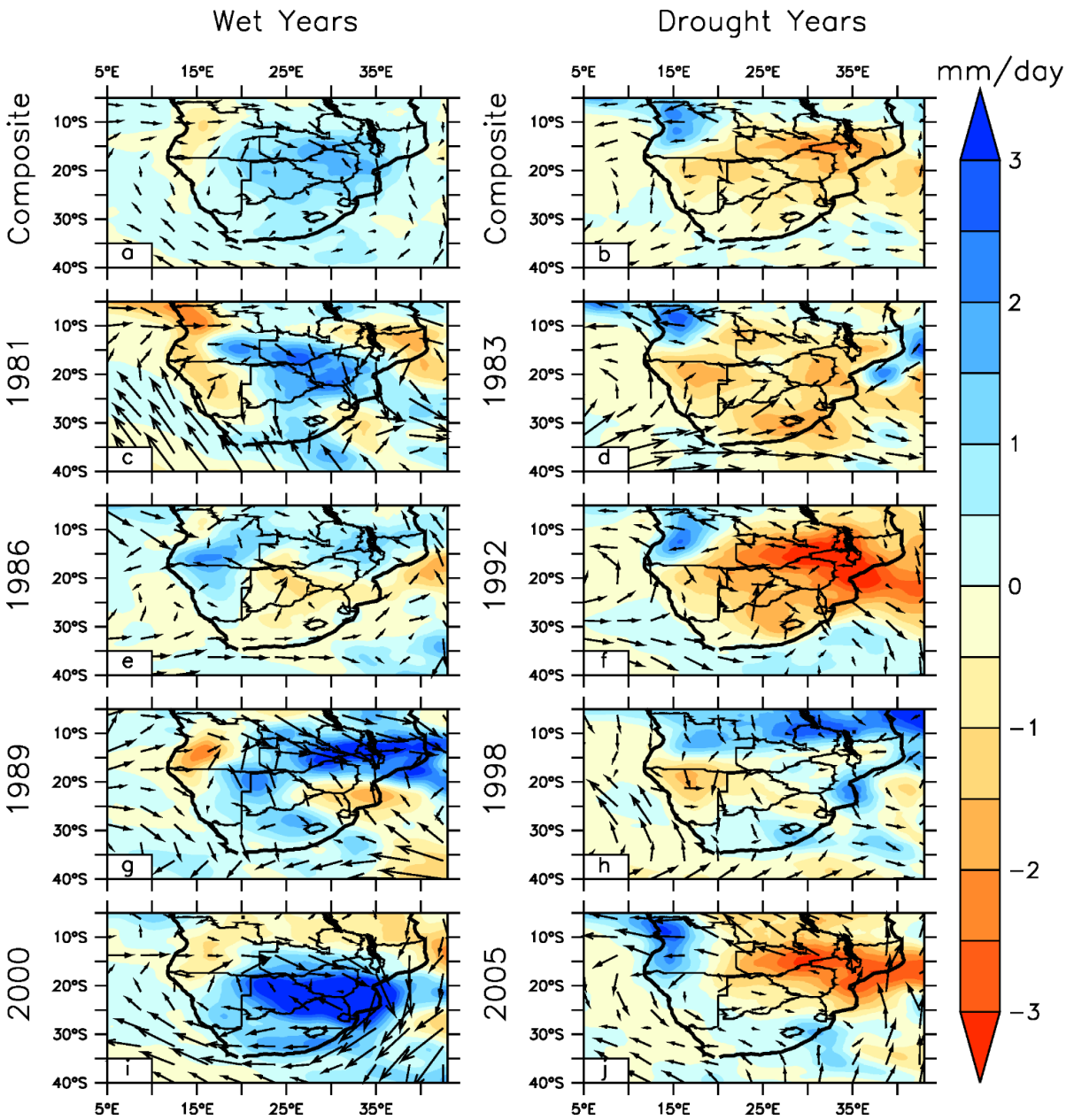

Fig 5. 9: Same as Fig. 5.7 but for rainfall and 850 hPa wind (m/s)

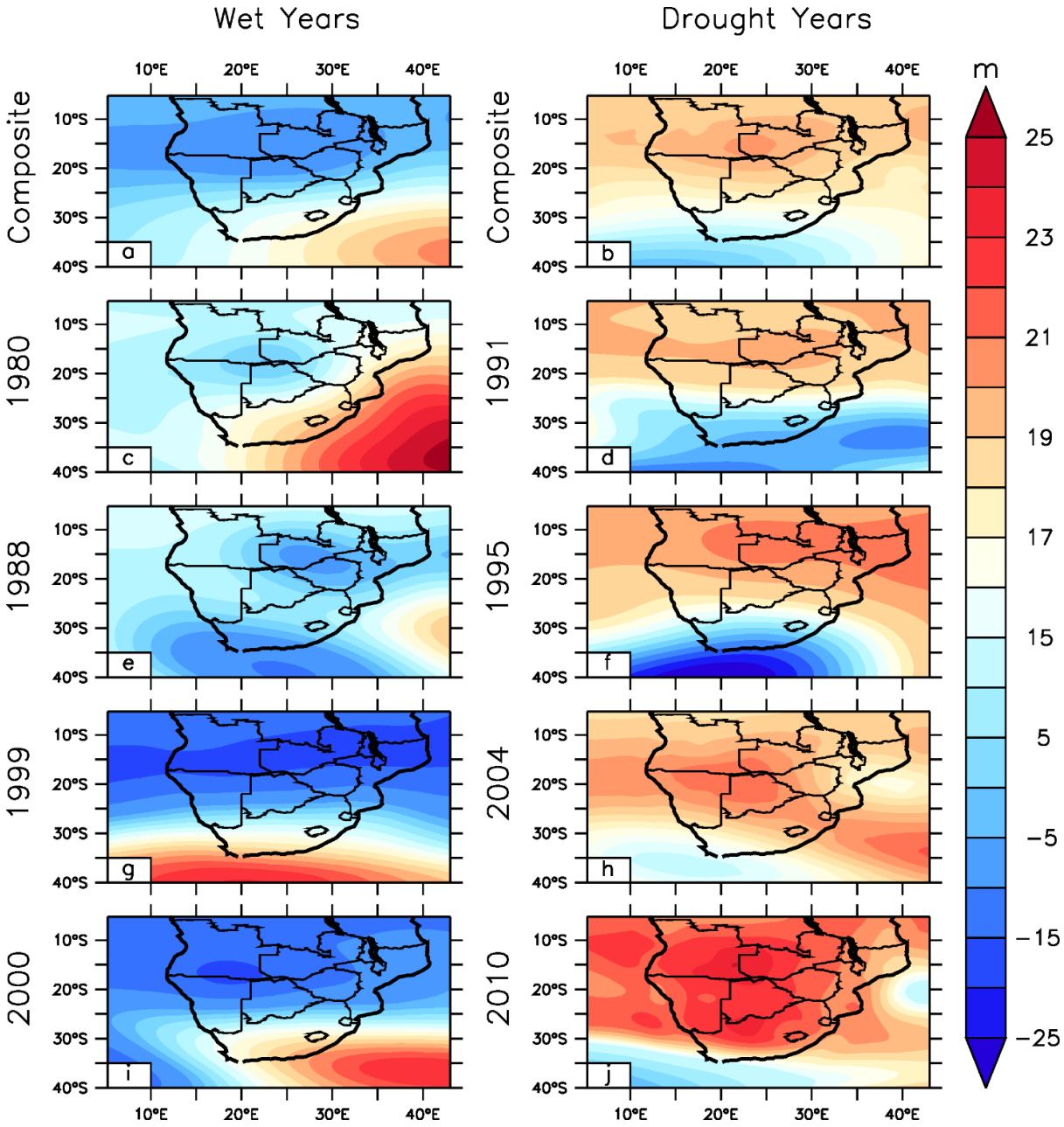

Fig 5. 10: Anomalies of JFM 500 hPa geopotential height during wet and drought years based on MPAS SPEI EOF (Fig. 5.5d). The mean used in calculating the anomalies was obtained using the 1980–2010 data

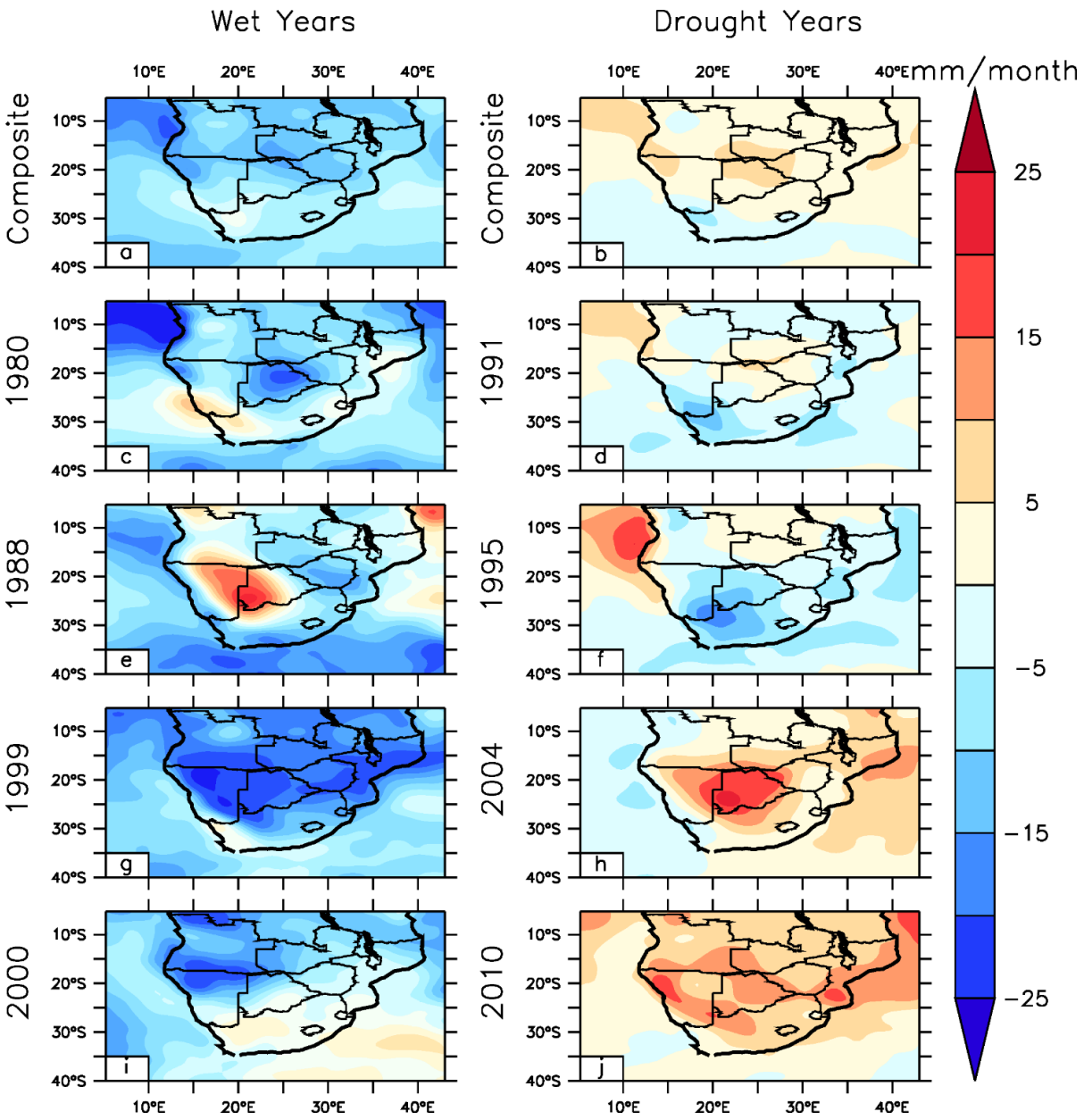

Fig 5. 11: Same as Fig 5.10 but for PET

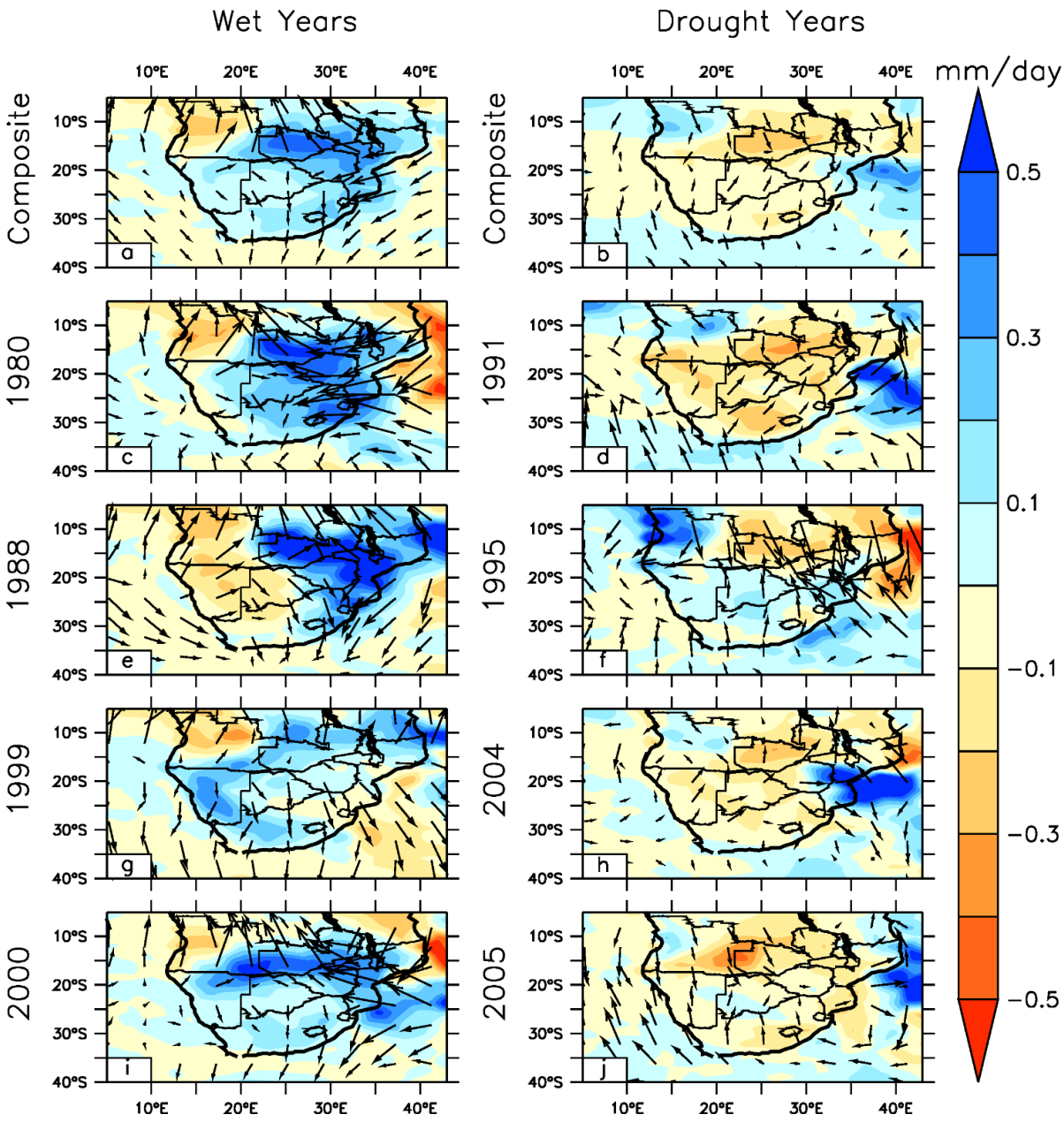

Fig 5. 12: Same as Fig 5.10 but for rainfall and 850 hPa winds

CHAPTER SIX: INVESTIGATING THE RESPONSE OF THE BOTSWANA HIGH TO EL NIÑO SOUTHERN OSCILLATION USING A VARIABLE-RESOLUTION GLOBAL CLIMATE MODEL

This study investigates the response of Botswana High to the 1982/1983, 1991/1992, 1997/1998 and 2009/2010 (hereafter 1983, 1992, 1998 and 2010 respectively) El Niños and 1984/1985, 1988/1989,1999/ 2000 and 2007/ 2008 (hereafter 1985, 1989, 2000 and 2008 respectively) La Niñas. Although this set does not include all ENSO events, we selected those years as they represent the strongest ENSO events between 1980 and 2010. We focus on the late summer season (JFM) when ENSO impacts are typically more significant and consistent than early summer (October to December) (Driver et al., 2017). For this investigation, we performed two experiments with the latest version of the MPAS (MPAS version 7.0; hereafter, MPAS) model. The first experiment (i.e., control experiment, hereafter CTRL) uses observed SST forcing everywhere, while in the second experiment (i.e., idealised experiment, hereafter NoENSO), observed SSTs were replaced by monthly climatological SSTs in the Pacific Ocean. We replaced observed SSTS with monthly climatology to remove the influence of ENSO and assay Botswana High's response to ENSO.

6.1 Relationship between the Botswana High and ENSO

Figure 6.1a shows a strong association in the interannual variability of the Botswana High and ENSO. The MPAS, MPAS5 and ERA5 show a high correlation between Botswana Highs and ENSO (r=0.84, r=0.81 and r=0.89, respectively). In addition, the Botswana High in MPAS shows a higher correlation with one in ERA5 (r=0.89) as compared to MPAS5 Botswana High (r=0.87). These results show that the MPAS model improves the simulation of the interannual variability of the Botswana High, although by a small margin. Both models and reanalysis indicate the strongest Botswana Highs during the strong El Niño years (1983, 1998 and 2010), while the weakest Botswana Highs occurred in La Niña years (1985, 1989, and 2000) (Fig 6.1a). This is in agreement with previous studies by Driver and Reason (2017). However, the relationship is not strictly linear as there are cases where the intensity of ENSO is not proportional to the intensity of the Botswana High (e.g. El Niño 1983 vs El Niño 1998). Kao and Yu (2009) showed that the nonlinear relationship could be explained by the internal variability of ENSO SST anomalies within the Pacific Ocean, creating different ENSO patterns. Furthermore, Johnson (2013) and Gore et al. (2019) identified eight ENSO SST

patterns over the Pacific Ocean (four El Niño patterns and four La Niña patterns) which might impact the strength of the Botswana High differently.

Figure 6.1b shows a scatter plot between the Botswana High and ENSO. As mentioned above, there seems to exist a quasi-linear relationship between the Botswana High and ENSO. At a 95% confidence limit, the adjusted R^2 values indicate that ENSO explains about 70%, 65%, and 79% of Botswana High variability in the MPAS, MPAS5 and ERA5 datasets, respectively. Again, the MPAS model improves the relationship between Botswana High and ENSO (70%) as compared to MPAS5 (65%). Given the strong association between the Botswana High and ENSO, the question then arises as to whether the Botswana High is a result of forcing from ENSO. To address this, the response of the Botswana High to the removal of ENSO forcing is discussed in section 6.3.

6.2 Composite Anomalies over Southern Africa

We evaluate the MPAS simulation over Southern Africa by comparing it with GPCP observation, ERA5 reanalysis and MPAS5 model data (Figs 6.2 and 6.3). The validation focuses on the spatial distribution of rainfall (Fig 6.2) and the 500 hPa geopotential height (Fig 6.3) in JFM of El Niño years (1983, 1992, 1998; and 2010) and La Niña Years (1985, 1989, 2000, and 2008). Figure 6.2 shows that MPAS simulates well spatial distribution of rainfall over Southern Africa, except that the simulation generally has a better agreement with GPCP during El Niño years composite (r=0.85; RMSE=1.67) than during La Niña years composite (r=0.80; RMSE=2.12). During the El Niño years, the model captures well the band of maximum rainfall over the tropics (associated with the South Indian Convergence Zone, SICZ) with a wet bias of about ±1 mm day^{-1}. It also reproduces well the rainfall over the eastern parts of the continent and areas of minimum rainfall over the central and western parts of South Africa and Namibia. Over Madagascar, the model fails to capture the local maximum rainfall as in GPCP. This lack of maximum rainfall over Madagascar may be attributed to the overestimation of deep convection over the Mozambique Channel (MC) area (Figs 6.2b, 6.2f, 6.2j, 6.2n and 6.2r), which may suppress convection over adjacent areas leading to the inability of MPAS to stimulate the local maximum rainfall over Madagascar.

During the La Niña years, the MPAS model underestimates the summer rainfall over the eastern and central parts of Botswana, Mozambique, and South Africa (by about 3 mm day^{-1}).

This may be attributed to the overestimated deep convection extending farther south of the MC (Figs 6.2d, 6.2h, 6.2l, 6.2p, and 6.2t), leading to the suppression of convective rainfall and a dry bias over the eastern and central parts of the Southern African continent. Furthermore, the overestimation of deep convection over the MC is greater in the MPAS variable grid than in the MPAS5 uniform-grid during La Niña. This reduces the accuracy of the MPAS in simulating the regional rainfall as compared to MPAS5. This result is consistent with Maoyi et al. (2017) and Driver et al. (2018), who noted a similar wet bias over the MC using a 50 km stretched-grid GCM (called CAM-EULAG). The wet bias could be due to the convective parameterisation in the model, which might be too sensitive to the warm boundary layer over the region. Another cause for this wet bias could be the horizontal resolution sensitivity of moist physics, as highlighted by Williamson (2008) or the parameterisation time step in the model simulation, as indicated by Williamson and Olson (2003).

MPAS shows good agreement with ERA5 on the spatial pattern of the 500 hPa geopotential height during El Niño years composite (r =0.96; RMSE=10.08) and La Niña years composite (r=0.96 RMSE=7.63). In general, both the MPAS and reanalysis show higher values of the 500 hPa geopotential height during El Niño years and Lower values during La Niña years, suggesting that El Niño (La Niña) summers may be the driving force in the strengthening (weakening) of the 500 hPa geopotential height over Southern Africa, which may lead to the strengthening (weakening) of the Botswana High. This result agrees with previous studies by Reason (2016) and Driver and Reason (2017), who also found that the high is always stronger (weaker) during El Niño (La Niña) summers. Furthermore, the strong spatial correlations (r > 0.9) indicate that the model has adequate skill in reproducing the dominating features of the 500 hPa geopotential height over Southern Africa but with some discrepancies. For instance, the model shows enhanced geopotential heights in the subtropics and lower anomalies poleward of 30°S as in ERA5. In addition to that, the model captures the local maximum geopotential height pattern over Southern Africa (which is reminiscent of the Botswana High) as in ERA5 (e.g. Figs 6.3a, 6.3e, 6.3i, 6.3m, 6.3q). Despite the higher resolution of the MPAS variable-grid simulation (48 km) than the MPAS5 uniform-grid simulation (240 km) over Southern Africa, MPAS results do not seem to always improve on that of MPAS5, as shown by the correlation and RMSE. While MPAS simulation outperforms the MPAS5 simulation in some years (i.e., 1992, 2010, 1989 and 2008), the opposite is true in other years (1983, 1998, 1985 and 2000). Several factors could make the higher-resolution MPAS simulation not always outperform the coarser-resolution MPAS5 simulation. For example, both models use different

land-use and topography data, which may impact results over high-lying regions over Southern Africa. Another reason could be the difference in the physics scheme between MPAS (WRF v4.0.3 physics) and MPAS5 (WRF v3.8.1 physics), which might have their strengths and weaknesses over Southern Africa.

6.3 Sensitivity Experiments

6.3.1 The response of the Botswana High to the removal of ENSO forcing

Figure 6.4 shows the interannual variability of the Botswana High in CTRL and NoENSO for the EOF analysis (Fig 6.4a) and spatial average analysis (Fig 6.4b). The time-series associated with the EOF Botswana High index (Fig 6.4a) shows good similarity with the spatial average Botswana High index. This result indicates that the EOF Botswana High is physically related to the temporal variability of the 500 hPa geopotential height over the Botswana High core region. Considering this, the impact of ENSO on the temporal variability of the Botswana High is evident. In general, NoENSO shows that with the removal of the ENSO forcing (El Niño or La Niña), the amplitude of variability in Botswana High reduces; however, the signal of the Botswana High variability still remains. This indicates that the Botswana High modes are independent of ENSO forcing while the magnitude of the variability is enhanced during ENSO events. Figure 6.4 also suggests that there are cases when ENSO forcing may alter the signs of the Botswana High mode, either from the +ve phase to the -ve phase (as in 1992) or from the +ve phase to the -ve phase (as in 2008). This may be due to the internal variability of ENSO SST anomalies within the Pacific Ocean, creating different ENSO flavours that may impact the Botswana High distinctively.

The 500 hPa geopotential height composites show good agreement with the Botswana High's interannual variability during El Niño Years (Figs 6.5a and 6.6a). At the regional scale (over Southern Africa), there is an overall decrease in the 500 hPa geopotential height over Southern Africa (Figs 6.5a, 6.5c, 6.5e, 6.5g and 6.5i) which is consistent with the decrease in the interannual variability of the Botswana High index in 1983, 1992, 1998 and 2010; however, the largest decrease is over the north-eastern parts of the Southern African region, which is typically an area of high precipitation associated with the SICZ. Basically, the removal of El Niño influence leads to increased convection over the SICZ area leading to increased precipitation over northern Madagascar, Mozambique Channel, and much of the north-eastern parts of the subcontinent. At the global scale (Figs 6.6a, 6.6c, 6.6e, and 6.6g), all El Niño years

(1983, 1992, 1998 and 2010) show that with the removal of an El Niño event, there is a decrease in the 500 hPa geopotential height over the tropics and an increase in the subtropics. This response represents a weakening of the Hadley circulation (Cook, 2000), and it is generally known from modelling and observational studies (Oort and Yienger, 1996; Roeckner et al., 1996). In addition to that, this decreases in the 500 hPa geopotential height over the tropics leads to a reduction in subsidence in the 500 hPa pressure level over Southern Africa (Figs 6.5a, 6.5c, 6.5e, 6.5g and 6.5i), which in turn reduces the strength of the Botswana High as seen in Fig 6.4.

La Niña composites (Figs 6.5b and 6.6b) show an opposite pattern in the 500 hPa geopotential heights compared to El Niño Composites. The regional circulation anomalies show an increase in subsidence over the region, especially over the Mozambique Channel, northern Mozambique, and northern Madagascar (Figs 6.5b, 6.5d, 6.5f, 6.5h and 6.5i). This anomalous increase in subsidence over the SICZ area may inhibit convection, increase temperatures, weaken the SICZ and lead to decreased precipitation. Reason (2016) attributed the formation of the Botswana High to heat released by tropical regions of high precipitation near the SICZ area. In light of this, the anomalous increase in subsidence and temperature over the SICZ may lead to the formation and strengthening of the Botswana High, as Reason (2016) stated. However, a model experiment similar to Lenters and Cook (1997) is required to prove the veracity of the results, which is beyond the scope of this work.

Globally, there is an overall increase in the 500 hPa geopotential height (NoENSO minus CTRL) over the tropics and a decrease over parts of the subtropics (Figs 6.6b, 6.6d, 6.6f and 6.6f). This pattern represents the strengthening of the Hadley circulation (Cook 2000). This increase in the 500 hPa geopotential height leads to an increase in subsidence over Southern Africa and strengthens the Botswana High, as shown by Maoyi and Abiodun (2021). The years 1985 and 1989 indicate a large increase in the 500 hPa geopotential height in the north-eastern regions of Southern Africa, which are the same years where there was the highest increase in the Botswana High strength due to the absence of La Niña (see Fig 6.4). In agreement with Maoyi and Abiodun (2021), this result implies that the Botswana High strength is sensitive to subsidence over this area during La Niña summers.

6.3.2 Atmospheric dynamics associated with El Niño

The difference in the 200 hPa velocity potential between NoENSO and CTRL years show an upper tropospheric divergence (negative velocity potential) over the Indian and Western Pacific Ocean (Figs 6.7a, 6.7c, 6.7e, 6.7g and 6.7i). This upper-level divergence is more pronounced over the northwest pacific and maritime continent, which coincides with deep convection from the warmer SSTs in the region. In contrast, there is a strong upper tropospheric convergence (positive velocity potential) over the eastern Pacific and South America, which coincides with cooler SSTs over that region. This convergence-divergence pattern across the Pacific is a reverse pattern of normal El Niño years and similar to a typical La Niña pattern. In normal El Niño years, the upper-level divergence is located over the eastern Pacific and South America, whilst the upper-level convergence is typically located over the western Pacific and maritime continent, including Australia. This normal pattern indicates a weakening of the Walker Circulation, which is typical during El Niño years (Reason and Jagadheesha, 2005, Ashok et al., 2007, Yuan et al., 2014, Gore et al., 2019). Therefore, the reverse pattern, which is the difference between NoENSO and CTRL, indicates that the Walker Circulation will strengthen in the absence of El Niño. 1983 and 1998 show the most strengthening of the Walker Circulation as they were the strongest El Niño years in the study period. The Southern African continent generally shows divergent flow, with some discrepancies. For example, the divergent flow over Southern Africa was weaker in 1998 and 2010 than it was in 1983 and 1992. This could be due to the Indian Ocean Dipole factor, which could also explain differences in ENSO impacts over Southern Africa (Chikoore and Jury, 2021). Despite that, the divergent flow over Southern Africa may strengthen the SICZ and aid in the formation of tropical temperate troughs (Tyson and Preston-Whyte, 2000) while weakening the strength of the Botswana High.

Figures 6.8a, 6.8c, 6.8e, 6.8g, and 6.8i show the difference between NoENSO and CTRL in the 200 hPa eddy stream function for each El Niño year, highlighting the large-scale stationary wave response. Taking the difference filters out the zonal mean response and only shows the difference in the wave response. All El Niño years show a strengthening of the cyclonic flow in the upper troposphere over the central and eastern Pacific Ocean, associated with the intensity of cooling of SSTs in the region. The strong ENSO event of 1998 generated the strongest anomalies, which indicates that the SST cooling was more intense during that year while the cyclonic flow extended as far as the western Pacific as in 2010. On the contrary, the South Atlantic and South Indian oceans show an increase in the upper tropospheric anticyclonic flow, indicating the warming of SSTs in the region. This warming of the two ocean basins may

increase convergence over the Southern African continent, leading to an overall weakening of subsidence in the 500 hPa level as in Figure 6.5, thus reducing the Botswana High's strength.

6.3.3 Atmospheric dynamics associated with La Niña

Figures 6.7b, 6.7d, 6.7f, 6.7h, and 6.7i show changes in the upper tropospheric divergence flow between NoENSO and CTRL. 1985, 1989 and 2008 show upper tropospheric divergence over much of the central and eastern Pacific and over much of the Atlantic Ocean, which coincides with deep convection from warmer SSTs. Contrary to that, there is an upper-level convergence (positive velocity potential) over much of the Indian Ocean, including Australia and the maritime continent, which corresponds to colder SSTs. This upper-level convergence over the Indian Ocean may result in a north-eastward shift of the SICZ (Cook, 2001) and tropical temperate troughs (Tyson and Preston-Whyte, 2000), strengthening drier conditions over Southern Africa. This convergence-divergence pattern is reminiscent of the weakening of the Walker Circulation (Gore et al., 2019) and typically takes place during El Niño events. In general, the weakening of the La Niña events will lead to an El Niño type of response in the atmosphere and vice versa. The year 2000 showed a similar pattern to other La Niña years, except for a weak convergence over the Pacific. 1985 and 1989 had the highest velocity potential over Southern Africa's northeast regions, which corresponds to the increase in subsidence over the region due to cooler SSTs. This corresponds well to the increase in the 500 hPa geopotential height as in Fig 6.6d and 6f and the larger strengthening of the Botswana High (1985, 1989) as in Fig 6.4 as compared to other La Niña Botswana High years (2000, 2008).

The difference in the eddy stream function at 200 hPa (NoENSO minus CTRL) shows anticyclones over the eastern and western Pacific Ocean (Figs 6.8b, 6.8d, 6.8f, 6.8h, and 6.8i). These anticyclones are characteristic of a Gill-Matsuno type response which is imminent due to the warming of Pacific Ocean SSTs (Cook, 2001; Wilson et al., 2014; Gore et al., 2019). This increase in the strength of anticyclones leads to a reduction in the cyclonic flow over the Pacific Ocean and the weakening of the Walker Circulation. All La Niña years indicate an increase in the cyclonic flow over the southern parts of South America, Africa, the Atlantic Ocean, and the Indian Ocean. This anomalous cyclonic flow in the upper troposphere indicates cooling SSTs over the region and may increase subsidence over Southern Africa, thus strengthening the Botswana High.

6.4 Summary

Previous studies have shown a strong relationship between ENSO and the Botswana High (Reason, 2016; Driver and Reason, 2017; Maoyi and Abiodun, 2021); however, the studies applied correlation and composite analysis, which cannot determine cause-and-effect in the relationship. Considering that, the present Chapter investigated the Botswana High response to ENSO using a variable-resolution GCM (MPAS) to better understand the relationship between the Botswana High and ENSO. Two experiments were performed. The first experiment used observed SST everywhere (control experiment, CTRL), while the second experiment used observed SSTs everywhere except over the Pacific Ocean, where monthly climatological SSTs were used (NoENSO experiment). The capability of MPAS in simulating the climatic features over Southern Africa and the temporal variability of the Botswana High were evaluated by comparing the models' historical simulations (CTRL, 1980-2010) with GPCP observation, ERA5 reanalysis and MPAS5 model data. The results of the study can be summarised as follows:

- The MPAS variable-resolution simulation reproduced the interannual variability of the Botswana High as in the ERA5 reanalysis. In all datasets, the Botswana High variability shows a strong link with ENSO ($r > 0.8$) and suggests a quasi-linear relationship between the Botswana High and ENSO.

- MPAS generally captures the summer (JFM) climatic variables over Southern Africa during El Niño and La Niña years, although with some biases across the region. However, in most cases, the results are comparable with GPCP observation and ERA5 reanalysis.

- Sensitivity experiments show that the Botswana High mode is independent of ENSO, but the amplitude of the modes amplifies during ENSO events.

- The removal of the El Niño forcing strengthens the Walker Circulation and results in upper-level divergence (200 hPa) over Southern Africa. This upper-level divergence weakens the 500 hPa geopotential height over the region resulting in a weak Botswana High. The opposite is true with the removal of the La Niña signal.

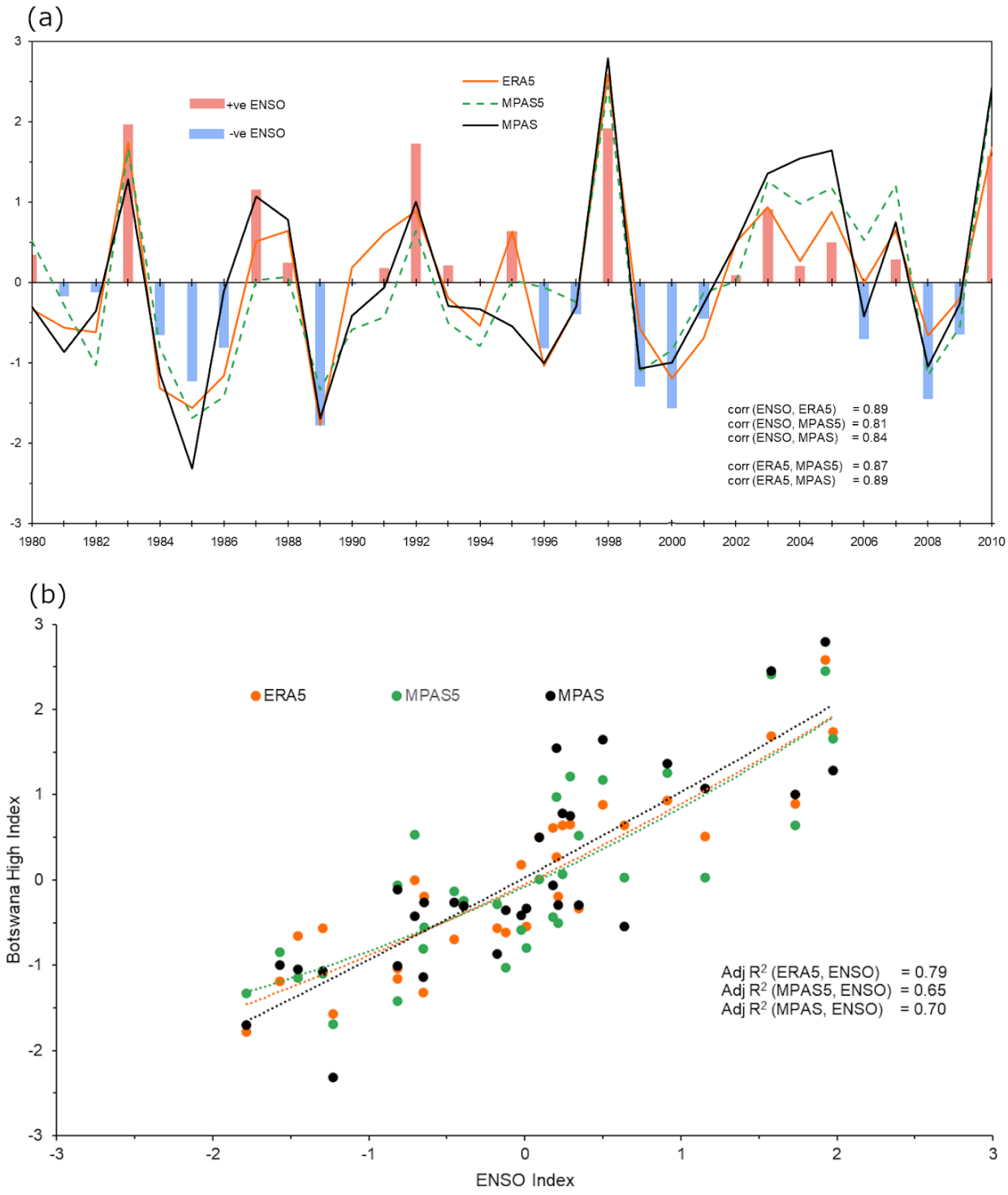

Fig 6. 1: (a) Interannual variability of the Botswana High as depicted by ERA5, MPAS and MPAS5. The bars show the ENSO Index. The Botswana High indices are derived from the scores of EOF-1 of JFM 500 hPa geopotential height over the study area (10-14°E, 0 -33°S) and the study period 1980-2010; (b) Scatter plot of the Botswana High Index (ERA5, MPAS and MPAS5) versus ENSO index for the same period. The lines represent the line of best fit, while R^2 is the coefficient of determination

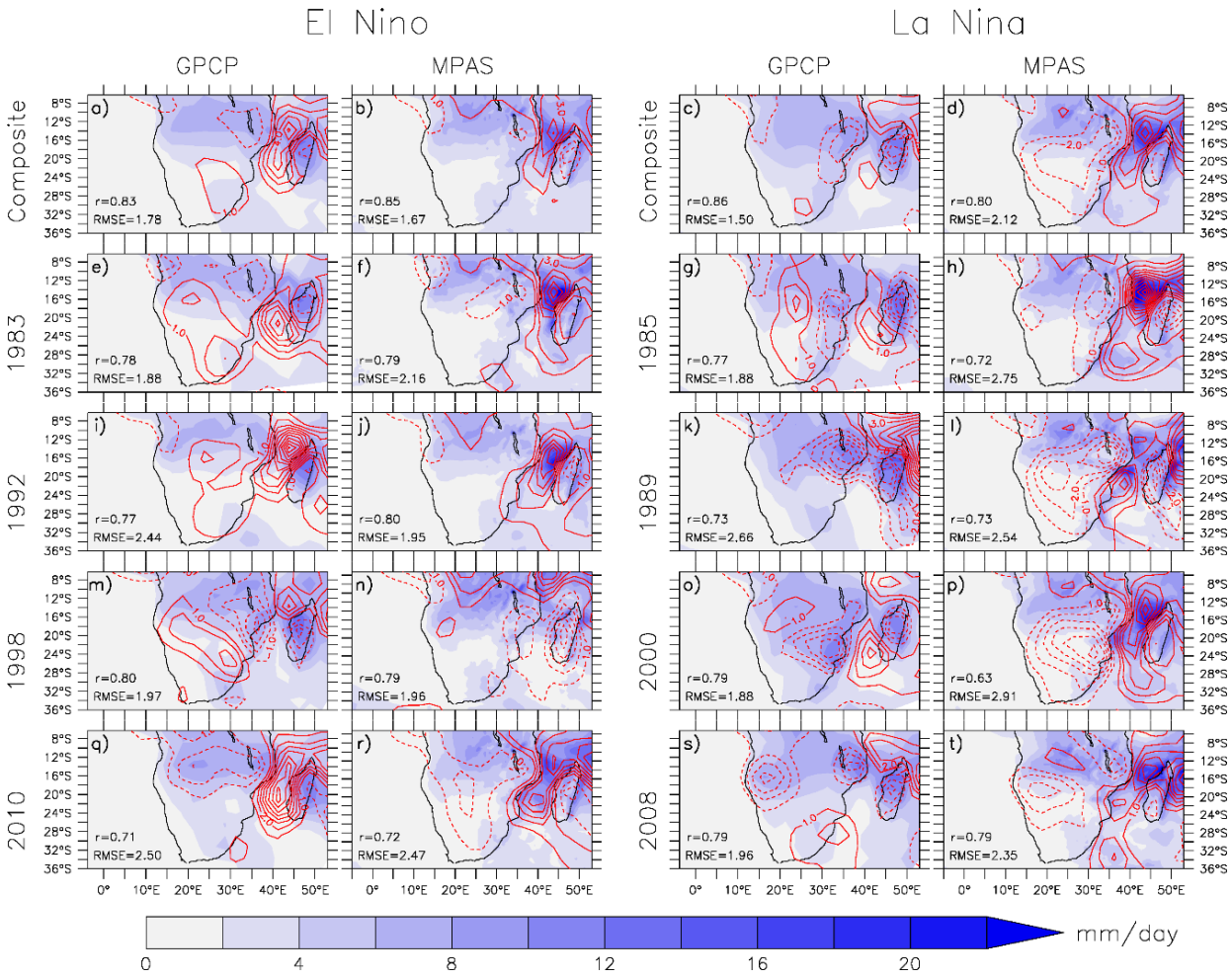

Fig 6. 2: The spatial distribution of JFM rainfall (mm/day; shaded) over Southern Africa as depicted by GPCP and MPAS during the El Niño years (columns 1 and 2) and La Niña years (columns 3 and 4). The contours in the GCPC panels show the bias in the MPAS5 model simulation with reference to the GCPC (i.e., MPAS5 - GPCP), while contours in the MPAS panels show the bias in the MPAS model simulation with reference to the GPCP (i.e., MPAS - GPCP). In the GPCP panels, the r-value represents the spatial correlation between GPCP and MPAS5 and RMSE represents the Root Mean Square Error. In the MPAS panels, the r-value represents the spatial correlation between GPCP and MPAS, and RMSE represents the Root Mean Square Error

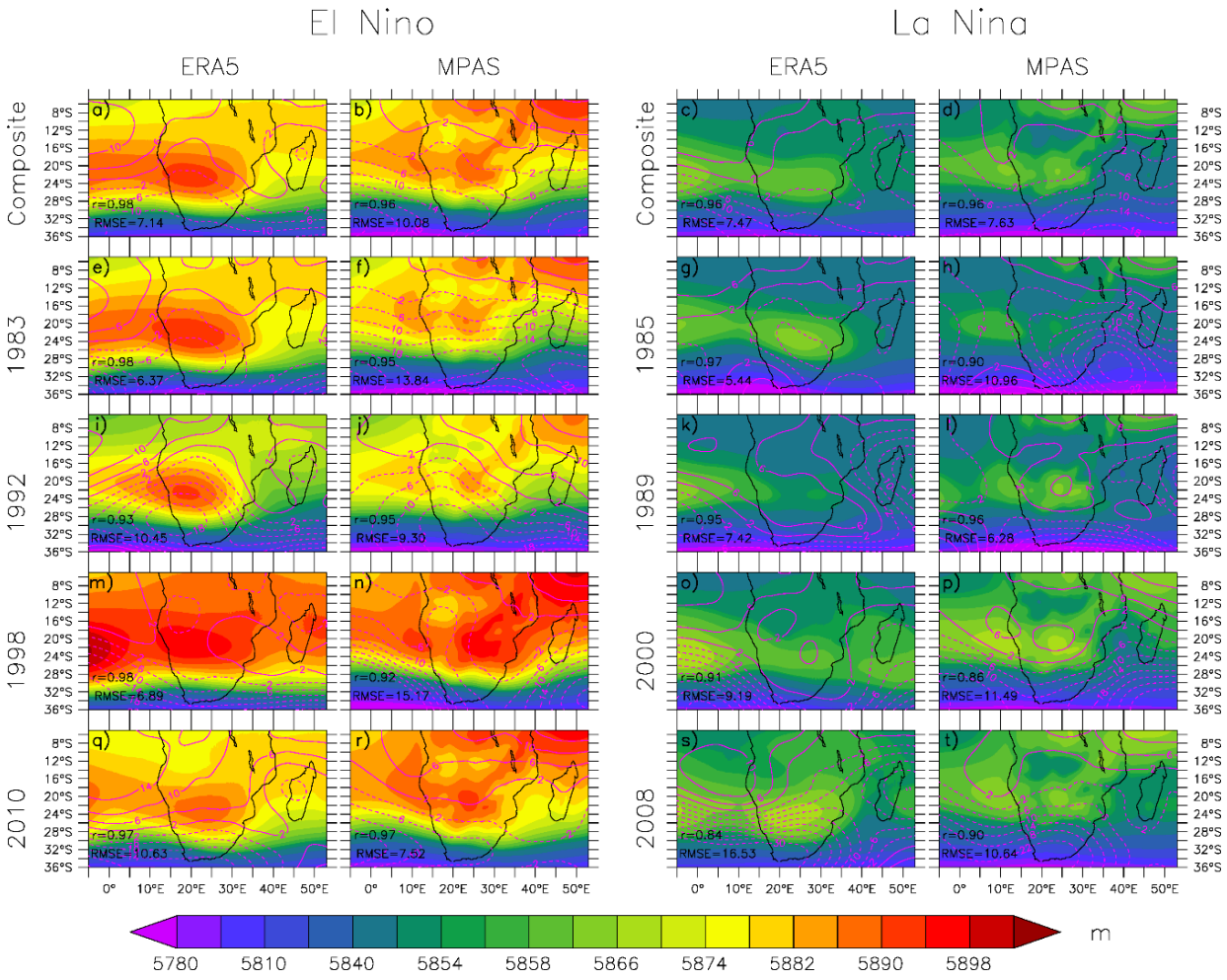

Fig 6. 3: Same as Figure 6.2 but for JFM 500 hPa geopotential height

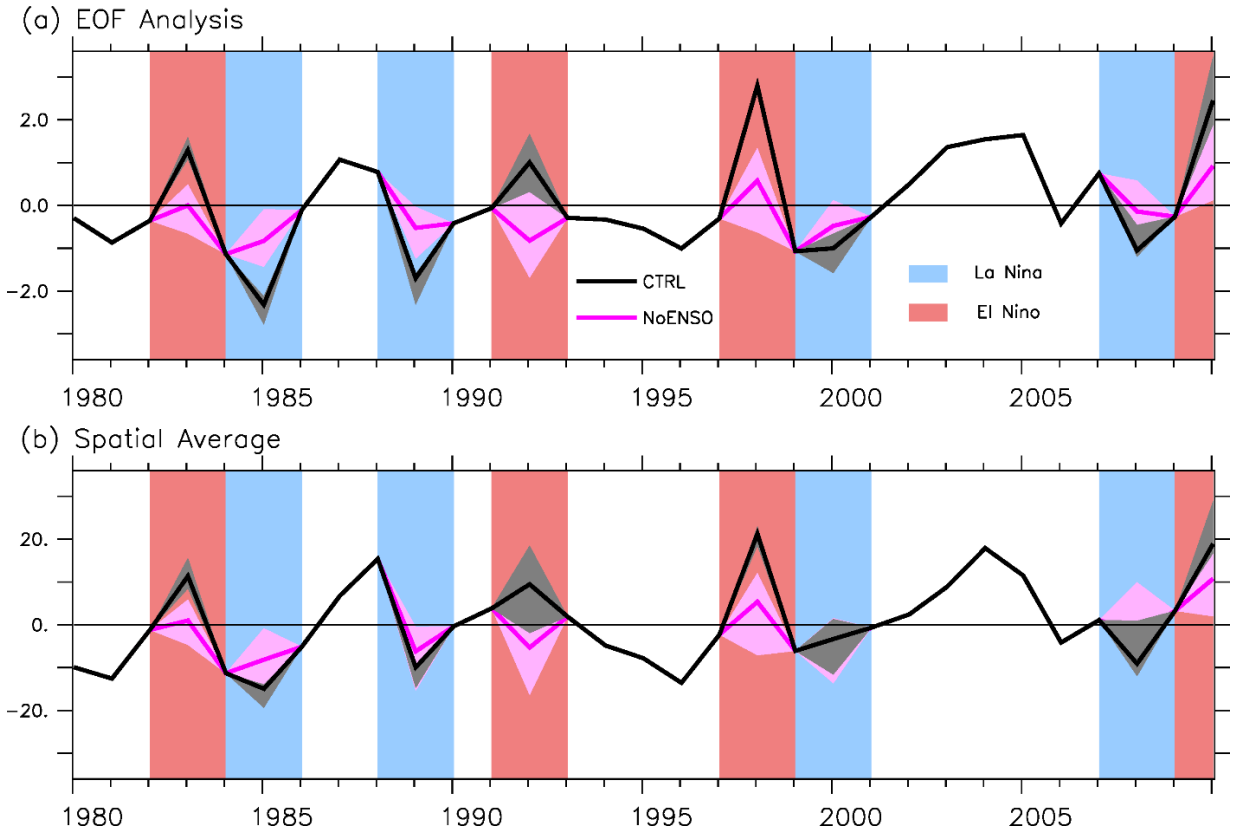

Fig 6. 4: The interannual variability of the simulated Botswana High in the control (CTRL) and no ENSO (NoENSO) experiments. (a) The Botswana High index was derived from the score of EOF-1 of JFM 500 hPa geopotential height over the study area (10-14°E, 0 -33°S). (b) The Botswana High index is derived from the spatial average of 500 hPa over the Botswana High core region (15°-22° E; 20° -25°S) shown in Fig. 3.3. The dashed lines represent the standard deviation of the Botswana High index in the CTRL experiment

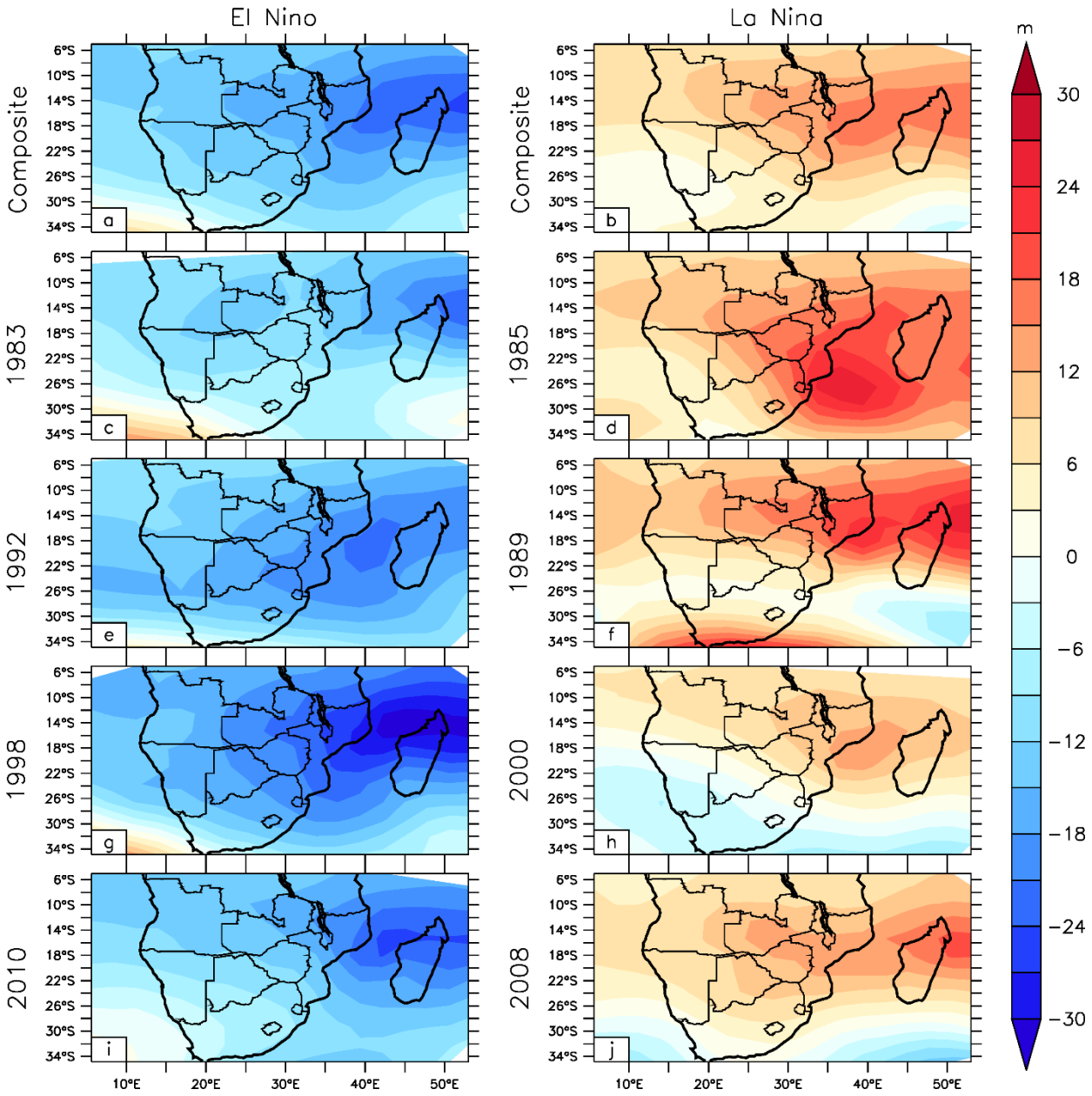

Fig 6. 5: Impact of the removal of ENSO forcing (NoENSO minus CTRL) on the 500 hPa geopotential height over Southern Africa during El Niño and La Niña Years

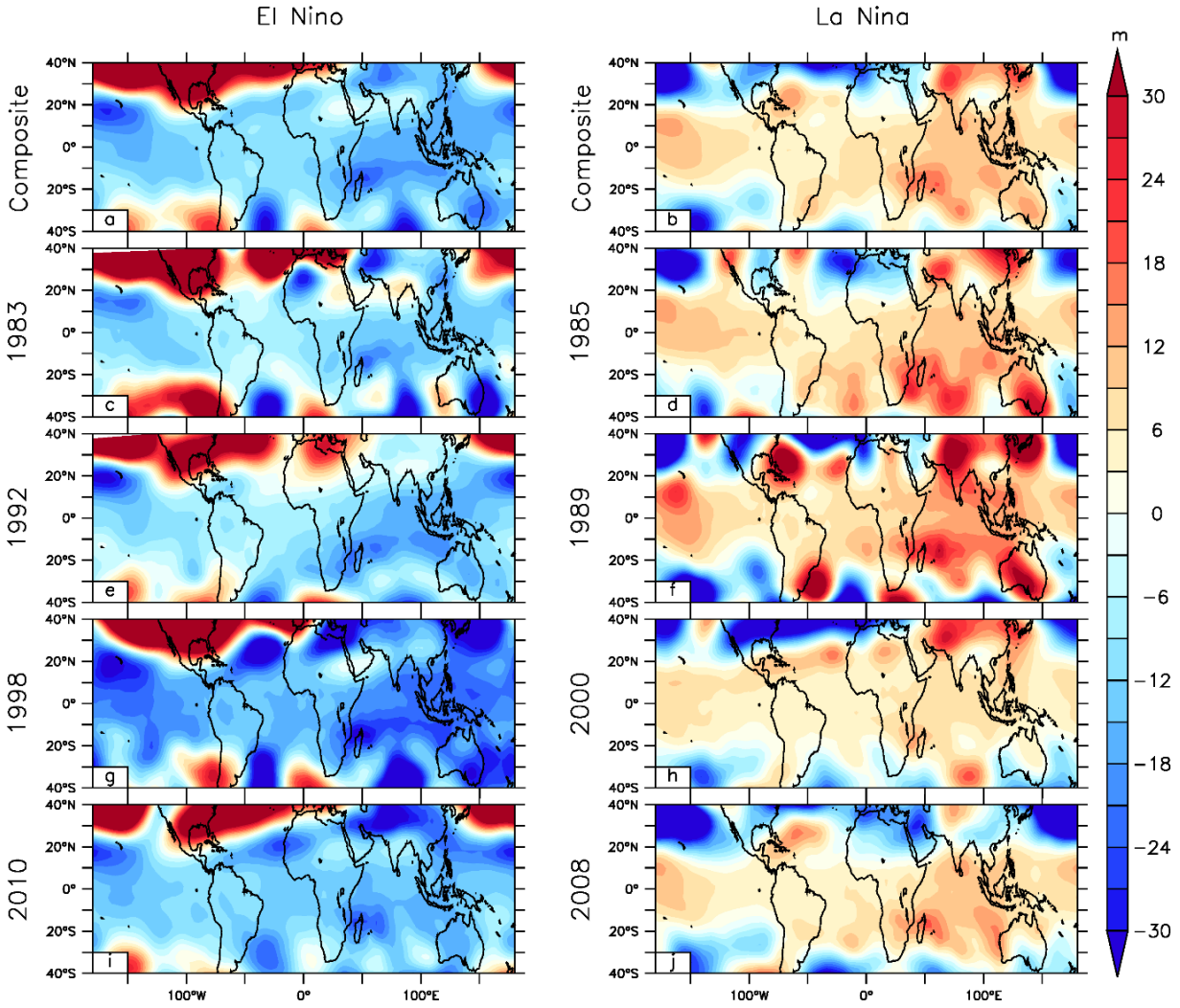

Fig 6. 6: Impact of the removal of ENSO forcing (NoENSO minus CTRL) on the global 500 hPa geopotential height during El Niño and La Niña Years

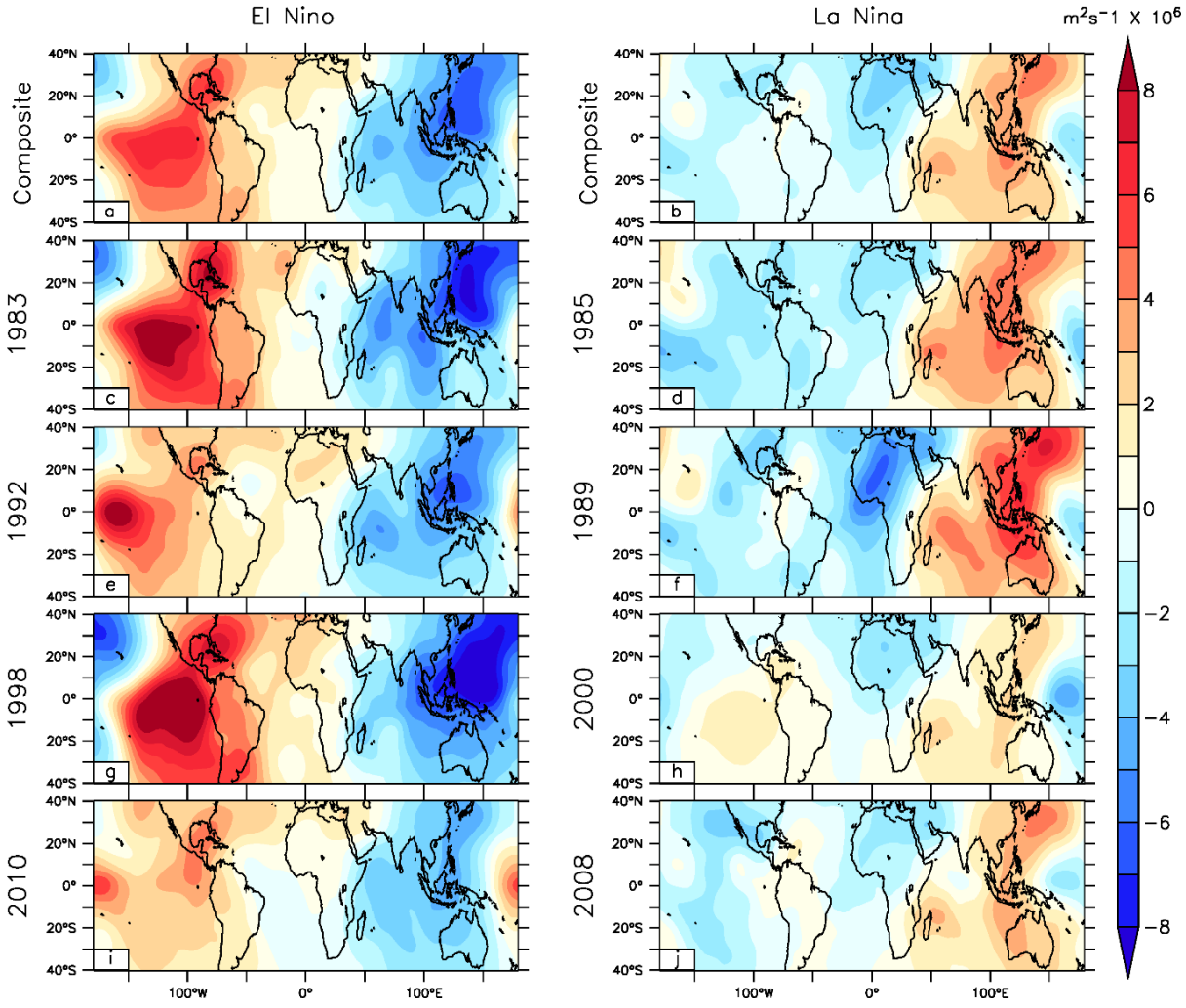

Fig 6. 7: Same as Figure 6.6 but for 200 hPa Velocity Potential

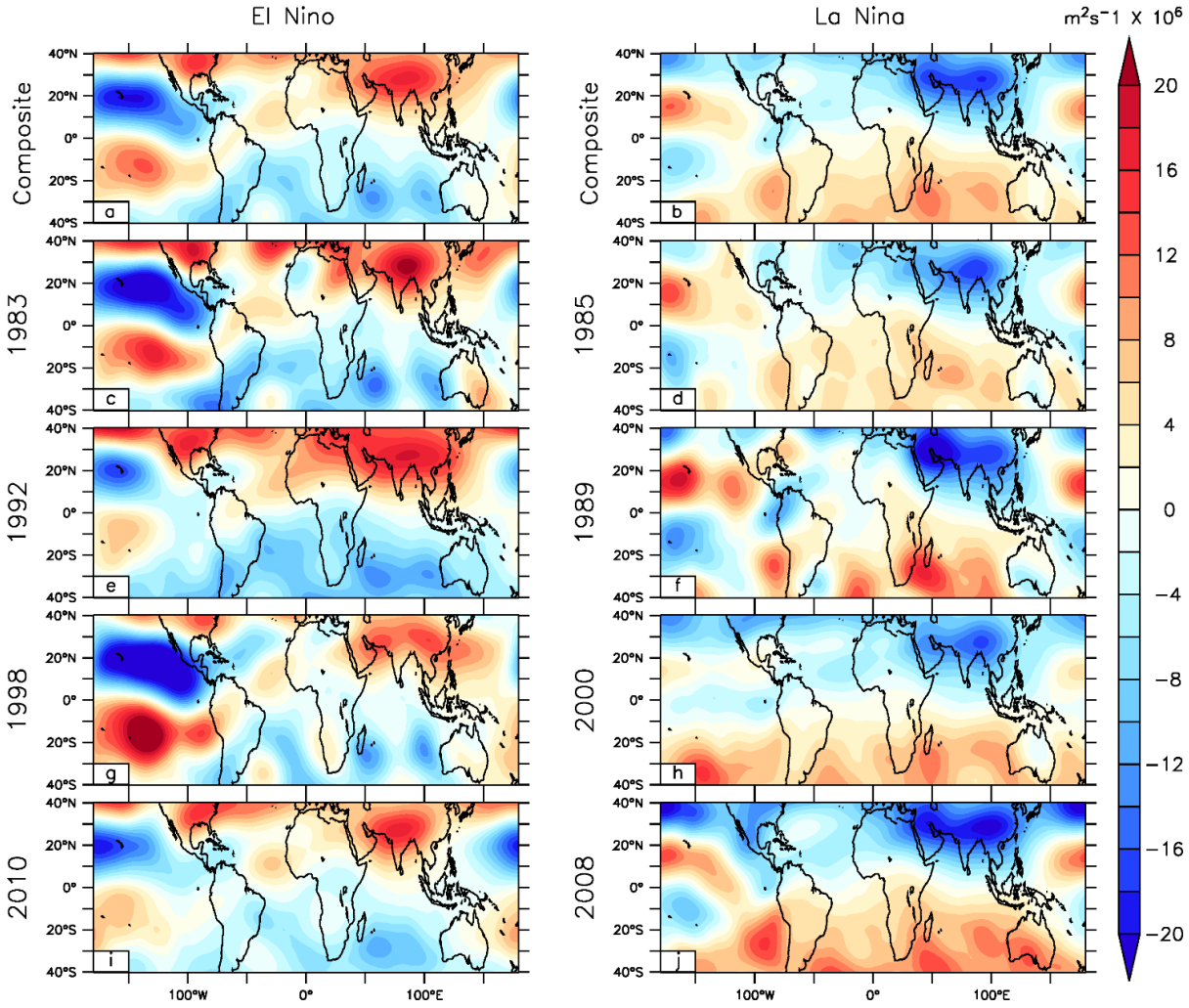

Fig 6. 8: Same as Figure 6.6 but for 200 hPa Stream Function

CHAPTER SEVEN: CONCLUSIONS AND RECOMMENDATIONS

7.1 Conclusions

The Botswana High remains an important component of the regional atmospheric circulation over Southern Africa during the austral spring, summer, and early autumn. This mid-level anticyclone is best expressed at 500 hPa and has been shown to impact rainfall, frequency of dry days and temperature extremes (Driver and Reason, 2017). However, the influence of the Botswana High on Southern African droughts has not been studied before. Furthermore, several studies have identified El Niño Southern Oscillation (ENSO) as one major cause of the Botswana High variability (Driver and Reason, 2017; Reason, 2018); however, previous studies have used correlation and composite analysis in determining the relationship between ENSO and the Botswana High, which cannot determine a cause-and-effect relationship. Therefore, it remains unknown if the Botswana Highs variability is a direct response to ENSO. Given this, this thesis investigated the skill of the Model Prediction Across Scales (MPAS) Global Climate Model in simulating the characteristics of the Botswana High and the influence of the High on Southern African droughts. The global model simulation covered a period of 31 years (1980–2010). The main focus was on the austral summer (January-February-March) as it represents the peak season of the Botswana High strength. Focusing on the Southern African domain, Empirical Orthogonal Function (EOF) analysis was used to extract the Botswana High feature from the 500 hPa geopotential height in the reanalysis and simulation datasets. To evaluate the skill of the model in capturing the spatial and temporal variability of the Southern African climate and the Botswana High, the simulated results were compared to the observational and reanalysis data using wavelet and correlation analysis. This thesis then investigated the spatio-temporal structures of Southern African drought patterns in observation, reanalysis and MPAS model simulation, showing how the temporal variability of the Botswana High influences the drought modes. Finally, the thesis investigated the Botswana High response to ENSO using the MPAS model with a variable resolution of 48 km over Southern Africa and 240 km worldwide to better understand the relationship between the Botswana High and ENSO.

The results of the thesis can be summarised as follows:

- In general, the MPAS model simulates well all of the climate variables over Southern Africa as in observation and reanalysis. The spatial variations in the 500 hPa

geopotential height are larger in the 20C reanalysis (about -16 to - 18m) and MPAS simulation (about -9 to 10 m) as compared to the ERA5 reanalysis. The simulated rainfall and temperature bias are about 3 mm/day and -2°C, respectively. However, the rainfall bias is more pronounced over the Mozambique Channel, which may be attributed to the overestimated deep convection by the model leading to the suppression of convective rainfall and dry bias over eastern and central parts of the Southern African region.

- The MPAS model captures well the spatial pattern of the Botswana High, and all datasets (i.e., reanalysis and model) agree that the Botswana High accounts for about 80% of the variability in the 500 hPa geopotential height over the Botswana area. However, the MPAS Botswana High spatial pattern features a better agreement with the ERA5 High than the 20C reanalysis High.

- The MPAS simulation reproduced the temporal variability of the Botswana High as in the reanalysis. In addition to that, the Botswana High's variability, which shows a strong correlation with ENSO ($r > 0.80$), suggests a quasi-linear relationship between the Botswana High and ENSO as in previous studies. Furthermore, R^2 analysis reveals that ENSO explains about 79%, 65% and 70% of the variability in the ERA5, uniform-grid MPAS (240km) and variable-resolution MPAS (48km - 240km) Botswana Highs, respectively.

- The MPAS model captured well the drought patterns over Southern Africa as compared to observation and reanalysis. In all the datasets (CRU, ERA5, 20C and MPAS), the most dominant five DMs (DM1-DM5) over Southern Africa jointly explain more than 60% of the interannual variability in the 3-month summer droughts for SPEI and SPI.

- ERA5 and MPAS agree that the Botswana High influences the interannual variability of DM1. However, the influence is stronger in ERA5 ($r = -0.85$) and moderate MPAS ($r = -0.42$). Wet years are distinguished by a weak Botswana High, while drought years are characterized by a strong Botswana High. Furthermore, the wet and dry years correspond to the -ve and +ve phases of the El Niño Southern Oscillation (ENSO). These findings imply that the Botswana High could be a conduit pipe through which ENSO signals influence DM1 in the region.

- During the positive phase of DM1, the core area of the drought mode is characterized by negative anomalies in 500 hPa geopotential height (i.e., weaker Botswana High), cooler temperature, weaker PET, net cyclonic flow, stronger moisture convergence, and positive anomalies in precipitation in both ERA5 and MPAS. The opposite is true for DMI's negative phase.

- Sensitivity experiments show that the Botswana High mode is independent of ENSO, but the modes' amplitude amplifies during ENSO events. Given that, removing the El Niño forcing strengthens the Walker Circulation and results in upper-level divergence (200 hPa) over Southern Africa. This upper-level divergence weakens the 500 hPa geopotential height over the region resulting in a weak Botswana High. The opposite is true with the removal of the La Niña signal.

7.2 Limitations and Recommendations

The results of this thesis suggest that MPAS can be applied for drought early warning systems over Southern Africa and for predicting the influence of the Botswana High variability on the annual variation of summer rainfall. However, more simulations and model improvements are still needed to establish the robustness of the results. For instance, due to the limited computational resources available for the study, we could only perform the MPAS simulation at about 240 km quasi-uniform horizontal grid over the globe. To resolve more regional-scale rainfall-producing systems that may be influenced by the Botswana High, future studies can take advantage of the variable-grid resolution of MPAS to perform more simulations with higher resolution over Southern Africa. Such studies could improve knowledge on the influence of uniform-grid vs variable-resolution grid in simulating the characteristics of the Botswana High. In addition, our results on the relationship between the Botswana High and drought, which is based on correlation and composite analysis, cannot determine causality in the relationships. Therefore, there is a need for a series of sensitivity experiments with MPAS to demonstrate and quantify the cause-and-effect relationships. However, the present study has demonstrated the capability of MPAS in simulating the characteristics and influence of the Botswana High on Southern African droughts.

The investigation into the influence of the Botswana High on drought modes could be improved in several ways. There are discrepancies among the datasets on the relationship between Botswana High and drought modes. Potential work following this thesis could consider using more observational, reanalysis, and model datasets to give a more robust assessment of the influence of the Botswana High on the drought modes (especially DMI). Future work could also look into understanding how the relationship of DM1 and the Botswana High would change in the future climate under global warming, which may also reduce future climate risks associated with drought occurrences over Southern Africa. Another area of study that needs attention is the influence of geopotential height patterns on Southern African climate, resulting in different climatic conditions over Southern Africa despite strong +ve or -ve Botswana High events. However, the present study supports the notion that different drought modes exist in Southern Africa and shows that there is a link between the Botswana High and the most dominant drought mode (DM1) in the region.

The results of the model sensitivity experiments affirm the idea that ENSO fuels the Botswana High variability, but the formation of the High is independent of ENSO. To that end, more model experiments are still needed to establish the formation mechanisms of the summertime Botswana High. Reason (2016) suggested that the Botswana High could form as a response to the heat released by tropical regions of high precipitation located to their northeast. In the Southern Africa region, this region is located near the SICZ. Therefore, future studies may apply the MPAS model to study the response of the Botswana High to condensational heating from the SICZ and assess whether the Botswana High forms as a response to areas of high precipitation to its northeast. Furthermore, it would also be useful to identify factors that influence the position of the Botswana High so that better forecasting is possible. Another area of study that requires attention could be the overestimation of rainfall over the MC in the MPAS model, which causes a dry bias over the Southern Africa region, especially during La Niña. Using variable-resolution models, Williamson (2008) showed that precipitation is highly sensitive to the parameterisation time step and horizontal resolution and suggested when resolution increases, the parameterisation time step must be decreased. Therefore, potential work following from this study would consider the impact of the parameterisation time step with respect to horizontal resolution, improving rainfall and Botswana High simulation over the region.

A common issue with EOF analysis is that its outcomes cannot be organised into an array of synoptic states spanning the continuum of events. Self-Organising Maps (SOMs), also known as Kohonen Maps (Kohonen, 1990), are an alternative approach in synoptic climatology that provide a mechanism for visualising the complex distribution of synoptic states while treating the data as a continuum (Hewitson and Crane, 2002). SOMs are a type of unsupervised artificial neural network used for various applications such as clustering, exploratory data analysis and visualisation, ordering of multidimensional data, sampling and feature extraction (Lobo, 2009; Meque, 2015). Despite the superiority of SOMs to EOFs, there is a dearth of studies on the application of SOMs in analysing mid-level subtropical highs like the Botswana High. In the Southern Africa region, SOM analysis has been used extensively by several authors (Maure et al., 2013; Oettlie et al., 2013; Meque, 2015; Abiodun et al., 2015), but to our knowledge, no study has used the algorithm to characterise Botswana High patterns. Given this, future studies should consider using SOM analysis to study the Botswana High and its associated circulation patterns.

REFERENCES

Abiodun BJ, Abba Omar S, Lennard C, Jack C (2015). Using regional climate models to simulate extreme rainfall events in the Western Cape, South Africa. International Journal of Climatology, 36(2):689-705. https://doi.org/10.1002/joc.4376

Abiodun BJ, Makhanya N, Petja B, Abatan AA, Oguntunde PG (2018) Future projection of droughts over major river basins in Southern Africa at specific global warming levels. Theor Appl Climatol 137(3–4):1785–1799. https://doi.org/10.1007/s00704-018-2693-0

Ali S, Dan L, Fu C, Yang Y (2015) Performance of convective parameterization schemes in Asia using RegCM: simulations in three typical regions for the period 1998–2002. Adv Atmos Sci 32(5):715–730. https://doi.org/10.1007/ s00376-014-4158-4

Ashok K, Behera SK, Rao SA, Weng H, Yamagata T (2007) El Niño Modoki and its possible teleconnection, J. Geophys. Res., 112, C11007. https://doi.org/10.1029/2006JC003798

Australian Government Burea of Meterology. The Indian Ocean Dipole (2021). http://www.bom.gov.au/climate/enso/history/ln-2010-12/IOD-what.shtml. . Accessed 18 September 2021

Bachèlery ML, Illig S, Rouault M (2020) Interannual coastal trapped waves in the Angola-Benguela upwelling system and Benguela Niño and Niña events. Journal of Marine Systems 203:103262

Barrett BS, Hameed S (2017) Seasonal variability in precipitation in central and southern Chile: Modulation by the South Pacific high. Journal of Climate 30(1):55–69. https://doi.org/10.1175/JCLI-D-16-0019.1

Behera SK, Yamagata T (2001) Subtropical SST dipole events in the southern Indian Ocean. Geophys. Res. Lett 28: 327–330. https://doi.org/10.1029/2000GL011451

Bhaktawar N, van Niekerk L (2012) South Africa Yearbook 2012/2013 | Government Communication and Information System (GCIS). https://www.gcis.gov.za/content/resourcecentre/sa-info/yearbook2012-13. Accessed 7 March 2021

Bolton Geography Portfolio (n.d) African Climate zones. https://sites.google.com/site/boltongeographyportfolio/home/african-climate-zones. Accessed 7 March 2021

Bridgman HA, Oliver JE (2006) The Global Climate System: Patterns, Processes, and Teleconnections. Cambridge University Press:359

Britannica The Editors of Encyclopaedia (2022) Subtropical High. *Encyclopedia Britannica*, 16 Aug. 2017, https://www.britannica.com/science/subtropical-high. Accessed 31 March 2022.

Burakowski EA, Tawfik A, Ouimette A, Lepine L, Zarzycki C, Novick K, Bonan G (2019) Simulating surface energy fluxes using the variable-resolution Community Earth System Model (VR-CESM). Theoretical and Applied Climatology 138(1):115-133. https://doi.org/10.1007/s00704-019-02785-0

Burls NJ, Blamey RC, Cash BA, Swenson ET, Fahad A, Bopape MJM, Straus, DM, Reason CJ C (2019) The Cape Town "Day Zero" drought and Hadley cell expansion. Npj Climate and Atmospheric Science 2(1):1–8. https://doi.org/10.1038/s41612-019-0084-6

Caian M, Geleyn JF (1997) Some limits to the variable-mesh solution and comparison with the nested-lam solution. Quarterly Journal of the Royal Meteorological Society, 123(539):743-766. https://doi.org/10.1002/qj.49712353911

Chang CP, Zhang Y, Li T (2000) Interannual and interdecadal variations of the East Asian summer monsoon and tropical Pacific SSTs. Part I: Roles of the subtropical ridge. Journal of Climate, 13(24), 4310-4325. https://doi.org/10.1175/1520-0442(2000)013%3C4310:IAIVOT%3E2.0.CO;2

Chikoore H (2016) Drought in Southern Africa: structure, characteristics and impacts. University of Zululand.http://uzspace.unizulu.ac.za/xmlui/handle/10530/1547. Accessed 8 March 2021

Chikoore H, Jury MR (2010) Intraseasonal variability of satellite-derived rainfall and vegetation over Southern Africa. Earth Interactions 14(3):1–26. https://doi.org/10.1175/2010EI267.1

Chikoore H, Jury MR (2021) South African drought, deconstructed. Weather and Climate Extremes 100334. https://doi.org/10.1016/j.wace.2021.100334

Choi W, Kim KY (2019). Summertime variability of the western North Pacific subtropical high and its synoptic influences on the East Asian weather. Scientific Reports 9(1):1–9. https://doi.org/10.1038/s41598-019-44414-w

Coelho CA, de Oliveira CP, Ambrizzi T, Reboita MS, Carpenedo CB, Campos JLPS, Rehbein A (2015). The 2014 southeast Brazil austral summer drought: regional scale

mechanisms and teleconnections. Climate Dynamics 46(11):3737-3752. https://doi.org/10.1007/s00382-015-2800-1

Colucci SJ (2003) Anticyclones. Encyclopedia of Atmospheric Sciences. Elsevier :142–146. doi:10.1016/b0-12-227090-8/00071-3

Cook KH (2000) The South Indian Convergence Zone and Interannual Rainfall Variability over Southern Africa, Journal of Climate 13(21):3789-3804. https://doi.org/10.1175/1520-0442(2000)013%3C3789:TSICZA%3E2.0.CO;2

Cook KH (2001) A Southern Hemisphere Wave Response to ENSO with Implications for Southern Africa Precipitation. Journal of the Atmospheric Sciences 58(15):2146-2162. https://doi.org/10.1175/1520-0469(2001)058%3C2146:ASHWRT%3E2.0.CO;2

Cooper PJM, Dimes J, Rao KPC, Shapiro B, Shiferaw B, Twomlow S (2008) Coping better with current climatic variability in the rain-fed farming systems of sub-Saharan Africa: An essential first step in adapting to future climate change? Agriculture, ecosystems & environment, 126(1-2):24-35. https://doi.org/10.1016/j.agee.2008.01.007

Crétat J, Pohl B, Dieppois B, Berthou S, Pergaud J (2018) The Angola Low: relationship with southern African rainfall and ENSO. Climate Dynamics 52(3):1783-1803. https://doi.org/10.1007/s00382-018-4222-3

Crétat J, Pohl B, Richard Y, Drobinski P (2011) Uncertainties in simulating regional climate of Southern Africa: sensitivity to physical parameterizations using WRF. Climate dynamics, 38(3):613-634. https://doi.org/10.1007/s00382-011-1055-8

Dahan A (2010) Putting the Earth System in a numerical box? The evolution from climate modeling toward global change. Studies in History and Philosophy of Science Part B - Studies in History and Philosophy of Modern Physics 41(3):282–292. https://doi.org/10.1016/j.shpsb.2010.08.002

Dames B (2014) Power System Emergency - 6 March 2014. https://www.eskom.co.za/OurCompany/MediaRoom/Documents/poweremergency6march.pdf. Accessed 7 March 2021

Davis RE, Hayden BP, Gay DA, Phillips WL, Jones GV (1997). The North Atlantic subtropical anticyclone. Journal of Climate 10(4):728–744. https://doi.org/10.1175/1520-0442(1997)010<0728: TNASA>2.0.CO;2

Davis CA, Ahijevych DA, Wang W, Skamarock WC (2016) Evaluating Medium-Range Tropical Cyclone Forecasts in Uniform- and Variable-Resolution Global Models. Monthly Weather Review. 144(11):4141-4160. https://doi.org/10.1175/MWR-D-16-0021.1

Davis-Reddy CL, Vincent K (2017) Risk and Vulnerability: a handbook for Southern Africa climate 2nd edn. https://www.csir.co.za/sites/default/files/Documents/SADC%20Handbook_Second%20Edition_full%20report.pdf

Dong X, Fan FX, Lin RP, Jin JB, Lian RX (2017) Simulation of the Western North Pacific subtropical high in El Niño Decaying Summers by CMIP5 AGCMs. Atmos Ocean Sci Lett 10(2):146–155. https://doi.org/10.1080/16742834.2017.2724 04

Driver P (2014) Rainfall Variability over Southern Africa. University of Cape Town. https://open.uct.ac.za/handle/11427/12830. Accessed 7 March 2021

Driver P, Abiodun B, Reason CJC (2018) Modelling the precipitation response over southern Africa to the 2009–2010 El Niño using a stretched grid global atmospheric model. Clim Dyn 52:3929–3949. https://doi.org/10.1007/s00382-018-4362-5

Driver P, Reason CJC (2017) Variability in the Botswana High and its relationships with rainfall and temperature characteristics over Southern Africa. Int J Climatol 37:570–581. https://doi.org/10.1002/joc.5022

Du Q, Faber V, Gunzburger M (1999) Centroidal Voronoi tessellations:applications and algorithms. SIAM Rev 41(4):637–676. https://doi.org/10.1137/S0036144599352836

Engelbrecht FA, McGregor JL, Engelbrecht CJ. (2008) Dynamics of the Conformal-Cubic Atmospheric Model projected climate-change signal over southern Africa. International Journal of Climatology 29:1013– 1033. https://doi.org/10.1002/joc.1742

Engelbrecht, C. J., Engelbrecht, F. A. and Dyson, L. L. (2012) High-resolution model-projected changes in mid-tropospheric closed-lows and extreme rainfall events over southern Africa. Int. J. Climatol 33: 173–187. https://doi.org/10.1002/joc.3420

Engelbrecht CJ, Landman WA, Engelbrecht FA, Malherbe J (2014) A synoptic decomposition of rainfall over the Cape south coast of South Africa. Climate Dynamics, 44(9-10): 2589-2607. https://doi.org/10.1007/s00382-014-2230-5

Fahad A, Burls NJ, Strasberg Z (2020) How will southern hemisphere subtropical anticyclones respond to global warming? Mechanisms and seasonality in CMIP5 and CMIP6 model projections. Climate Dynamics 55(3):703–718. https://doi.org/10.1007/s00382-020-05290-7

Fauchereau N, Trzaska S, Richard Y, Roucou P, Camberlin P (2003) Sea-surface temperature co-variability in the southern Atlantic and Indian Oceans and its connections with the atmospheric circulation in the Southern Hemisphere. Int. J. Climatol 23:663–677. https://doi.org/10.1002/joc.905

Florenchie P, Lutjeharms JRE, Reason CJC, Masson S, Rouault M (2003) The source of Benguela niños in the South Atlantic Ocean. Geophysical Research Letter 30. https://doi.org/10.1029/2003GL017172

Florenchie P, Reason CJC, Lutjeharms JRE, Rouault M, Roy C, Masson S (2004): Evolution of interannual warm and cold events in the Southeast Atlantic Ocean. Journal of Climate 17:2318–2334. https://doi.org/10.1175/1520-0442(2004)017%3C2318:EOIWAC%3E2.0.CO;2

Food and Agricultural Organization of the United Nations (2016) AGRICULTURE AND FOOD INSECURITY RISK MANAGEMENT IN AFRICA Concepts, lessons learned and review guidelines. http://www.fao.org/3/a-i5936e.pdf. Accessed 7 March 2021

Fowler LD, Skamarock WC, Grell GA, Freitas SR, Duda MG (2016) Analyzing the Grell–Freitas Convection Scheme from Hydrostatic to Nonhydrostatic Scales within a Global Model, Monthly Weather Review, 144(6):2285-2306. https://doi.org/10.1175/MWR-D-15-0311.1

Fox-Rabinovitz M, Cote J, Dugas B, Deque M, McGregor JL, Belochitski A (2008) Stretched-grid Model Intercomparison Project: decadal regional climate simulations with enhanced variable and uniform-resolution GCMs. Meteorology and atmospheric physics 100(1):159-178. https://doi.org/10.1007/s00703-008-0301-z

Fuenzalida H (1982) A country of extreme climate (in Spanish). Chile: Essence and Evolution. Instituto de Estudios Regionales Universidad de Chile 27–35

Gamble DW, Parnell DB,Curtis S (2008) Spatial variability of the Caribbean mid-summer drought and relation to north Atlantic high circulation. International Journal of Climatology 28(3):343–350. https://doi.org/10.1002/joc.1600

Gates WL (1992) AN AMS continuing series: Global CHANGE--AMIP: The atmospheric model intercomparison project. Bulletin of the American Meteorological Society 73(12):1962-1970. https://doi.org/10.1175/1520-0477(1992)073%3C1962:ATAMIP%3E2.0.CO;2

Giannini A, Biasutti M, Held IM, Sobel AH (2008) A global perspective on African climate. Clim Change 90:359–383. doi:10.1007/ s10584-008-9396-y

Giannini A, Kushnir Y, Cane MA (2000) Interannual variability of Caribbean rainfall, ENSO, and the Atlantic Ocean. J Clim 13:297–311. https://doi.org/10.1175/1520-0442(2000)013%3C0297:IVOCRE%3E2.0.CO;2

Giorgi F, Gutowski Jr WJ (2015) Regional dynamical downscaling and the CORDEX initiative. Annual Review of Environment and Resources 40:467-490. https://www.annualreviews.org/doi/10.1146/annurev-environ-102014-021217

Giorgi F, Mearns LO (1999) Introduction to special section: Regional climate modelling revisited. J Geophys Res 104:6335–6352. https://doi.org/10.1029/98JD02072

Grimm AM, Reason CJC (2010) Does the South American Monsoon Influence African Rainfall? J. Climate 24:1226-1238. https://doi.org/10.1175/2010JCLI3722.1

Gore M, Abiodun BJ, Kucharski F (2019) Understanding the influence of ENSO patterns on drought over southern Africa using SPEEDY. Clim Dyn 54:307–327. https://doi.org/10.1007/s00382-019-05002-w

Hameed S, Iqbal MJ, Collins D (2011) Impact of the Indian Ocean high pressure system on winter precipitation over western and southwestern Australia. Australian Meteorological and Oceanographic Journal, 61(3):159

Hersbach H, Bell B, Berrisford P, Biavati G, Horányi A, Muñoz Sabater J, Nicolas J, Peubey C, Radu R, Rozum I, Schepers D, Simmons A, Soci C, Dee D, Thépaut J-N (2018) ERA5 hourly data on single levels from 1979 to present. Copernicus Climate Change Service (C3S) Climate Data Store (CDS). https://doi.org/10.24381/cds.adbb2d47

Hewitson BC, Crane RG (2002) Self-organizing maps: applications to synoptic climatology. Climate Research 22(1):13-26. https://www.int-res.com/articles/cr2002/22/c022p013.pdf

Hansingo K, Reason CJC (2009) Modelling the atmospheric response over southern Africa to SST forcing in the southeast tropical Atlantic and southwest subtropical Indian Oceans.
Int. J. Climatol 29:1001–1012. https://dx.doi.org/10.1002/joc.1919

Hart NCG, Reason CJC, Fauchereau N (2010) Tropical–extratropical interactions over southern Africa: Three cases of heavy summer season rainfall. Monthly weather review, 138(7):2608-2623. https://doi.org/10.1175/2010MWR3070.1

He C, Wu B, Zou L, Zhou T (2017) Responses of the summertime subtropical anticyclones to global warming. J Clim 30(16):6465–6479. https://doi.org/10.1175/JCLI-D-16-0529.1

Heim RR (2002) A Review of Twentieth-Century Drought Indices Used in the United States. Bulletin of the American Meteorological Society 83(8):1149–1166. https://doi.org/10.1175/1520-0477-83.8.1149

Held IM, Hou AY (1980) Nonlinear axially symmetric circulations in a nearly inviscid atmosphere. J. Atmos. Sci 37:515–533

Hermes JC and Reason CJC (2005) Ocean model diagnosis of interannual coevolving SST variability in the south Indian and South Atlantic Oceans. J. Climate 18:2864–2882. https://doi.org/10.1175/JCLI3422.1

Hohenegger C, Brockhaus P, Schaer C (2008) Towards climate simulations at cloud-resolving scales. Meteorol Z 17(4):383–394. https://doi.org/10.127/0941-948/2008/0303

Horel JD, Hahmann AN, Geisler JE (1989) An investigation of the Annual Cycle of Convective Activity over the Tropical Americas. Journal of Climate 2(11):1388–1403. https://doi.org/10.1175/1520-0442(1989)002<1388: aiotac>2.0.co;2

Hoskins BJ (1996) On the existence and strength of the summer subtropical anticyclones. Bull. Amer. Meteor. Soc, 77:1287–1291

Ingpen B (2015) Ocean Currents. Maritime Studies South Africa. https://maritimesa.org/grade-10/ocean-currents/. Accessed 7 March 2021

Johnson NC (2013) How many ENSO flavors can we distinguish? Journal of Climate. American Meteorological Society, 26(13):4816–4827. https://doi.org/10.1175/JCLI-D-12-00649.1

Jolliffe IT (2002) Principal Component Analysis, 2nd edition. Springer :519

Judt F (2018) Insights into atmospheric predictability through global convection-permitting model simulations. J. Atmos. Sci., 75:1477–1497. https://doi.org/10.1175/JAS-D-17-0343.1

Judt F (2020) Atmospheric predictability of the tropics, middle latitudes, and polar regions explored through global storm-resolving simulations, Journal of the Atmospheric Sciences. American Meteorological Society, 77(1): 257–276. https://doi.org/10.1175/JAS-D-19-0116.1

Jury MR (2013) Climate trends in southern Africa. South African Journal of Science 109(1/2):1-11. http://dx.doi.org/10.1590/ sajs.2013/980

Keyantash J, National Center for Atmospheric Research Staff (Eds) (2018) The Climate Data Guide: Standardized Precipitation Index (SPI). https://climatedataguide.ucar.edu/climate-data/standardized-precipitation-index-spi. Accessed 23 October 2021

Klemp JB, Skamarock WC, Dudhia J (2007) Conservative split explicit time integration methods for the compressible nonhydrostatic equations. Mon Wea Rev 135(8):2897–2913. https://doi.org/10.1175/MWR3440.1

Knaff JA (1997) Implications of summertime sea level pressure anomalies in the tropical Atlantic region. J Clim 10:789–804. https://doi.org/10.1175/1520-0442(1997)010%3C0789:IOSSLP%3E2.0.CO;2

Knight J, Grab S (2015) The Drakensberg escarpment: mountain processes at the edge. In Landscapes and Landforms of South Africa 47-55. http://dx.doi.org/10.1007/978-3-319-03560-46

Kohonen T (1990). The self-organizing map. Proceedings of the IEEE 78(9):1464-1480. https://doi.org/10.1109/5.58325

Kousky VE, Kagano MT (1981) A climatological study of the trospospheric circulation over the Amazon region. Acta Amazonica 11(4):743-758

Lake PS (2011) Drought and Aquatic Ecosystems: Effects and Responses, Drought and Aquatic Ecosystems: Effects and Responses.John Wiley & Sons. https://doi.org/10.1002/9781444341812

Lawal K (2015) Understanding the variability and predictability of seasonal climates over West and Southern Africa using climate models. University of Cape Town. https://open.uct.ac.za/handle/11427/16556. Accessed 7 March 2021

Lee HT (2014) Climate Algorithm Theoretical Basis Document (C-ATBD): Outgoing Longwave Radiation (OLR) - Daily. NOAA's Climate Data Record (CDR) Program, CDRP-ATBD-0526:46

Lee SS, Seo YW, Ha KJ, Jhun JG (2013) Impact of the western North Pacific subtropical high on the East Asian monsoon precipitation and the Indian Ocean precipitation in the boreal summertime. Asia-Pacific Journal of Atmospheric Sciences, 49(2):171–182. https://doi.org/10.1007/s13143-013-0018-x

Lenters JD, Cook KH (1997) On the Origin of the Bolivian High and Related Circulation Features of the South American Climate, Journal of the Atmospheric Sciences, 54(5):656-678. https://doi.org/10.1175/1520-0469(1997)054%3C0656:OTOOTB%3E2.0.CO;2

Li W, Li L, Fu R, Deng Y, Wang H (2011) Changes to the North Atlantic subtropical high and its role in the intensification of summer rainfall variability in the southeastern United States. Journal of Climate 24(5):1499–1506. https://doi.org/10.1175/2010JCLI3829.1

Lindesay JA (1988) South African rainfall, the Southern Oscillation and a Southern Hemisphere semi-annual cycle. J Climatol 8(1):17–30. https://doi.org/10.1002/joc.3370080103

Lindzen RS, Hou AY (1988) Hadley circulations for zonally averaged heating centered off the equator. J. Atmos. Sci 45:2416–2427

Liu YM, Wu GX, Liu H, Liu P (2001) Condensation heating of the Asian summer monsoon and the subtropical anticyclone in the Eastern Hemisphere. Climate Dynamics, 17(4):327-338. https://doi.org/10.1007/s003820000117

Lobo VJ (2009) Application of self-organizing maps to the maritime environment. In Information Fusion and Geographic Information Systems 19-36. https://doi.org/10.1007/978-3-642-00304-2_2

Lu R (2001) Interannual Variability of the Summertime North Pacific Subtropical High and its Relation to Atmospheric Convection over the Warm Pool. Journal of the Meteorological Society of Japan 79(3):771–783. https://doi.org/10.2151/jmsj.79.771

Lutjeharms JRE (2006) The agulhas current. https://doi.org/10.1007/3-540-37212-1

Magadza C (1994) Climate change: some likely multiple impacts in Southern Africa. Food Policy 19(2):165–191. https://doi.org/10.1016/0306-9192(94)90068-X

Mahlalela PT, Blamey RC, Reason CJC (2018). Mechanisms behind early winter rainfall variability in the southwestern Cape, South Africa. Climate dynamics 53(1):21-39. https://doi.org/10.1007/s00382-018-4571-y

Manatsa D, Morioka Y, Behera SK, Matarira CH, Yamagata T (2013) Impact of Mascarene High variability on the East African 'short rains'. Climate dynamics, 42(5-6), 1259-1274. https://doi.org/10.1007/s00382-013-1848-z

Manatsa D, Reason CJC, Mukwada G (2012) On the decoupling of the IODZM from southern Africa summer rainfall variability. Int J Climatol 32(5):727–746. doi:10.1002/joc.2

Maoyi ML, Abiodun BJ (2021) How well does MPAS-atmosphere simulate the characteristics of the Botswana High? Climate Dynamics 1-20. https://doi.org/10.1007/s00382-021-05797-7

Maoyi ML, Abiodun BJ, Prusa JM, Veitch JJ (2017) Simulating the characteristics of tropical cyclones over the South West Indian Ocean using a Stretched-Grid Global Climate Model. Climate dynamics 50(5): 1581-1596. https://doi.org/10.1007/s00382-017-3706-x

Mason SJ, Jury MR (1997) Climatic variability and change over southern Africa: a reflection on underlying processes. Progress in Physical Geography: Earth and Environment 21(1):23–50. https://doi.org/10.1177%2F030913339702100103

Matarira CH (1990) Drought over Zimbabwe in a regional and global context. Int J Climatol 10(6):609–625. https://doi.org/10.1002/joc.33701 00605

Matsumura S, Horinouchi T (2016) Pacific Ocean decadal forcing of long-term changes in the western Pacific subtropical high. Scientific reports 6(1):1-7. https://doi.org/10.1038/srep37765

Maúre GA (2013) Effects of biomass-burning aerosol loading on Southern African climate. PhD Thesis, University of Cape Town, Cape Town South Africa

McKee TB, Doesken NJ, Kleist J (1993) The relationship of drought frequency and duration to time scales. In: Proceedings of the 8th conference on applied climatology, vol 17, pp 179–183

Meadows ME (2006) Global change and southern Africa. Geographical Research 44(2):135-145. https://doi.org/10.1111/j.1745-5871.2006.00375.x

Meque A (2015) Investigating the link between southern African droughts and global atmospheric teleconnections using regional climate models. In: Thesis, University of Cape Town. https://open.uct.ac.za/handle/11427/16686

Miyasaka T, Nakamura H (2005) Structure and formation mechanisms of the Northern Hemisphere summertime subtropical highs. J. Climate 18:5046–5065. https://doi.org/10.1175/JCLI3599.1

Miyasaka T, Nakamura H (2010) Structure and mechanisms of the Southern Hemisphere Summertime subtropical anticyclones. J Clim 23(8):2115–2130. https:// doi. org/ 10. 1175/ 2009JCLI3008.1

Mizuta R, Oouchi K, Yoshimura H, Noda A, Katayama K, Yukimoto S, Nakagawa M. (2006). 20-km-mesh global climate simulations using JMA-GSM model—mean climate states—. Journal of the Meteorological Society of Japan Ser. II 84(1):165-185. https://doi.org/10.2151/jmsj.84.165

Morioka Y, Tozuka T, and Yamagata T (2010) Climate variability in the southern Indian

Ocean as revealed by self organizing maps. Climate Dyn 35:1059–1072. https://doi.org/10.1007/S00382-010-0843-X

Morioka Y, Tozuka T, Yamagata T (2011) On the growth and decay of the subtropical dipole mode in the South Atlantic. J. Climate 24:5538–5554. doi:10.1175/2011JCLI4010.1

Morioka Y, Tozuka T,Masson S, Terray P, Luo JJ, Yamagata T (2012) Subtropical dipole modes simulated in a coupled general circulation model. J. Climate 25:4029–4047. doi:10.1175/JCLI-D-11-00396.1

Muvuyani F (2016). Millions threatened by drought and hunger in southern Africa. dw.com. https://www.dw.com/en/millions-threatened-by-drought-and-hunger-in-southern-africa/a-18988565. Accessed 7 March 2021

Naik M (2015) Modeling the potential impacts of Vegetation change on the future climate of Southern Africa. University of Cape Town. https://open.uct.ac.za/handle/11427/1558. Accessed 7 March 2021

National Oceanic and Atmospheric Administration (n.d) 20CR Climate Indices:AAO. https://psl.noaa.gov/data/20thC_Rean/timeseries/monthly/AAO/. Accessed 7 March 2021.

Nguyen H, Lucas C, Evans A, Timbal B, Hanson L (2015) Expansion of the Southern Hemisphere Hadley cell in response to greenhouse gas forcing. Journal of Climate 28(20):8067-8077. https://doi.org/10.1175/JCLI-D-15-0139.1

Nicholson SE, Entekhabi D (1987) Rainfall variability in equatorial and southern Africa: relationships with sea surface temperatures along the southwestern coast of Africa. Journal of Climate & Applied Meteorology 26(5):561–578. https://doi.org/10.1175/1520-0450(1987)026%3C0561:RVIEAS%3E2.0.CO;2

Nicholson SE (2011): Dryland Climatology. Cambridge University Press:530

Nicholson SE, Kim J (1997) The relationship of the El Niño-Southern oscillation to African rainfall. Int J Climatol 17(2):117–135. https://doi.org/10.1002/(SICI)1097-0088(199702)17:2%3C117::AID-JOC84%3E3.0.CO;2-O

Nkurunziza IF, Guirong T, Ngarukiyimana JP, Sindikubwabo C (2019) Influence of the Mascarene High on October-December rainfall and their associated atmospheric circulation anomalies over Rwanda. J. Environ. Agric. Sci, 20, 1-20.

Ogwang BA, Ongoma V, Xing L, Ogou KF (2015) Influence of Mascarene high and Indian Ocean dipole on East African extreme weather events. Geographica Pannonica 19(2):64-72

Abba Omar SA (2020) Understanding the Characteristics of Cut-off Lows over the Western Cape, South Africa. University of Cape Town. https://open.uct.ac.za/handle/11427/32478. Accessed 7 March 2021

Oettli P, Tozuka T, Izumo T, Engelbrecht FA, Yamagata T (2014) The self-organizing map, a new approach to apprehend the Madden-Julian Oscillation influence on the intraseasonal variability of rainfall in the southern African region. Climate dynamics 43(5-6):1557. DOI:10.1007/s00382-013-1985-4

Oort AH, Yienger JJ (1996) Observed Interannual Variability in the Hadley Circulation and Its Connection to ENSO, Journal of Climate, 9(11):2751-2767. https://doi.org/10.1175/1520-0442(1996)009%3C2751:OIVITH%3E2.0.CO;2

O'Regan V (2021) Eskom blackouts: blame it on the rain…. https://www.dailymaverick.co.za/article/2021-02-07-eskom-blackouts-blame-it-on-the-rain/. Accessed 7 March 2021

Paek H, Yu JY, Hwu JW, Lu MM, Gao T (2015) A SOURCE of AGCM bias in simulating the Western Pacific Subtropical high: different sensitivities to the two types of ENSO. Mon Wea Rev143(6):2348–2362. https://doi.org/10.1175/MWR-D-14- 00401.1

Park JY, Jhun JG, Yim SY, Kim WM (2010) Decadal changes in two types of the western North Pacific subtropical high in boreal summer associated with Asian summer monsoon/El Niño–Southern Oscillation connections. Journal of Geophysical Research 115(D21): D21129. https://doi.org/10.1029/2009JD013642

Perkins R (2018) New Climate Model to Be Built from the Ground Up. Caltech. https://www.caltech.edu/about/news/new-climate-model-be-built-ground-84636. Accessed 19 September 2021

Persson A (1998) How do we understand the Coriolis force? Bulletin of the American Meteorological Society 79(7):1373-1386

Pontes, G. M. et al. (2020) 'Drier tropical and subtropical Southern Hemisphere in the mid-Pliocene Warm Period', Scientific Reports, 10(1), pp. 1–11.

Pontes GM, Wainer I, Taschetto AS, Gupta AS, Abe-Ouchi A, Brady EC, Zhang Z (2020) Drier tropical and subtropical Southern Hemisphere in the mid-Pliocene Warm Period. Scientific reports 10(1) :1-11. https://doi.org/10.1038/s41598-020-68884-5

Porcù F, Carrassi A, Medaglia CM, Prodi F, Mugnai A (2006) A study on cut-off low vertical structure and precipitation in the Mediterranean region. Meteorology and Atmospheric Physics 96(1):121-140. https://doi.org/10.1007/s00703-006-0224-5

Ratna SB, Behera S, Ratnam JV, Takahashi K, and Yamagata T (2012) An index for tropical temperate troughs over southern Africa. Climate dynamics 41(2):421–44. https://doi.org/10.1007/s00382-012-1540-8

Reboita MS, Ambrizzi T, Silva BA, Pinheiro RF, Da Rocha RP (2019) The South Atlantic subtropical anticyclone: present and future climate. Frontiers in Earth Science 7:8. https://doi.org/10.3389/feart.2019.00008

Rummukainen M (2010) State-of-the-art with regional climate models. Wiley Interdisciplinary Reviews: Climate Change 1(1):82–96. https://doi.org/10.1002/wcc.8

Reason CJC, RJ Allan, JA Lindesay and TJ Ansell (2000) ENSO and climatic signals across the Indian Ocean basin in the global context: part I, interannual composite patterns. Int. J. Climatol 20: 1285–1327. https://doi.org/10.1002/1097-0088(200009)20:11%3C1285::AID-JOC536%3E3.0.CO;2-R

Reason CJC (2001) Subtropical Indian Ocean SST dipole events and southern African rainfall. Geophys. Res. Lett 28:2225–222. https://doi.org/10.1029/2000GL012735

Reason CJC (2016) The Bolivian, Botswana, and Bilybara highs and southern hemisphere drought/floods. Geophys Res Lett 43(3):1280–1286. https://doi.org/10.1002/2015GL0672 28

Reason, C. J. C. (2017). Variability in rainfall over tropical Australia during summer and relationships with the Bilybara High. Theoretical and applied climatology, 132(1), 313-326

Reason CJC, Jagadheesha D (2005) A model investigation of recent ENSO impacts over southern Africa. Meteorology and Atmospheric Physics 89(1–4):181–205. https://doi.org/10.1007/s00703-005-0128-9

Reason CJC, Landman W, Tennant W (2006) Seasonal to decadal prediction of southern African climate and its links with variability of the Atlantic Ocean. Bulletin of the American Meteorological Society 87(7):941–955. https://doi.org/10.1175/BAMS-87-7-941

Reason CJC (2018) Low-frequency variability in the Botswana High and southern African regional climate. Theor Appl Climatol 137(1):321–1334. https://doi.org/10.1007/s00704-018-2661-8

Reason CJC, Rouault M (2005) Links between the Antarctic Oscillation and winter rainfall over western South Africa. Geophysical research letters, 32(7). https://doi.org/10.1029/2005GL022419

Reboita MS, Amaro TR, de Souza MR (2017) Winds: intensity and power density simulated by RegCM4 over South America in present and future climate. Climate Dynamics 51(1–2): 187–205. https://doi.org/10.1007/s00382-017-3913-5

Reboita MS, Gan MA, Rocha RP, Ambrizzi T (2010) Regimes de precipitação na América do Sul: uma revisão bibliográfica. Revista Brasileira de Meteorologia, 25(2):185–204. https://doi.org/10.1590/s0102-77862010000200004

Reboita MS, Rodrigues M, Silva LF, Alves MA (2015) ASPECTOS CLIMÁTICOS DO ESTADO DE MINAS GERAIS (CLIMATE ASPECTS IN MINAS GERAIS STATE). Revista Brasileira de Climatologia 17(0). https://doi.org/10.5380/abclima.v17i0.41493

Richard Y, Fauchereau N, Poccard I, Rouault M, Trzaska S (2001) 20th century droughts in southern Africa: spatial and temporal variability, teleconnections with oceanic and atmospheric conditions. International Journal of Climatology 21(7): 873-885. https://doi.org/10.1002/joc.656

Rodwell MJ, Hoskins BJ (1996) Monsoons and the dynamics of deserts. Quarterly Journal of the Royal Meteorological Society, 122(534):1385-1404. https://doi.org/10.1002/qj.49712253408

Rodwell MJ, Hoskins BJ (2001) Subtropical anticyclones and summer monsoons. J Clim 14(15):3192–3211. https://doi.org/10.1175/1520-0442(2001)014%3C3192:SAASM%3E2.0.CO;2

Roeckner E, Oberhuber JM, Bacher A, Christoph M, Kirchner I (1996) ENSO variability and the atmospheric response in a global coupled atmosphere–ocean GCM. Climate Dyn, 12:737–754. https://doi.org/10.1007/s003820050140

Rojas O, Vrieling A, Rembold F (2011) Assessing drought probability for agricultural areas in Africa with coarse resolution remote sensing imagery. Remote Sensing of Environment 115(2):343–352. https://doi.org/10.1016/j.rse.2010.09.006

Rouault M, Florenchie P, Fauchereau N, Reason CJC (2003) Southeast tropical Atlantic warm events and southern African rainfall. Geophysical Research Letter 30: 8009. DOI: 10.1029/2002GL014840

Rouault M, Illig S, Barthlomae C, Reason CJC, Bentamy A (2007) A Propagation and origin of warm anomalies in the Angola Benguela upwelling system in 2001. Journal of Marine Systems 68:473–488. https://doi.org/10.1016/j.jmarsys.2006.11.010

Rouault M, Richard Y (2005) Intensity and spatial extension of drought in South Africa at different time scales. WaterSA 29(4):489–500

SADC (2001) Southern African Development Community. Annual Report 2001-2002. https://www.sadc.int/files/6813/5333/8099/SADC_Annual_Report_2001-2002.pdf.pdf. Accessed 7 March 2021

SADC (2012a) Southern African Development Community:: Poverty Eradication & Policy Dialogue. https://www.sadc.int/themes/poverty-eradication-policy-dialogue/. Accessed 7 March 2021

SADC (2012b) Southern African Development Community:: Disaster Risk Management. .https://www.sadc.int/themes/disaster-risk-management/. Accessed 7 March 2021

SADC (2012c) Southern African Development Community:: SADC Overview. https://www.sadc.int/about-sadc/overview/. Accessed 7 March 2021

SADC (2012d) Southern African Development Community:: Agriculture & Food Security. https://www.sadc.int/themes/agriculture-food-security/. Accessed 7 March 2021

SADC (2012e) Southern African Development Community:: Food Security https://www.sadc.int/themes/agriculture-food-security/food-security/. Accessed 7 March 2021

SADC (2012f) Southern African Development Community:: Mining. https://www.sadc.int/themes/economic-development/industry/mining/. Accessed 7 March 2021

SADC (2012g) Southern African Development Community:: Electricity Generation. https://www.sadc.int/themes/infrastructure/en/electricity-generation/. Accessed 7 March 2021

SADC (2018) SADC Selected Economic and Social Indicators 2018. https://www.sadc.int/files/6215/6630/2592/SADC_Selected_Indicators_2018.pdf. Accessed 7 March 2021

Saha S, Moorthi S, Wu X, Wang J, Nadiga S, Tripp P, Behringer D, Hou Y, Chuang H, Iredell M, Ek M, Meng J, Yang R, Mendez MP, Van den Dool H, Zhang Q , Wang W, Chen M, Becker, E. (2014). The NCEP climate forecast system version 2. Journal of climate, 27(6):2185-2208. https://doi.org/10.1175/JCLI-D-12-00823.1

Saji NH, Goswami BN, Vinayachandran PN, Yamagata T (1999) A dipole mode in the tropical Indian Ocean. Nature 401:360–363. https://doi.org/10.1038/43854

Schmidt DF, Grise KM (2019) Impacts of subtropical highs on summertime precipitation in North America. Journal of Geophysical Research: Atmospheres, 124(21):11188-11204. https://doi.org/10.1029/2019JD031282

Scholvin S (2014) South Africa's Energy Policy: Constrained by Nature and Path Dependency. Journal of Southern African Studies 40(1):185–202. https://doi.org/10.1080/03057070.2014.889361

Seager R, Murtugudde R, Naik N, Clement A, Gordon N, Miller, J (2003) Air–sea interaction and the seasonal cycle of the subtropical anticyclones. Journal of climate 16(12):1948-1966. https://doi.org/10.1175/1520-0442(2003)016%3C1948:AIATSC%3E2.0.CO;2

Singleton AT, Reason C J C (2007) A numerical model study of an intense cutoff low pressure system over South Africa. Monthly Weather Review 135(3):1128–1150. https://doi.org/10.1175/MWR3311.1

Shannon LV, Boyd AJ, Brundrit GB, and Taunton-Clark J (1986) On the existence of an El Niño-type phenomenon in the Benguela system. Journal of Marine Research 44: 495–520. https://doi.org/10.1357/002224086788403105

Shongwe ME, Van Oldenborgh GJ, Van Den Hurk BJJM, De Boer B, Coelho CAS, Van Aalst MK (2009) Projected changes in mean and extreme precipitation in Africa under global warming. Part I: Southern Africa. Journal of climate, 22(13): 3819-3837. https://doi.org/10.1175/2009JCLI2317.1

Siddharta (2020) Intertropical Convergence Zone. https://siddhartha01writes.medium.com/intertropical-convergence-zone-itcz-7de592bbd7ef. Accessed 7 March 2021

Smillie S (2019) Load shedding: Eskom's wet coal boogeyman is back. https://www.iol.co.za/saturday-star/news/load-shedding-eskoms-wet-coal-boogeyman-is-back-38796659. Accessed 7 March 2021

Skamarock WC, Klemp JB, Duda MG, Fowler LD, Park S (2013) Uniform and variable resolution nonhydrostatic global atmospheric simulations using Voronoi meshes in MPAS-atmosphere (Invited). In: AGUFM Abstract, pp A31H-01

Spector JB (2012) South Africa: Mining for change. Or change for mining? Daily Maverick. https://www.dailymaverick.co.za/article/2012-06-20-south-africa-mining-for-change-or-change-for-mining/. Accessed 7 March 2021

Stahle DW, Cleaveland MK (1992) Reconstruction and analysis of spring rainfall over the southeastern US for the past 1000 years. Bulletin - American Meteorological Society, 73(12): 1947–1961. https://doi.org/10.1175/1520-0477(1992)073<1947:RAAOSR>2.0.CO;2

Sun X, Cook KH, Vizy EK (2017) The South Atlantic subtropical high: Climatology and interannual variability. Journal of Climate 30(9):3279–3296. https://doi.org/10.1175/JCLI-D-16-0705.1

Nishizawa T, Tanaka M (1983) The annual change in the tropospheric circulation and the rainfall in South America. Archives for Meteorology, Geophysics, and Bioclimatology Series B 33(1–2):107–116. https://doi.org/10.1007/BF02273994

Thompson DW, Wallace, JM (2000). Annular modes in the extratropical circulation. Part I: Month-to-month variability. Journal of climate 13(5):1000-1016. https://doi.org/10.1175/1520-0442(2000)013%3C1000:AMITEC%3E2.0.CO;2

Tyson, PD, Preston-Whyte RA (2000) Weather and climate of southern Africa. Oxford University Press

University Corporation for Atmospheric Science (2021) The Highs and Lows of Air Pressure | UCAR Center for Science Education. In: UCAR - Center for Science Education. https://scied.ucar.edu/learning-zone/how-weather-works/highs-and-lows-air-pressure. Accessed 8 March 2021

Ujeneza EL, Abiodun BJ (2014) Drought regimes in Southern Africa and how well GCMs simulate them. Climate Dynamics 44(5):1595-1609. https://doi.org/10.1007/s00382-014-2325-z

Unganai LS, Mason SJ (2002) Long-Range predictability of Zimbabwe summer rainfall. Int J Climatol 22(9):1091–1103. https://doi.org/10.1002/joc.786

Venegas SA, Mysak LA, and Straub DN (1997) Atmosphere– ocean coupled variability in the South Atlantic. J. Climate 10:2904–2920. https://doi.org/10.1175/1520-0442(1997)010%3C2904:AOCVIT%3E2.0.CO;2

Vicente-Serrano SM, Beguería S, López-Moreno JI (2010) A multiscalar drought index sensitive to global warming: the standardized precipitation evapotranspiration index. J Clim 23(7):1696–1718. https://doi.org/10.1175/2009JCLI2909.1

Vicente-Serrano SM, National Center for Atmospheric Research Staff (Eds) (2015) The Climate Data Guide: Standardized Precipitation Evapotranspiration Index (SPEI).

https://climatedataguide.ucar.edu/climate-data/standardized-precipitation-evapotranspiration-index-spei. Accessed 23 October 2021

Vigaud N, Richard Y, Rouault M, Fauchereau N (2008) Moisture transport between the South Atlantic Ocean and southern Africa: relationships with summer rainfall and associated dynamics. Climate Dynamics, 32(1):113-123. https://doi.org/10.1007/s00382-008-0377-7

Wainer I, Prado LF, Khodri M, Otto-Bliesner B (2020) The South Atlantic sub-tropical dipole mode since the last deglaciation and changes in rainfall. Climate Dynamics 56(1):109-122

Wang B, Xiang B, Lee JY (2013) Subtropical High predictability establishes a promising way for monsoon and tropical storm predictions. Proceedings of the National Academy of Sciences of the United States of America 110(8):2718–2722. https://doi.org/10.1073/pnas.1214626110

Wardlow BD, Anderson MC ad Verdin JP (2012) Remote Sensing of Drought. Innovative Monitoring Approaches 472

Wilks DS (2011) Statistical Methods in Atmospheric Sciences 3rd ed. Int. Geophy. Series V.100, :688

Williamson DL (2008) Convergence of aqua-planet simulations with increasing resolution in the Community Atmospheric Model, Version 3, Tellus A: Dynamic Meteorology and Oceanography, 60(5) :848-862, https://doi.org/10.1111/j.1600-0870.2008.00339.x

Williamson DL, Olson JG (2003), Dependence of aqua-planet simulations on time step. Q.J.R. Meteorol. Soc., 129: 2049-2064. https://doi.org/10.1256/qj.02.62

Wilson AB, Bromwich DH, Hines KM, Wang S (2014) El Niño Flavors and Their Simulated Impacts on Atmospheric Circulation in the High Southern Latitudes, Journal of Climate, 27(23):8934-8955. https://doi.org/10.1175/JCLI-D-14-00296.1

Woods Hole Oceanographic Institution (2021) Indian Ocean Dipole. https://www.whoi.edu/multimedia/indian-ocean-dipole/. Accessed 7 March 2021

Wu G, Liu Y (2003) Summertime quadruplet heating pattern in the subtropics and the associated atmospheric circulation. Geophysical research letters 30(5). https://doi.org/10.1029/2002GL016209

Xiang B, Wang B, Yu W, Xu S (2013) How can anomalous western North Pacific subtropical high intensify in late summer? Geophysical Research Letters, 40(10): 2349-2354. https://doi.org/10.1002/grl.50431

Xue F, Wang H, He J (2004) Interannual Variability of Mascarene High and Australian High and Their Influences on East Asian Summer Monsoon. Journal of the Meteorological Society of Japan 82(4):1173–1186. https://doi.org/10.2151/jmsj.2004.1173

Xulu NG, Chikoore H, Bopape MJM, Nethengwe NS (2020) Climatology of the mascarene high and its influence on weather and climate over Southern Africa. Climate 8(7):86. https://doi.org/10.3390/cli8070086

Yuan C, Tozuka T, Landman WA, Yamagata T (2014) Dynamical seasonal prediction of Southern African summer precipitation. Climate dynamics, 42(11-12):3357-3374. https://doi.org/10.1007/s00382-013-1923-5

Zhang F, Bei N, Rotunno R, Snyder C, Epifanio CC (2007) Mesoscale Predictability of Moist Baroclinic Waves: Convection-Permitting Experiments and Multistage Error Growth Dynamics, Journal of the Atmospheric Sciences, 64(10):3579-3594. https://doi.org/10.1175/JAS4028.1

Zhao C, Leung LR, Park SH, Hagos S, Lu J, Sakaguchi K, Yoon J, Harrop BE, Skamarock W, Duda MG (2016) Exploring the impacts of physics and resolution on aqua-planet simulations from a nonhydrostatic global variable-resolution modeling framework. Journal of Advances in Modeling Earth Systems, 8(4):1751-1768. https://doi.org/10.1002/2016MS000727

Zhao YJ (2011) Subtropical Indian Ocean Dipole. https://commons.wikimedia.org/wiki/File:Subtropical_Indian_Ocean_Dipole.jpg. Accessed 7 March 2021

Zhou C (2021) Empirical Orthogonal Function (EOF) analysis. MATLAB Central File Exchange. https://www.mathworks.com/matlabcentral/fileexchange/54416-empirical-orthogonal-function-eof-analysis. Accessed 19 September 2021

Ziervogel G, Cartwright A, Tas A, Adejuwon J, Zermoglio F, Shale M, Smith B (2008) Climate change and adaptation in African agriculture. Stockholm environment institute 17-19. https://www.sei.org/publications/climate-change-adaptation-african-agriculture/

Zinyengere N, Crespo O, Hachigonta S (2013) Crop response to climate change in southern Africa: A comprehensive review. Global and Planetary Change 111:118–126. doi: 10.1016/j.gloplacha.2013.08.010

Zhou TJ (2005). Atmospheric water vapor transport associated with typical anomalous summer rainfall patterns in China. Journal of Geophysical Research 110(D8): D08104. https://doi.org/10.1029/2004JD005413